MeV-scale reheating temperature and thermalization of active and sterile neutrinos in the early Universe

Takuya Hasegawa

Ph.D. dissertation
2019/12/10

Supervisor: Prof. Kazunori Kohri

Department of particle and nuclear physics
School of high energy accelerator science
The Graduate University for Advanced Studies, SOKENDAI

Abstract

In this thesis, we investigate a possibility of an MeV-scale reheating temperature of the Universe and discuss the active- and sterile neutrino thermalization in the scenario. Focusing on the roles of neutrinos in the light element production in the big-bang nucleosynthesis, we obtain observational constraints on i) lower bounds on the reheating temperature, and ii) a possibility of existence of light sterile neutrinos inferred from results of short-baseline neutrino experiments, which are summarized in Refs. [1, 2].

Contents

Chapter 1

Introduction

In this chapter, we describe the outline and the organization of this thesis. Also, we refer to the unit system and notations of variables and constants adopted in this thesis.

1.1 Outline of this thesis

Observations of the light element abundances produced in the epoch of big-bang nuclosynthesis (BBN) have a great capacity to study the physical phenomena which occurred in the early Universe. Also, we can test an underlying theory of cosmology and particle physics by comparing theoretical- and observed abundances of light elements.

In this thesis, we especially focus on a possibility of an MeV-scale reheating temperature of the Universe, motivated by theories beyond the standard model of particle physics which include long-lived massive particles with masses around the weak scale $\sim \mathcal{O}(100)$ GeV, decaying only through gravitational interaction.

The other main focus of this thesis is on neutrino physics. As will be seen in this thesis, neutrinos play important roles in cosmological phenomena in the early Universe. This is because they are one of the most abundant species in the epoch of big-bang nucleosynthesis and recombination, and they are therefore closely related to the expansion history and the dynamics of the phenomena. For this reason, it is important or almost essential to understand property and behavior of neutrinos in extreme environments realized in the hot Big-Bang Universe. Apart from a cosmological interest, neutrinos physics have been drawing strong attention to many physicists, working in vast research fields such as the astrophysics, particle physics, and nuclear physics. To provide a deep understanding and a verification of physics related to the above fields, many observational- and experimental programs have been performed in the past, *e.g.* neutrino oscillation experiments, neutrinoless double beta decay experiments, and neutrino mass measurements. In particular, a theoretical prediction of neutrino oscillation, the transition from a state of one flavor to another, has been experimentally verified, and many researchers believe that it should be clear evidence of the physics beyond the standard model of particle physics. Besides, researchers are currently planning a lot of future programs as explained later. In this thesis,

we also look into a possible existence of sterile neutrinos with a wide range of masses, motivated by a long-standing problem present in the short-baseline neutrino oscillation experiments and a possibility that sterile neutrinos constitute the dark matter.

This thesis is mainly based on our studies summarized in the papers:

[1] T. Hasegawa, N. Hiroshima, K. Kohri, R. S. L. Hansen, T. Tram, and S. Hannestad. "*MeV-scale reheating temperature and thermalization of oscillating neutrinos by radiative and hadronic decays of massive particles.*" *JCAP* **12** (2019) 012 [arXiv: 1908.10189],

[2] T. Hasegawa, K. Kohri, S. Wang, R. S. L. Hansen, T. Tram, and S. Hannestad. "*MeV-scale reheating temperature and cosmological constraints on sterile neutrinos*", In preparation (2019),

both of which focus on the possibility of the MeV-scale reheating temperature, but their purposes are different. The first paper aims to investigate a lower bound on the reheating temperature, and that of the second paper is to explore a possibility of sterile neutrinos with a wide range of masses in the range of $\mathcal{O}$(eV) to $\mathcal{O}$(keV) from cosmological point of view.

In the first paper [1], we perform a numerical computation of the neutrino thermalization in the reheating and evaluate its effects on the production of light elements. As a result, we obtain the lower bound on the reheating temperature $T_{\rm RH} \gtrsim 1.8$ MeV when some massive particle X, responsible for the reheating, dominantly decays into radiation, *i.e.* $X \to \gamma + \ldots$ or $X \to l + \ldots$ where γ is photons and l is charged leptons. Meanwhile, we obtain $T_{\rm RH} \gtrsim$ 4–5 MeV when X dominantly decays into hadrons, *i.e.* $X \to q + \ldots$ or $X \to g + \ldots$, where g is gluons and q is quarks, depending on the mass of X and the hadronic branching ratio of the decay.

In the second paper [2], we calculate the thermalization of sterile neutrinos and find that light sterile neutrinos with its mass of eV-scale, whose existence is inferred from experimental results of short-baseline neutrino oscillation experiments, is consistent with cosmology if $T_{\rm RH} \sim \mathcal{O}(1)$ MeV, in contrast to the case of the standard big-bang model with an *implicit* assumption that $T_{\rm RH} >> \mathcal{O}(1)$ MeV.

We elaborate the first- and the second papers in Chapters 5 and 6, respectively.

1.2 Organization of this thesis

The organization of this thesis is as follows:

In Chapter 2, we review the standard theory of cosmology, the standard big-bang model, and then in Chapter 3 we explain the production of light elements in the early Universe predicted in the standard big-bang model, the standard big-bang nucleosynthesis (SBBN). In Chapter 4, in order to prepare for the later chapters, we survey neutrino oscillation phenomena, first focusing on neutrino oscillation in a vacuum, and then explaining how matter effects affect the phenomena.

Chapters 5 and 6 are devoted to descriptions of our studies [1,2]. Particularly, in Chapter 5 we focus on Ref. [1], where we present our results of the neutrino thermalization in the reheating and light element abundances synthesized in BBN assuming an MeV-scale reheating temperature. Particular attention is paid to treatment of neutrino thermalization calculations. Also, we demonstrate how neutrino oscillation and neutrino self-interaction, *i.e.* collisional processes among neutrinos, affect flavor-dependent neutrino abundances and light element abundances. In Chapter 6, we then focus on Ref. [2], where we discuss cosmological constraints on sterile neutrinos, whose existence is motivated by *e.g.* the discovery of neutrino oscillation, searches for the dark matter, and results of short-baseline neutrino oscillation experiments.

Finally, in Chapter 7 we draw our conclusion and comment on prospects of our studies summarized in this thesis.

1.3 System of units

In this thesis, we adopt the natural unit, where $c = \hbar = k_{\rm B} = 1$. Therefore, dimensions of time $[T]$, length $[L]$, and mass $[M]$ are related to the dimension of energy $[E]$ as $[L]^{-1} = [T]^{-1} = [M] = [E]$. Also, temperature has units of energy, and it is measured in terms of eV.

1.4 Notations of variables and constants

In this section, we present notations and definitions of physical variables and constants which often appear in this thesis.

Symbol	Definition
c	Speed of light.
h	Planck constant.
$\hbar$	Reduced Planck constant, $\hbar \equiv h/2\pi$.
k_{B}	Boltzmann constant.
G	Gravitational constant.
m_e	Electron mass.
m_p	Proton mass.
m_n	Neutron mass.
m_N	Atomic mass unit, $m_N \equiv m_{^{12}\mathrm{C}} \simeq 931.5$ MeV.
M_{pl}	Planck mass, $M_{\mathrm{pl}} \equiv \sqrt{c\hbar/G}$.
m_{pl}	Reduced planck mass, $m_{\mathrm{pl}} \equiv M_{\mathrm{pl}}/\sqrt{8\pi}$.
τ_n	Neutron lifetime.
G_{F}	Fermi coupling constant.
K	Space curvature.
Λ	Cosmological constant.
γ^μ	Gamma matrix ($\mu = 1, 2, 3, 4$).
γ_5	Chirality, $\gamma_5 \equiv i\gamma^0\gamma^1\gamma^2\gamma^3$.

Table 1.1: Symbols and definitions of physical- and mathematical constants.

Symbol	Definition
a	Scale factor.
z	Red shift.
H	Hubble parameter, $H \equiv (da/dt)/a$.
ρ	Total energy density.
ρ_B	Energy density of baryons.
p	Total pressure.
n	Total number density.
n_B	Number density of baryons.
$\bar{n}_B$	Number density of anti-baryons.
n_L	Number density of leptons.
$\bar{n}_L$	Number density of anti-leptons.
n_γ	Number density of photons.
w	Equation of state parameter, $w \equiv p/\rho$.
T	Cosmic temperature.
T_γ	Photon temperature.
T_e	Electron temperature.
T_ν	Neutrino temperature.
$T_{\rm RH}$	Reheating temperature.
ds	Line element.
r	Radial distance.
θ	Azimuthal angle.
ϕ	Polar angle.
$g_{\mu\nu}$	Space-time metric.
$R_{\mu\nu}$	Ricci tensor.
R	Ricci scalar, $R \equiv R^{\mu\nu} g_{\mu\nu}$.
η_B	Baryon asymmetry, $\eta_B \equiv (n_B - \bar{n}_B)/n_\gamma$.
η_L	Lepton asymmetry, $\eta_L \equiv (n_L - \bar{n}_L)/n_\gamma$.
$N_{\rm eff}$	Effective number of neutrino species.

Table 1.2: Symbols and definitions of physical variables.

Symbol	Definition
f_ν	Distribution function of neutrinos.
ν_α	Flavor eigenstates of neutrinos (where $\alpha = e, \mu, \tau, s$).
ν_i	Mass eigenstates of neutrinos ($i = 1, 2, 3, \dots$).
θ_{12}	Mixing angle between ν_1 and ν_2.
θ_{23}	Mixing angle between ν_2 and ν_3.
θ_{13}	Mixing angle between ν_1 and ν_3.
δm^2_{12}	Squared mass difference between ν_1 and ν_2, $\delta m^2_{12} \equiv m^2_2 - m^2_1$.
δm^2_{23}	Squared mass difference between ν_2 and ν_3, $\delta m^2_{23} \equiv m^2_3 - m^2_2$.
δm^2_{13}	Squared mass difference between ν_1 and ν_3, $\delta m^2_{13} \equiv m^2_3 - m^2_1$.
$\delta_{\rm D}$	Dirac CP phase.
$\alpha_{\rm M}$	Majorana CP phase.
$U_{\rm PMNS}$	Flavor mixing matrix .
H	Hydrogen.
D	Deuterium.
T	Tritium.
^{3}He	Helium 3.
^{4}He	Helium 4.
^{6}Li	Lithium 6.
^{7}Li	Lithium 7.
^{7}Be	Beryllium 7.
^{12}C	Carbon 12.
$n_{\rm H}$	Number density of H.
$n_{\rm D}$	Number density of D.
$n_{\rm T}$	Number density of T.
$n_{^3{\rm He}}$	Number density of ^{3}He.
$n_{^4{\rm He}}$	Number density of ^{4}He.
$n_{^6{\rm Li}}$	Number density of ^{6}Li.
$n_{^7{\rm Li}}$	Number density of ^{7}Li.
$n_{^7{\rm Be}}$	Number density of ^{7}Be.
D/H	Number density ratio of D to H, D/H $\equiv n_{\rm D}/n_{\rm H}$.
Y_p	Mass fraction of ^{4}He, $Y_p \equiv m_{^4{\rm He}} n_{^4{\rm He}}/\rho_B$

Table 1.3: Symbols and definitions of physical variables.

Chapter 2

Standard Big-Bang Model

In this chapter, we review the standard theory of cosmology, the standard big-bang model, which is usually assumed in the field of cosmology.

The standard big-bang model is a widely believed theory of cosmology, which describes the time- and temperature evolution of the Universe from a hot and dense state right after the big bang to the current epoch. According to the model, the Universe was born about 13.8 billion years ago, and then it has been cooling down due to the cosmic expansion until today. The maximum temperature of the Universe attained in the "big-bang" (*i.e.* the reheating) is still unknown, but roughly speaking it should be higher than ~ 1 MeV for explaining light element abundances synthesized in BBN and cosmic microwave background (CMB) observed in the Universe. In contrast, the current temperature of the Universe is known to be less than 3 K from observations of CMB [3]. This vast difference between the maximum and the current temperatures means that the Universe can be regarded as a testing ground of both high-energy and low-energy physics.

The standard big-bang model is built on the cornerstones of modern physics, namely the general relativity and the standard theory of particle physics, which are well-tested theories of macroscopic and microscopic phenomena, respectively. The standard big-bang model offers comprehensive explanations for various physical phenomena in the Universe. Particularly, there are four important events which are known as evidence for the validity of the model; namely

(i) Light element abundances produced in the big-bang nucleosynthesis (BBN),

(ii) Cosmic microwave background (CMB) radiation, emitted in the recombination processes of atomic nuclei with electrons,

(iii) Large-scale structure (LSS) of the Universe, formed from density perturbations generated in the early Universe,

(iv) Redshifts associated with galaxies, explained by the Hubble's law.

The theoretical predictions and observational results of these events are in reasonable agreement with each other, and that is the reason that most researchers regard the big-bang model as "standard theory" of cosmology.

In the following, we explain the formulations of the standard big-bang model. In Section 2.1, we first introduce fundamental equations of the model, which describe an expansion of the Universe. More thorough discussions should be found in great textbooks, *e.g.* Refs. [4–7].

2.1 Dynamical equations of the Universe

In this section, we introduce fundamental equations of the standard big-bang model, paying particular attention to explicit- and implicit assumptions of the model.

2.1.1 General relativity

The standard big-bang model is built on the general relativity, established by A. Einstein in the early 19th century. According to the theory, a behavior of the standard model particles in the expanding Universe can be described by the Einstein field equation, which provides a relation between space-time and matter:

$$R_{\mu\nu} - \frac{1}{2}Rg_{\mu\nu} = 8\pi G T_{\mu\nu} + \Lambda g_{\mu\nu}, \tag{2.1}$$

where $R_{\mu\nu}$ is the Ricci curvature tensor, $R(= R^{\mu}{}_{\mu})$ is the Ricci scalar, $g_{\mu\nu}$ is the space-time metric, G is the gravitational constant, $T_{\mu\nu}$ is the energy-momentum tensor of matter, and Λ is the cosmological constant. The Ricci tensor can be expressed in terms of the Christoffel symbols:

$$R_{\mu\nu} = \Gamma^{\alpha}_{\mu\nu,\alpha} - \Gamma^{\alpha}_{\mu\alpha,\nu} + \Gamma^{\alpha}_{\beta\alpha}\Gamma^{\beta}_{\mu\nu} - \Gamma^{\alpha}_{\beta\nu}\Gamma^{\beta}_{\mu\alpha}, \tag{2.2}$$

where $\Gamma^{\alpha}_{\mu\nu,\alpha} \equiv \frac{\partial \Gamma_{\mu\nu,\alpha}}{\partial x^{\alpha}}$, and the Christoffel symbols are defined as

$$\Gamma^{\mu}_{\alpha\beta} = \frac{g^{\mu\nu}}{2}\left[g_{\alpha\nu,\beta} + g_{\beta\nu,\alpha} - g_{\alpha\beta,\nu}\right], \tag{2.3}$$

where again $g_{\alpha\nu,\beta} \equiv \frac{\partial g_{\alpha\nu,\beta}}{\partial x^{\alpha}}$. As is obvious from Eqs. (2.1)–(2.3), once we have expressions of the space-time metric $g_{\mu\nu}$ and the energy-momentum tensor $T_{\mu\nu}$, we can understand gravitational effects on particles in the Universe. Then, how can we determine them? Next, we focus on this question.

2.1.2 Cosmological principle

In the standard big-bang model, we impose a working hypothesis called "cosmological principle", which states that the Universe is isotropic and homogeneous on large scales.

This hypothesis is well consistent with precise observations of the cosmic microwave background and the large-scale structure of the Universe, and it seems to be a providence of nature. The spacetime metric which satisfies the cosmological principle is uniquely determined except for a choice of the space curvature K. It is called the Friedman-Lemaitre-Robertson-Walker (FLRW) metric [8–11]:

$$ds^2 = -c^2dt^2 + a(t)^2\left[\frac{dr^2}{1-Kr^2} + r^2\big(d\theta^2 + \sin^2\theta\, d\phi^2\big)\right], \tag{2.4}$$

where $K = +1, 0, -1$ respectively corresponds to the open, flat, and closed space-time of the Universe. Also, $a(t)$ is the scale factor, which measures the size of the Universe at a given time.

2.1.3 Friedman equation

Due to the requirement of the cosmological principle, *viz.* a homogeneity and isotropy of the Universe, together with the Lorentz invariance, an expression of the energy-momentum tensor of the Universe is uniquely determined as:

$$T_{\mu\nu} = p\, g_{\mu\nu} + (p+\rho)\, u_\mu u_\nu, \tag{2.5}$$

where u_μ is a four-velocity of the observer, and it can be written as $u_\mu = (1,0,0,0)$ in the comoving frame, in which the observer is at rest with respect to the expanding space-time. Also, p and ρ are the pressure and the energy density of the system, respectively. It should be stressed that the energy-momentum tensor in Eq. (2.5) has the same expression as the perfect fluid, but it is not an assumption by hand. It can be derived from the more fundamental requirements mentioned above.

The evolution equations of the expanding Universe are obtained by substituting the FLRW metric, Eq. (2.4), and the energy-momentum tensor, Eq. (2.5), into the Einstein field equation, Eq. (2.1):

$$H^2 \equiv \left(\frac{\dot{a}}{a}\right)^2 = \frac{8\pi G}{3}\rho - \frac{K}{a^2} + \frac{\Lambda}{3} = \frac{\rho}{3m_{\rm pl}^2} - \frac{K}{a^2} + \frac{\Lambda}{3}, \tag{2.6}$$

where $m_{\rm pl}(\equiv 1/\sqrt{8\pi G}) \sim 10^{18}$ GeV is the reduced Planck constant, and H is the Hubble parameter, which gives the expansion rate of the Universe at the time t. The Eq. (2.6) is called the Friedman equation, and it originates from the spatial part of the Einstein field equation, Eq. (2.1). The second term of Eq. (2.6) is due to the spacial curvature of the Universe. It is usually neglected because its contribution is expected to be very small after the inflation, which causes a rapid expansion of the Universe. In addition to the Friedman equation in Eq. (2.6), we can derive the following equation from the time component of the field equation Eq. (2.1):

$$\dot{\rho} + 3H(\rho + p) = 0\,, \tag{2.7}$$

which corresponds to the conservation of energy and momentum of the Universe.

Once we have an equation of state of the Universe, it is possible to obtain a thermodynamic evolution of the Universe by combining it with Eqs. (2.6)–(2.7). In the simple case where a specific particle component dominates the total energy density of the Universe, and hence the equation of state is nearly constant with time, we can analytically solve the equations. In general, particle components are roughly fallen into three types; namely

1. Relativistic particles - radiation,

2. Non-relativistic particles - matter,

3. Dark energy,

which are characterized by the equation of state parameters $w \equiv p/\rho = 1/3$, 0, and -1, respectively. [1] For a constant value of w, we can find the relation between the total energy density of the Universe ρ and the scale factor $a(t)$:

$$\rho \propto a^{-3(1+w)}\,, \tag{2.8}$$

which leads to

$$\rho \propto a^{-4} \quad \text{for} \quad w = 1/3, \tag{2.9}$$
$$\rho \propto a^{-3} \quad \text{for} \quad w = 0, \tag{2.10}$$
$$\rho = \text{const.} \quad \text{for} \quad w = -1. \tag{2.11}$$

Since the second term in the right-hand side of Eq. (2.6) is basically negligible, the scale factor $a(t)$ always increases with time. Thus, it follows from Eqs. (2.9)–(2.11) that radiation components dominate the energy density of the Universe in the early epoch when the scale factor is still relatively small. This stage of the Universe is called the radiation-dominated (R.D.) epoch. Afterwards, as the energy density of radiations rapidly decreases with time, matter contributions surpass it at a certain time, and the matter-dominated (M.D.) epoch realizes. Finally, total energy density is dominated by the dark energy, whose energy density is always constant, and the Universe enters into the dark-energy-dominated (D.E.D.) epoch. A schematic picture of the evolution of the total energy density of the Universe is shown in Figure 2.1, where possible existences of the inflation epoch and the early matter-dominated epoch realized by the inflaton oscillating at around its potential minimum, called oscillation epoch, are not depicted in the figure.

[1] The origin of dark energy is still unknown, but the recent observational results favor the equation of state parameter which is very close to unity [12]. Thus, the vacuum energy and the cosmological constant, both of which are characterized by $w = -1$, are favored as candidates of the dark energy. However, energy density of the vacuum energy derived from the standard model of particle physics $\rho_{\rm vac} \sim m_{\rm pl}^4 \sim 10^{76}$ GeV^4 is too large to explain the observational value of the dark energy $\rho_{\rm DE} \sim 3 \times 10^{-47}$ GeV^4, This problem is called "cosmological constant problem", and it is a long-standing problem in the fields of cosmology and particle physics.

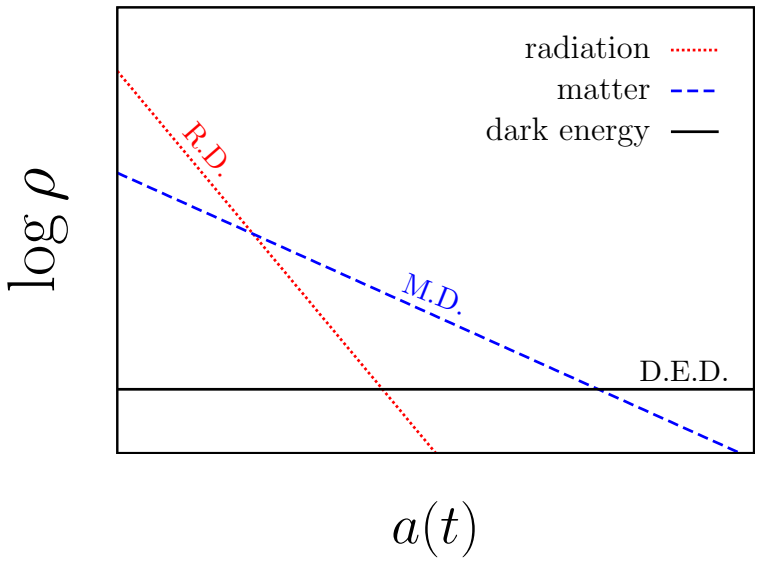

Figure 2.1: Schematic picture of the evolution of the energy density. The x-axis is the scale factor $a(t)$, and the y-axis is the energy density for each particle component, namely the red-dotted line is for radiation ($\rho_{\rm rad}$), the blue dashed line is for matter ($\rho_{\rm mat}$), and the black solid line is for the dark energy ($\rho_{\rm DE}$). The value in the x-(y-) axis increases towards the right (upward) direction.

In the same way, we can obtain the relation between the cosmic time t and the scale factor $a(t)$ by combining Eqs. (2.6) and (2.7):

$$a \propto t^{\frac{2}{3(1+w)}} \quad \text{for} \quad w \neq -1\,, \tag{2.12}$$
$$a \propto e^{Ht} \quad \text{for} \quad w = -1\,, \tag{2.13}$$

where we assume $\Lambda = 0$ and $K = 0$ for simplicity. The former condition is well satisfied in the early Universe where $\rho_{\rm rad}$ and $\rho_{\rm mat}$ are much larger than $\rho_{\rm DE}$, and the latter is also approximately true if we assume existence of the inflationary phase in the early Universe. Substituting the equation of state parameters w into Eq. (2.13), it follows from Eq. (2.13) that

$$a \propto t^{1/2} \quad \text{for R.D. epoch}\,, \tag{2.14}$$
$$a \propto t^{2/3} \quad \text{for M.D. epoch}\,, \tag{2.15}$$
$$a \propto e^{Ht} \quad \text{for D.E.D. epoch}\,. \tag{2.16}$$

Thus, the scale factor $a(t)$ is proportional to the power of time t in the R.D. and M.D. epochs, while it exponentially grows with time in the D.E.D. epoch as in the inflationary phase or in the current Universe.

2.2 Thermal history of the Universe

In this section, we briefly explain the thermal history of the Universe in the standard big-bang model. The interested readers can consult more comprehensive reviews in Refs. [5, 6, 13].

As we have seen in the previous section, the standard big-bang model is based on the standard model of particle physics. We summarize in Table 2.1 the particle content of the standard model together with its mass and internal degrees of freedom g_f. Since the time at which each cosmic event occurs is determined by the cosmic temperature rather than the cosmic time, the evolution of the Universe is called the "thermal history".

For concreteness, let us assume that the cosmic temperature far exceeds the Electroweak (EW) scale in the very early epoch of the Universe, *i.e.* $T >> \mathcal{O}(100)$ GeV. Then, all of the cosmic events can be summarized in Table 2.2. We refrain from explaining each event in detail, but we instead only refer to the important aspects of the thermal history in the following.

2.2.1 Effective number of relativistic species

At high temperature right after the inflation and the subsequent reheating (*i.e.* the 'Big-Bang'), the cosmic temperature is expected to be very high so that a large number of particle species are excited in the system since all of the standard model particles are ultra-relativistic in such epochs. Due to the cosmic expansion, the temperature gradually decreases, and some of the standard model particles become non-relativistic. Since the number- and energy densities of non-relativistic particles are Boltzmann-suppressed and fall exponentially with the temperature, their contributions decrease to be negligible. As some particle becomes non-relativistic, the energy and entropy of the particle are transferred to other particle species which are still relativistic. In this way, an effective number of relativistic species becomes smaller and smaller as the Universe expands and the temperature decreases. Figure 2.2 shows the evolution of the effective number of relativistic degrees of freedom g^*, which is defined as

$$\rho_{\rm rad} = \sum_i \rho_i = \frac{\pi^2}{30} g^*(T) T^4, \tag{2.17}$$

where $\rho_{\rm rad}$ is the total energy density of relativistic particles ('radiations'), and i runs over all relativistic species. As can be seen from Table 2.1, the most massive species in the standard model is the top quark, whose masses is $\simeq 173$ GeV. All the standard model particles are therefore excited at $T >> \mathcal{O}(100)$ GeV, and $g^* = 106.75$ in such epochs (see Figure 2.2). After the EW symmetry breaking at $T \sim 100$ GeV, the scalar- and vector bosons (namely $H^0, W^\pm$, and Z^0) together with the heavy quarks (t) disappear from the system at around temperatures corresponding to their masses. As the temperature further goes down, other species also start to decay or annihilate into lighter species, and their abundances become vanishing. The effective number of species is $g^* \sim 61.75$ just before

types	species & symbols	mass	g_f
Gauge bosons	photon: γ	0	2
	W boson: $W^{\pm}$	80 GeV	$2 \cdot 3 = 6$
	Z boson: Z^0	91 GeV	3
	gluon: g	0	$8 \cdot 2 = 16$
Scalar boson	Higgs boson: H^0	125 GeV	1
Lepton	electron: $e^{\pm}$	0.511 MeV	$2 \cdot 2 = 4$
	muon: $\mu^{\pm}$	106 MeV	
	tau lepton: $\tau^{\pm}$	1777 MeV	
	electron neutrino: ν_e, $\bar{\nu}_e$	< 0.6 eV	$2 \cdot 1 = 2$
	mu neutrino: ν_μ, $\bar{\nu}_\mu$	< 0.6 eV	
	tau neutrino: ν_τ, $\bar{\nu}_\tau$	< 0.6 eV	
Quark	up quark: u, $\bar{u}$	2 MeV	$2 \cdot 2 \cdot 3 = 12$
	down quark: d, $\bar{d}$	5 MeV	
	charm quark: c, $\bar{c}$	1 GeV	
	strange quark: s, $\bar{s}$	100 MeV	
	top quark: t, $\bar{t}$	173 GeV	
	bottom quark: b, $\bar{b}$	4 GeV	

Table 2.1: Particle content of the standard model of particle physics together with its mass and the internal degrees of freedom g_f [13].

the QCD transition occurs at $T \sim 150$ MeV, after which its value goes down to $g^* \sim 10.75$ due to the hadronization, in which quarks and gluons ('hadrons') are combined to form baryons or mesons. In this epoch, the thermal bath of the cosmic plasma consists of only three particle species, namely photons, electrons, and neutrinos ($g^* = g_\gamma + \frac{7}{8}g_e + \frac{7}{8}g_\nu = 2 + \frac{7}{8} \cdot 2 \cdot 2 + \frac{7}{8} \cdot 2 \cdot 3 = 10.75$ where the factor $\frac{7}{8}$ is a correction for Fermions). Among them, $e^{\pm}$ have relatively large mass $m_e \simeq 0.5$ MeV and start to annihilate at the corresponding temperature, slightly later than the neutrino decoupling at $T \sim 1$ MeV. Therefore, for $T \lesssim 0.5$ MeV there remains photon- and neutrino degrees of freedom, and thereby $g^* = g_\gamma + \frac{7}{8}g_\nu = 2 + \frac{7}{8} \cdot 2 \cdot 3 \cdot \left(\frac{4}{11}\right)^{4/3} \simeq 3.38$, where the factor $\left(\frac{4}{11}\right)^{4/3}$ originates from

cosmic event	temperature T	time t
Inflation	?	?
Reheating	?	?
Baryogenesis	?	?
EW transition	100 GeV	20 ps
QCD transition	150 MeV	20 μs
Neutrino decoupling	1 MeV	1 s
e^-e^+ annihilation	500 keV	6 s
Big-Bang nucleosynthesis	100 keV	3 min
Matter-radiation equality	0.75 eV	60 kyr
Recombination	0.26–0.33 eV	260–380 kyr
Photon decoupling	0.23–0.28 eV	380 kyr
Reionization	2.6–7.0 meV	100–400 Myr
Dark energy-matter equality	0.33 meV	9 Gyr
Present	0.24 meV	13.8 Gyr

Table 2.2: Standard picture of the thermal history of the Universe and cosmic events in the standard big-bang model [13]. The epochs in which the inflation, the reheating, and the baryogenesis take place are still unknown.

the dilution of neutrinos due to the e^-e^+ annihilation, as explained later in Section 3.2.1.

As can be seen in Eq. (2.6), the expansion rate H depends on the total energy density of the Universe, and it can be written as $H^2 = \frac{\rho}{3m_{\rm pl}^2} + \cdots = \frac{\pi^2}{90} g^* T^4 / m_{\rm pl}^2 + \cdots$. Therefore, the evolution of g^* determines the relation between the cosmic temperature T and the expansion rate H, and this gives the reason that g^* is an important parameter for understanding the thermal history of the Universe.

2.2.2 Freeze-out of particles

If all of the particles are always in equilibrium with other particles until today, number densities of non-relativistic particles would be strongly suppressed by the Boltzmann factor and almost completely vanishing in the current Universe. In contrast, there are non-negligible abundances of heavy particles such as nuclear elements (and possibly the dark

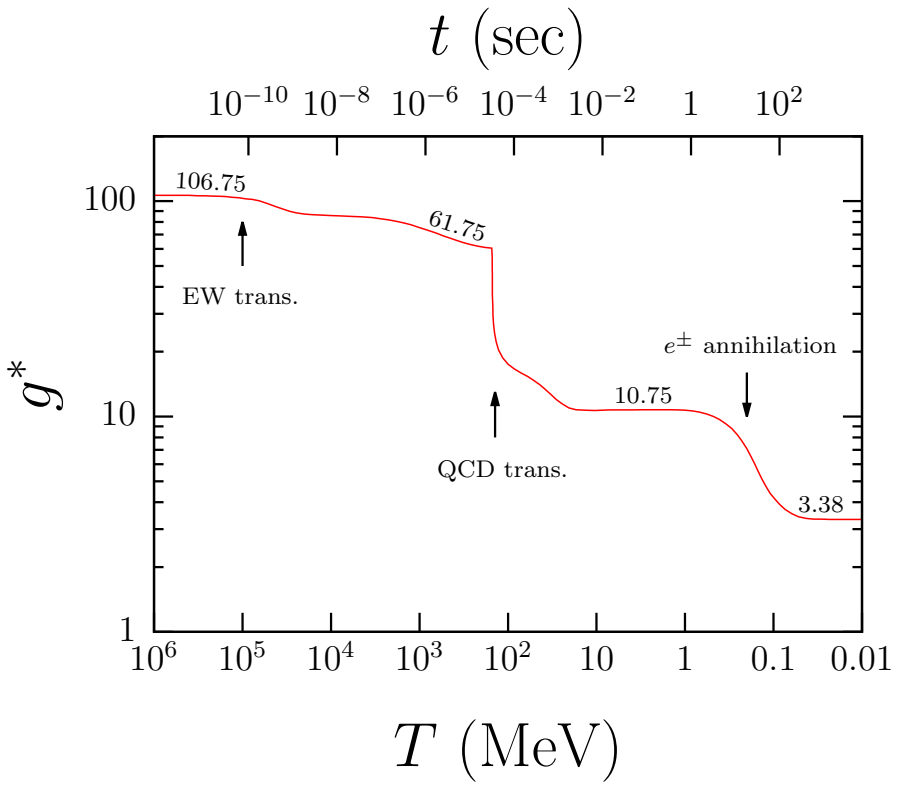

Figure 2.2: Evolution of the effective number of relativistic degrees of freedom g^* as functions of the cosmic temperature and time [13].

matter) around us. That is because the creation- and destruction of some particle species effectively finish ('decouple') and afterwards the particle abundance is conserved during the expansion of the Universe. This is called the 'freeze-out' of the particle, and it happens when the Hubble expansion rate becomes equal to the reaction rates for creation- and destruction processes relevant to the particle, $\Gamma \sim H$, which is often called the 'Gamow's criterion'.

Figure 2.3 shows a schematic picture for the evolution of the number density per unit volume ($V = a^3$). Since the freeze-out often takes place when the temperature is of the same order as the particle mass, it is convenient to follow the evolution as a function of m/T. As in Figure 2.3, the destruction processes decouple at *freeze-out temperature*, and there survives a larger abundance than the equilibrium one, which is proportional to $\exp[-m/T]$.

2.2.3 Boltzmann equation

In the previous subsection, we have seen the freeze-out temperature of particles T_f is determined by the simple criterion, $\Gamma(T_f) = H(T_f)$. This gives a rough estimate of the

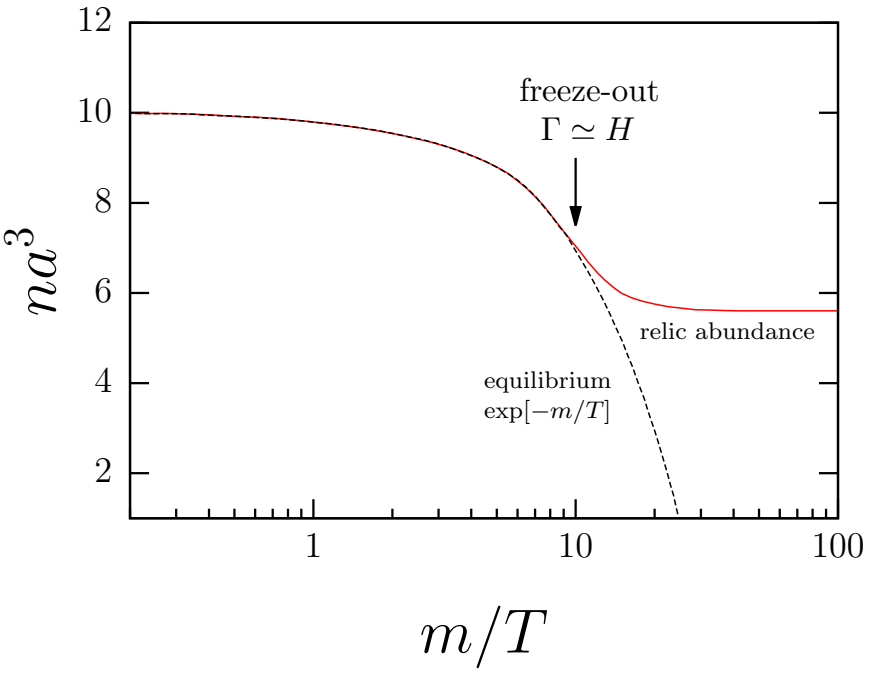

Figure 2.3: Schematic picture of the evolution of the comoving number density of particles na^3. The actual- and equilibrium abundances are shown by the red solid- and the black dashed lines, respectively [13].

relic abundance if and only if the particle under consideration is in equilibrium with the rest of the cosmic plasma, and therefore the reaction rate Γ can be expressed as a simple analytical function of the cosmic temperature T. Otherwise, it is essential to solve the Boltzmann equation to describe the evolution beyond equilibrium:

$$\frac{df}{dt} = C[f, t], \tag{2.18}$$

which describes an evolution of a distribution function f, *i.e.* the number density in a unit phase-space volume, of some particle as functions of its momentum and the cosmic time. The term in the right-hand side of Eq. (2.18), $C[f(p,t),t]$, is the collision term of the particle, whose concrete expressions depend on the specific collisional processes under consideration, and it can be calculated from scattering matrix elements, $\mathcal{M}_{\alpha\beta}$, where α and β are arbitrary initial- and final states of the collisional process. If we write the distribution function as functions of its three momentum $\boldsymbol{p}$, space coordinates $\boldsymbol{x}$, and the cosmic time t, $f = f(\boldsymbol{x}, \boldsymbol{p}, t)$, the total derivative of the distribution function with respect to time (*i.e.* the left-hand side) in Eq. (2.18) can be rewritten as follows:

$$\left(\frac{\partial}{\partial t} + \dot{\boldsymbol{x}} \cdot \frac{\partial}{\partial \boldsymbol{x}} + \dot{\boldsymbol{p}} \cdot \frac{\partial}{\partial \boldsymbol{p}}\right) f(\boldsymbol{x}, \boldsymbol{p}, t) = C[f(\boldsymbol{x}, \boldsymbol{p}, t), t], \tag{2.19}$$

where $\dot{\boldsymbol{x}}$ and $\dot{\boldsymbol{p}}$ are time derivatives of the space coordinate and the three-momentum with respect to time, respectively. Since we assume the homogeneity and the isotropy of the Universe, the distribution function does not depend on the space coordinate $\boldsymbol{x}$ and the direction of momentum $\boldsymbol{p}$. In the current situation, we can therefore write $f = f(p,t)$, where $p\,(\equiv |\boldsymbol{p}|)$ is the absolute momentum. Finally, we find

$$\frac{df(p,t)}{dt} = \left(\frac{\partial}{\partial t} - Hp\frac{\partial}{\partial p}\right) f(p,t) = C[f(p,t),t], \tag{2.20}$$

which is the Boltzmann equation for the homogeneous and the isotropic Universe. In the derivation of Eq. (2.20), we have used the relation, $\partial p/\partial t = -Hp$. We note that the term proportional to the Hubble rate H stems from the redshift of momentum due to the cosmic expansion, $p \propto a^{-1}$.

Chapter 3

Standard Big-Bang Nucleosynthesis

In this chapter, we review the standard theory of the big-bang nucleosynthesis, the standard big-bang nucleosynthesis (SBBN), and an inference of the primordial abundances of light elements from observations. The knowledge of this chapter is useful for understanding our results in Chapters 5 and 6, where we discuss observational constraints on the reheating temperature and sterile neutrinos imposed by BBN, respectively.

3.1 Overview

The big-bang nucleosynthesis is a sequence of nuclear reaction processes responsible for the production of light elements such as Hydrogen (H), Deuterium (D), Tritium (T), Helium (^{3}He, ^{4}He), Lithium (^{6}Li, ^{7}Li), and Beryllium (^{7}Be), which took place at around $t \sim 0.01$–100 sec ($T \sim 10$–0.1 MeV). Among these, T and ^{7}Be are later converted into ^{3}He and ^{7}Li through beta decays with their half-lives of 12.32 yrs and 53.2 days, respectively. Thus, the primordial abundance of ^{3}He (^{7}Li) is given by a sum of ^{3}He and T abundances (^{7}Li and ^{7}Be abundances) right after the end of BBN $\sim \mathcal{O}(10^4$–$10^5)$ sec.

Elements heavier than carbon (^{12}C), *i.e.* elements with the mass number $A \geq 12$, are only slightly produced in the nucleosynthesis although these elements are more stable than the elements with $A < 12$. This is because there is no stable nucleus with $A = 5$ and 8, and the density of particles in the BBN epoch is so sparse that the three-body reaction $3\,\alpha \rightarrow {}^{12}$C ("Triple alpha process") is inefficient, where we label ^{4}He as α. Such heavier elements present in our surroundings such as C, O, or Fe are mainly synthesized in massive stars through *e.g.* s- and r processes. On the ground that there is no way to accurately estimate the primordial abundances of such "rare" elements from observations for the time being, we are not able to compare theoretical- and observational abundances of such heavier elements. Therefore, we only consider the production of light elements with $A < 8$ listed above.

In this thesis, light element abundances are denoted by

$$\mathrm{D/H} = n_{\mathrm{D}}/n_{\mathrm{H}}, \tag{3.1}$$
$$^3\mathrm{He/D} = n_{^3\mathrm{He}}/n_{\mathrm{D}}, \tag{3.2}$$
$$Y_p = \rho_{^4\mathrm{He}}/\rho_B, \tag{3.3}$$
$$^6\mathrm{Li/H} = n_{^6\mathrm{Li}}/n_{\mathrm{H}}, \tag{3.4}$$
$$^7\mathrm{Li/H} = n_{^7\mathrm{Li}}/n_{\mathrm{H}}, \tag{3.5}$$

where n_i is the number density of nuclear species i, $\rho_{^4\mathrm{He}}$ is the mass density of ^{4}He, and ρ_B is the energy density of baryons, *i.e.* $\rho_B \approx m_N (n_B - \bar{n}_B)$ where $m_N \approx 931.5$ MeV is the atomic mass unit, whereas n_B and $\bar{n}_B$ are the number densities of baryons and anti-baryons, respectively.

As can be seen later in this chapter, the theory of SBBN is in excellent agreement with "inferred" primordial abundances of light elements, and therefore a comparison between predicted- and inferred abundances of light elements provides a powerful tool to test the theory of cosmology and its underlying theory, *viz.* the theory of gravity and particle physics.

History of research

The notion of the big-bang nucleosynthesis (also called primordial nucleosynthesis) dates back to the paper written by G. Gamow in 1946 [14], and the first calculation of the ^{4}He abundance was given by R. Alpher, H. Bethe, and G. Gamow in their well-known paper [15], which is also known as "$\alpha\beta\gamma$ theory" named after their names. Afterwards, F. Hoyle and R. Tayler provided an analytical estimate of the ^{4}He abundance in 1964 [16]. Then, P. Peebles [17] and R. Wagoner, W. Fowler, A. William, and F. Hoyle [18] developed a detailed code for the numerical calculation of the nucleosynthesis in 1996 and 1967, respectively. Particularly, the latter considered a complicated network of nuclear reactions, and not only the calculation of ^{4}He abundance but also that of other light element abundances were available. Henceforth, some other authors also independently offered nucleosynthesis codes [19–21], and among them the updated version of the Wagoner's code [21] has become the standard code of BBN. Since then, nuclear reaction rates of the nucleosynthesis have been updated every several years, and finite temperate effects and Coulomb corrections were subsequently incorporated into the code [22]. More recently, the Wagoner's code has been greatly improved by L. Kawano [23], and it turned out to be more user-friendly, much faster, and more documented, which facilitated other researchers in working in this field of study. Still, new nucleosynthesis codes have been offered. Among them, famous ones are PArthENoPE code [24], and AlterBBN code [25], which enable researchers to easily consider some non-standard scenario of cosmology and particle physics.

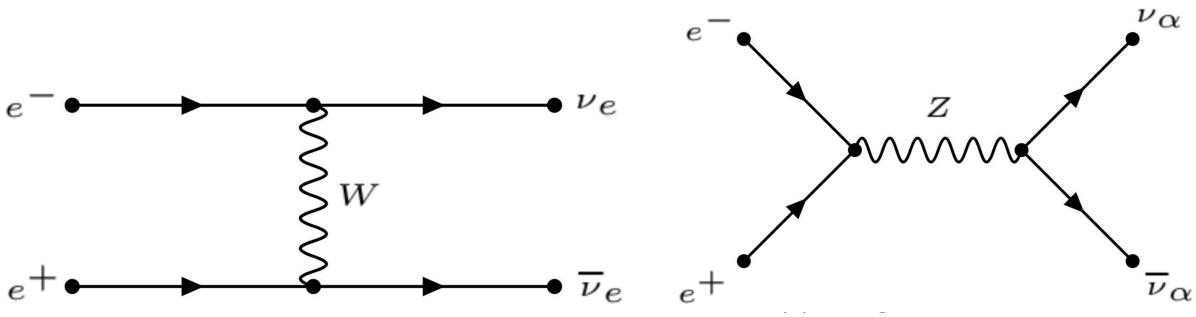

Figure 3.1: Feynman diagrams of charged-current (left) and neutral-current (right) interactions of neutrinos with electrons mediated by W- and Z bosons, respectively. The process in the left panel applies only to electron neutrinos ν_e, while the right panel applies to all flavors of neutrinos, namely $\nu_\alpha = \nu_e, \nu_\mu$, and ν_τ.

3.2 Theory of standard big-bang nucleosynthesis

In this section, we explain the big-bang nucleosynthesis from the theoretical point of view, especially focusing on the theory of SBBN predicted in the framework of the standard big-bang model. First, we introduce a thermal history around the epoch of BBN, and then we discuss an analytical estimation of the primordial abundances of light elements.

3.2.1 Thermal history around BBN

The production of light elements occurs around $t \sim 0.01$–100 sec and $T \sim 10$ MeV to 0.1 MeV, which corresponds to the era well within the radiation-dominated (R.D.) epoch as described in Chapter 2. In this epoch, only three particle species are relevant to the dynamics of the Universe, namely photons γ, electrons e^-, neutrinos ν since an abundance of any particle with its mass larger than the cosmic temperature T is non-relativistic and therefore its contribution to the total energy density and pressure is strongly suppressed compared to radiation components listed above. Thus, neutrons and protons, which constitute nuclear elements, are almost irrelevant to the dynamics of the Universe at least in this case. In particular, there are mainly two important events around the BBN epoch:

1. Neutrino decoupling,

2. Electron annihilation.

In the following, we briefly describe them.

Neutrino decoupling

In the standard big-bang model, we believe that all particles are thermalized by thermal- and non-thermal production during- or after the reheating, and all particles are assumed to be in thermal- and chemical equilibrium at the 'initial' time. In contrast, neutrinos only interact through weak interaction in the process, *e.g.* $e^- + e^+ \to \nu_\alpha + \bar{\nu}_\alpha$, $e^\pm + \nu_\alpha \to e^\pm + \bar{\nu}_\alpha$, and $\nu_\alpha + \nu_\beta \to \nu_\alpha + \nu_\beta$ where α and $\beta (\neq \alpha)$ are flavors of neutrinos, *viz.* e, μ, or τ. The reaction rate of them is approximately written as

$$\Gamma_\nu = n_e \sigma_\nu |v| \simeq G_F^2 T^5, \tag{3.6}$$

where n_e is the electron number density, $|v|$ is the absolute velocity of neutrinos, G_F is the Fermi coupling constant, and we have approximated the electron number density and the cross-section of weak interaction to their thermal ones, *i.e.* $n_e \simeq T^3$ and $\sigma_\nu \mapsto \langle \sigma_\nu \rangle \simeq G_F T^2$. As can be seen from Eq. (3.6), the reaction rate depends on the number density of electrons, whose mass is $m_e \simeq 0.511$ MeV. Thus, when the cosmic temperature drops as the same order or below the mass of electrons, their number density rapidly decreases from $n_e \simeq T^3$ to $n_e \simeq (m_e T)^{3/2} e^{-m_e/T}$ due to the exponential suppression by the Boltzmann factor, leading to a fast drop of the reaction rate of neutrinos. Since a physical process whose reaction rate is much smaller than the Hubble expansion rate is no longer effective and it "decouples" from the system, neutrinos cannot be in equilibrium if $\Gamma_\nu << H$. For neutrinos, the temperature of the decoupling can be estimated as

$$\frac{\Gamma_\nu}{H} \simeq \frac{G_F^2 T^5}{T^2/m_{\rm pl}^2} \simeq \left(\frac{T}{1\,{\rm MeV}} \right)^3, \tag{3.7}$$

where we have used $H = \sqrt{8\pi G \rho/3} = \sqrt{g^* T^4/m_{\rm pl}^2} \simeq T^2/m_{\rm pl}$ with the relativistic degrees of freedom g^* defined by

$$\rho = \frac{\pi^2}{30} g^* T^4, \tag{3.8}$$

where ρ is the total energy density, and it can be approximately written as

$$\rho \simeq \rho_{\rm rad} \simeq \rho_\gamma + \rho_e + \rho_\nu = \frac{\pi^2}{30} g_\gamma T^4 + \frac{7}{8} \left(\frac{\pi^2}{30} g_e T^4 \right) + \frac{7}{8} \left(\frac{\pi^2}{30} g_\nu T^4 \right). \tag{3.9}$$

around the epoch of BBN, *i.e.* $T \sim 10$ MeV to 0.1 MeV. In the above, $\rho_{\rm rad}$ is the energy density of radiations, ρ_i and g_i are the energy density and the statistical degrees of freedom of a particle i $(= \gamma, e, \text{and } \nu)$, respectively. Note that the factor 7/8 in the expressions of ρ_e and ρ_ν accounts for the difference between Fermi- and Bose statistics. From Eq. (3.9), we can see that $g^* \simeq g_\gamma + \frac{7}{8} g_e + \frac{7}{8} g_\nu = 2 + 7/2 + 21/4 = 10.75$, which justifies the approximation used in Eq. (3.7). Therefore, neutrinos decouple at around $T \sim \mathcal{O}(1)$ MeV.

The decoupling temperature of electron neutrino ν_e is in fact smaller than that of μ neutrino ν_μ and τ neutrinos ν_τ. This is because electron neutrinos additionally react with electrons through charged-current interactions (left panel in Figure 3.1) along with neutral-current ones (right panel in Figure 3.1), and thereby $\Gamma_{\nu_e} > \Gamma_{\nu_x}$ where $\nu_x = \nu_\mu$ or ν_τ.

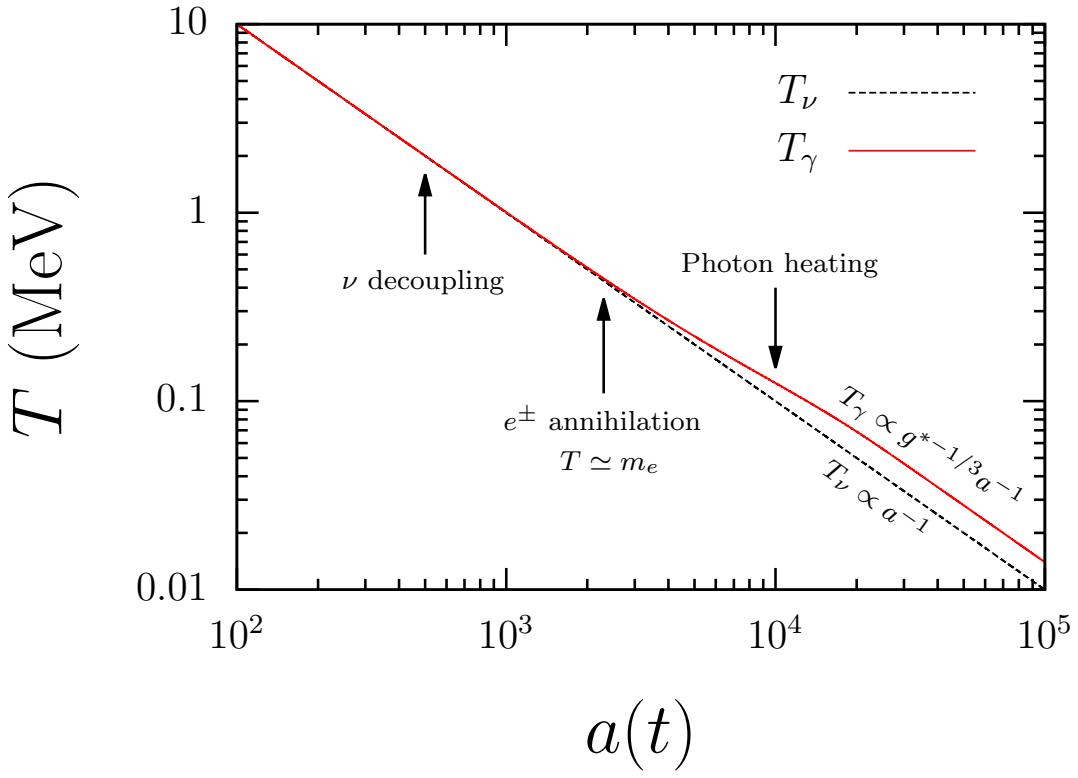

Figure 3.2: Evolution of the temperatures of neutrinos and photons as a function of the scale factor $a(t)$ [13]. The scale factor is normalized by its value at high temperature $T(>> m_e)$. The black dashed line is the neutrino temperature T_ν, and the red solid line is the photon temperature T_γ. In the figure, both photons and neutrinos are assumed to be thermalized at the initial time.

Electron annihilation

For the cosmic temperature below 1 MeV, neutrinos are almost completely decoupled from the thermal bath consisting of electromagnetic particles, namely photons, and electrons. In this epoch, neutrinos still contribute to the total energy density and thereby affecting background dynamics, but they are irrelevant to the evolution of the thermal bath.

When the temperature of photons and electrons drop to the same order or below the electron mass $m_e(\simeq 0.511$ MeV), the annihilation of electrons and positrons begins. Since neutrinos already decouple at this time, their energy and entropy are entirely transferred to photons, and the photon temperature T_γ becomes slightly greater than the neutrino temperature T_ν. On the ground that the cosmic expansion is an adiabatic process, the total entropy in the Universe is conserved, which means

$$(s_\gamma + s_e)\, a^3_{\rm before} = s_\gamma\, a^3_{\rm after}, \tag{3.10}$$

where $a_{\rm before}$ and $a_{\rm after}$ are the scale factor long before- and after the electron annihilation, and s_γ and s_e are the entropy density of photons and electrons, respectively:

$$s_\gamma = \frac{2\pi^2}{45} g^*_{s,\gamma} T_\gamma^3 \ , \quad s_e = \frac{7}{8}\left(\frac{2\pi^2}{45} g^*_{s,e} T_e^3\right), \tag{3.11}$$

where the temperature of electrons T_e is equal to the photon temperature T_γ since they continue to interact with each other even after the electron annihilation. [1] Assuming that the electron-positron annihilation instantaneously starts and finishes at $T_\gamma = m_e$, Eq. (3.11) results in

$$\frac{T_\gamma}{T_\nu} = \left(\frac{11}{4}\right)^{\frac{1}{3}} \simeq 1.40, \tag{3.12}$$

for $T_\gamma << m_e$.

It is important to accurately follow the evolution of the energy density of radiation components, namely photons, electrons, and neutrinos, by taking into account this temperature difference between photons and neutrinos due to the electron annihilation. This is because, as explained in the next section, neutrino abundances and the total energy density of the Universe are main factors which controls the neutron-to-proton ('np') ratio n/p just before the nucleosynthesis, and it is closely related to the final abundances of light elements.

Figure 3.2 shows the evolution of the photon temperature T_γ and the neutrino temperature T_ν as functions of the scale factor $a(t)$, where assume neutrinos are completely thermalized before the neutrino decoupling or the electron annihilation. The result is obtained by simultaneously solving the Friedman equation Eq. (2.6) and the conservation equation of energy and momentum Eq. (2.7) with an input of the thermal energy density and pressure of each particle.

3.2.2 Neutron-to-proton ratio

In the above, we have seen that the neutrino decoupling and the electron annihilation are the most important events in the epoch around BBN. This is because these events are closely related to the freeze-out value of the neutron-to-proton ratio before the nucleosynthesis, which is one of the decisive parameters for the final abundances of light elements. In this subsection, we therefore focus on the evolution of the neutron-to-proton ratio.

[1] Photons and electrons no longer interact with each other after the Compton scattering $\gamma + e^- \to \gamma + e^-$ decouples in the epoch of recombination $T_\gamma \sim 1$ eV.

Inter-converting processes between neutrons and protons

In the early Universe, the neutron-to-proton ratio is regulated by the following processes mediated by the weak interaction:

$$n + \nu_e \leftrightarrow p + e^-, \tag{3.13a}$$
$$n + e^+ \leftrightarrow p + \bar{\nu}_e, \tag{3.13b}$$
$$n \leftrightarrow p + e^- + \bar{\nu}_e. \tag{3.13c}$$

The general form of their reaction rates can be written as a nine dimensional integral with respect to momentum:

$$\Gamma_{12\to34} = \frac{1}{2E_1}\sum\int \frac{d^3p_2}{2E_2(2\pi)^3}\frac{d^3p_3}{2E_3(2\pi)^3}\frac{d^3p_4}{2E_4(2\pi)^3} \times (2\pi)^4\delta^{(4)}\left(p_1+p_2-p_3-p_4\right) S\langle|M|^2_{12\to34}\rangle F\left(p_1,p_2,p_3,p_4\right), \tag{3.14}$$

for the processes (3.13a) and (3.13b), and

$$\Gamma_{1\to234} = \frac{1}{2E_1}\sum\int \frac{d^3p_2}{2E_2(2\pi)^3}\frac{d^3p_3}{2E_3(2\pi)^3}\frac{d^3p_4}{2E_4(2\pi)^3} \times (2\pi)^4\delta^{(4)}\left(p_1-p_2-p_3-p_4\right) S\langle|M|^2_{1\to234}\rangle F\left(p_1,p_2,p_3,p_4\right), \tag{3.15}$$

for the process (3.13c), where S is the symmetric factor which gives a factor of 1/2 if particles in the initial- and final states are identical, $\delta^{(4)}\left(p_1+p_2-p_3-p_4\right)$ is the 4D Dirac delta function corresponding to the conservation of four-momentum, $\langle|M|^2\rangle$ is the spin-averaged and summed square of the nuclear matrix element, and $F\left(p_1,p_2,p_3,p_4\right)$ is the phase space factor including Pauli blocking effects, which can be expressed as

$$F\left(p_1,p_2,p_3,p_4\right) \equiv f(p_1)f(p_2)\left(1-f(p_3)\right)\left(1-f(p_4)\right), \tag{3.16}$$

for the processes (3.13a) and (3.13b), and

$$F\left(p_1,p_2,p_3,p_4\right) \equiv \ f(p_1)\left(1-f(p_2)\right)\left(1-f(p_3)\right)\left(1-f(p_4)\right), \tag{3.17}$$

for the process (3.13c). Some of the above integrals can be analytically performed (see *e.g.* Refs. [6, 26, 27]):

$$\Gamma_{n+\nu_e\to p+e^-} = K\int_q^\infty d\epsilon \frac{\epsilon\sqrt{\epsilon^2-1}(\epsilon-q)^2}{\{1+\exp(-\epsilon z)\}[1+\exp\{(\epsilon-q)z_\nu\}]}, \tag{3.18a}$$
$$\Gamma_{n+e^+\to p+\bar{\nu}_e} = K\int_1^\infty d\epsilon \frac{\epsilon\sqrt{\epsilon^2-1}(\epsilon+q)^2}{\{1+\exp(\epsilon z)\}[1+\exp\{-(\epsilon+q)z_\nu\}]}, \tag{3.18b}$$
$$\Gamma_{p+\bar{\nu}_e\to e^++n} = K\int_1^\infty d\epsilon \frac{\epsilon\sqrt{\epsilon^2-1}(\epsilon+q)^2}{\{1+\exp(-\epsilon z)\}[1+\exp\{(\epsilon+q)z_\nu\}]}, \tag{3.18c}$$
$$\Gamma_{p+e^-\to n+\nu_e} = K\int_q^\infty d\epsilon \frac{\epsilon\sqrt{\epsilon^2-1}(\epsilon-q)^2}{\{1+\exp(\epsilon z)\}[1+\exp\{-(\epsilon-q)z_\nu\}]}, \tag{3.18d}$$
$$\Gamma_{n\to p+e^-+\bar{\nu}_e} = K\int_1^q d\epsilon \frac{\epsilon\sqrt{\epsilon^2-1}(\epsilon-q)^2}{\{1+\exp(-\epsilon z)\}[1+\exp\{(\epsilon-q)z_\nu\}]}, \tag{3.18e}$$
$$\Gamma_{p+e^-+\bar{\nu}_e\to n} = K\int_1^q d\epsilon \frac{\epsilon\sqrt{\epsilon^2-1}(\epsilon-q)^2}{\{1+\exp(\epsilon z)\}[1+\exp\{-(\epsilon-q)z_\nu\}]}, \tag{3.18f}$$

where $\epsilon = E_e/m_e, z = m_e/T_e, z_\nu = m_e/T_{\nu_e}$ and $q = Q/m_e$ where $Q = m_n - m_p \simeq 1.293$ MeV is the mass difference between neutrons and protons, where we have assumed that electron neutrinos are thermalized and have a temperature of T_{ν_e}. Also, $K = \frac{G_F^2}{2\pi^3}\left(1+3g_A^2\right)m_e^5$ with the axial vector coupling of nucleons g_A is a constant factor, which is related to the free neutron lifetime τ_n:

$$\tau_n = \Gamma^{-1}_{n\to pe\nu} \tag{3.19}$$

$$= \left[\frac{G_F^2}{2\pi^3}\left(1+3g_A^2\right)m_e^5\Lambda\right]^{-1} \simeq K^{-1}, \tag{3.20}$$

where $\Lambda \equiv \int_1^q d\epsilon\epsilon(\epsilon-q)^2\left(\epsilon^2-1\right)^{1/2} \simeq 1.636$. The total reaction rates of the reactions Γ_{np} is given by $\Gamma_{np} = \Gamma_{n\to p} + \Gamma_{p\to n}$, where

$$\Gamma_{n\to p} = \Gamma_{n+\nu_e\to p+e^-} + \Gamma_{n+e^+\to p+\nu_e} + \Gamma_{n\to p+e^-+\nu_e}, \tag{3.21}$$

$$\Gamma_{p\to n} = \Gamma_{p+e^-\to n+\nu_e} + \Gamma_{p+\nu_e\to e^++n} + \Gamma_{p+e^-+\nu_e\to n}. \tag{3.22}$$

Focusing on $\Gamma_{p+e^-\to n+\nu_e}$, it takes values at high- and low temperatures below [6]:

$$\Gamma_{pe^-\to n+\nu_e} \sim \begin{cases} \tau_n^{-1}\left(T/m_e\right)^3\exp(-Q/T) & \text{for } T << Q \\ \frac{\pi}{60}\pi\left(1+3g_A^2\right)G_F^2T^5 \simeq G_F^2T^5 & \text{for } T >> Q \end{cases}. \tag{3.23}$$

Initial and freeze-out values of n/p ratio

Since the Hubble rate can be written as $H \simeq T^2/m_{\rm pl}$ (see Eq. (3.7)), reaction rates of the exchange reactions between protons and neutrons are much larger than the Hubble expansion rate of the Universe at high temperatures, and the opposite is true at low temperatures, as can be seen from Eq. (3.23). By equating the Hubble rate and the exchange rates, we obtain the temperature at which the exchange process decouples, the "freeze-out temperature" T_f: [2]

$$\frac{\Gamma_{pe^-\to n+\nu_e}}{H} \sim \frac{G_F^2T^5}{T^2/m_{\rm pl}} \sim \left(\frac{T}{0.7\text{ MeV}}\right), \tag{3.24}$$

which means $T_f \sim 0.7$ MeV. The evolution of the $n-p$ exchange rate and the Hubble rate obtained by numerical computations is shown in Figure 3.3, where we can see that the Hubble rate H actually exceeds the $n-p$ exchange rate $\Gamma_{pe^-\to n+\nu_e}$ at around $T \sim 0.7$ MeV. Therefore, all of the process (3.13a)–(3.13b) are both in *kinetic*- and *chemical* equilibrium

[2]The free neutron decay (3.13c) continues even after the processes (3.13a)–(3.13b) decouple, and it further decreases the neutron-to-proton ratio before the nucleosynthesis of light elements. However, the freeze-out value of the neutron-to-proton ratio is more important because the neutron decay is still inert just when the nucleosynthesis proceed rapidly at around $T \simeq 0.08$ MeV and $t \simeq 200$ sec [28].

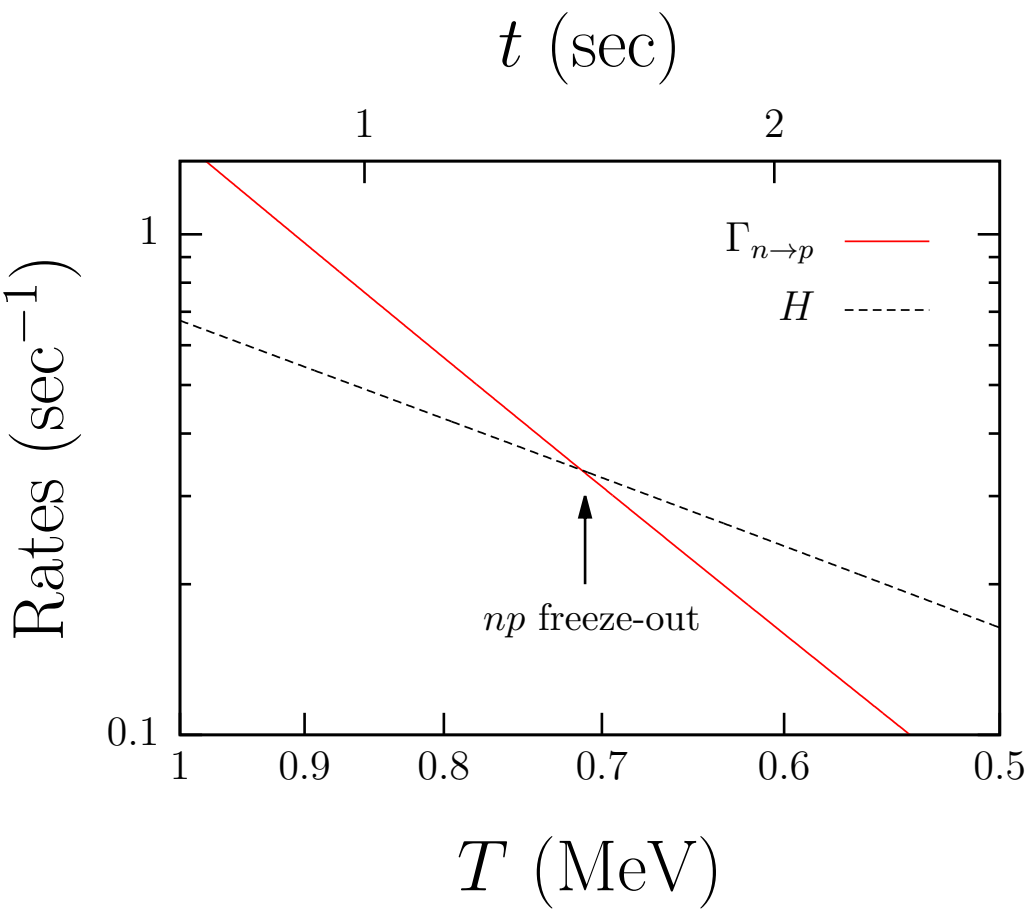

Figure 3.3: Evolution of the forward reaction rate of the np exchanging processes and the Hubble expansion rate as functions of the cosmic temperature and time. The temperature at which the Hubble rate exceeds the forward rate corresponds to the freeze-out temperature T_f for the weak processes. The red solid line is the forward rate $\Gamma_{n\to p}$, and the black dashed line is the Hubble rate H. The baryon-to-photon ratio, the neutron lifetime, and the effective number of neutrino species are fixed to be $\eta_B = 6.0 \times 10^{-10}$, $\tau_n = 880$ sec, and $N_{\rm eff} = 3.046$, respectively.

for $T(\equiv T_\gamma = T_e = T_\nu) >> T_f$. In such cases, the number density for non-relativistic neutrons and protons can be written as

$$n_i = g_i \left(\frac{m_i T}{2\pi}\right)^{3/2} \exp\left(\frac{-m_i + \mu_i}{T}\right), \tag{3.25}$$

where $i = n, p$ and g_i is the statistical degrees of freedom. In addition, the sum of chemical potentials of initial- and final states are equal:

$$\mu_n + \mu_{\nu_e} = \mu_p + \mu_e. \tag{3.26}$$

Therefore, neutron-to-proton ratio $n/p \equiv n_n/n_p$ can be given by

$$n/p \simeq \exp[-\{(m_n - m_p) + (-\mu_n + \mu_p)\}/T] = \exp[-\{Q + (\mu_e - \mu_{\nu_e})\}/T]. \tag{3.27}$$

The contribution of chemical potentials μ_e and μ_{ν_e} on the neutron-to-proton ratio is normally assumed to be negligible. This is because the order of μ_e/T and μ_{ν_e}/T are expected to be the same as the baryon-to-photon ratio $\sim \mathcal{O}(10^{-10})$ due to the charge neutrality of the Universe and the standard mechanism of the baryogenesis, *i.e.* the sphaleron process. If this is true, the neutron-to-proton ratio has the following values at high- ($T >> Q$) and low ($T \sim T_f$) temperatures:

$$n/p \simeq \exp[-Q/T] \tag{3.28}$$

$$\simeq \begin{cases} 1 & \text{for } T >> Q \\ 1/6 & \text{for } T \sim T_f \end{cases}, \tag{3.29}$$

which implies that there is the same number of neutrons and protons, $n_n = n_p$, at high temperature. Since neutrons spontaneously decay into protons and light species with its lifetime $\tau_{\rm n} = 880.2 \pm 1.0$ sec (68% C.L.) [29], the freeze-out value of the neutron-to-proton ratio $(n/p)_f = \exp[-Q/T_f] \simeq 1/6$ further decreases down to $\simeq 1/7$ [28]. The temperature evolution of the n/p ratio obtained by numerical computations is shown in Figure 3.4, where it can be seen that the n/p ratio actually deviates from the prediction under equilibrium, *i.e.* $n/p \sim \exp[-Q/T]$. The rapid decrease of the n/p ratio at $T \simeq 0.1$ MeV is due to the onset of the nucleosynthesis.

3.2.3 Predicted abundances of light elements

Predictions of the light element abundances as a result of BBN have been provided both in analytical- and numerical ways. First, we discuss analytical calculations and then we describe numerical analyses. More thorough discussions can be found in *e.g.* Refs. [6,30,31] (see Refs. [28, 32] for more recent papers).

Analytical estimation

The analytical estimate of the light element abundances can be obtained by viewing the nucleosynthesis as a series of departures from "*nuclear statistical equilibrium*" (NSE) of nuclear reactions. The most simple case was discussed in Subsection 3.2.2, where we described how the freeze-out value of the neutron-to-proton ratio is determined. The purpose of this section is to express the production abundances of light elements in terms of the neutron- and proton abundances so that we can obtain an analytical picture of BBN.

When *all* of the nuclear reactions which are responsible for production or destruction of some nuclear species are much faster than the expansion rate of the Universe, the nuclear species are in both *kinetic* and *chemical* equilibrium, and in this case the nuclear species are

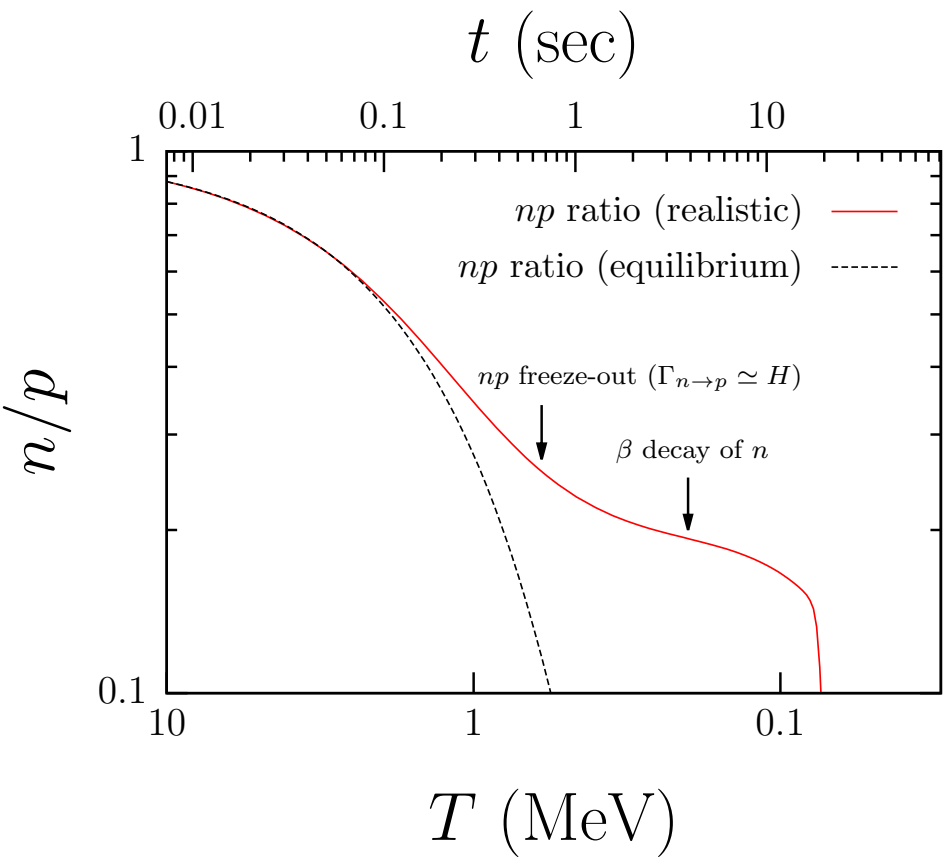

Figure 3.4: Evolution of the neutron-to-proton ratio n/p as functions of the comic temperature T and time t [28]. The black dashed line is the equilibrium value $\simeq \exp[-Q/T]$, and the red solid line is the realistic n/p ratio obtained by numerical computations. The baryon-to-photon ratio, the neutron lifetime, and the effective number of neutrino species are fixed to be $\eta_B = 6.0 \times 10^{-10}$, $\tau_n = 880$ sec, and $N_{\rm eff} = 3.046$, respectively.

under the nuclear statistical equilibrium. In the same way as for neutrons and protons, in *kinetic equilibrium*, the number density of non-relativistic nuclear species with the atomic number Z and the mass number A can be written as

$$n_A = g_A \left(\frac{m_A T}{2\pi}\right)^{\frac{3}{2}} \exp\left(\frac{\mu_A - m_A}{T}\right), \tag{3.30}$$

where m_A, μ_A, and g_A are the mass, the chemical potential, and the statistical degrees of freedom of the nuclear species, respectively. If *chemical equilibrium* is also attained, the chemical potential μ_A is related to those of neutrons (μ_n) and protons (μ_p):

$$\mu_A = Z\mu_p + (A - Z)\mu_n. \tag{3.31}$$

${}^{A}Z$	B_A	g_A
^{2}H (D)	2.22 MeV	3
^{3}H (T)	8.48 MeV	2
^{3}He	7.72 MeV	2
^{4}He	28.3 MeV	1
^{12}C	92.2 MeV	1

Table 3.1: The binding energy B_A and the statistical degrees of freedom g_A of the nuclear species of each nuclear species ${}^{A}Z$ with the mass number A and the atomic number Z.

Then, by using Eq. (3.31) we can rewrite the exponential part of Eq. (3.30) in terms of the number density of neutrons and protons as follows:

$$\exp\left(\mu_A/T\right) = \exp\left[\left(Z\mu_p + (A-Z)\mu_n\right)/T\right] \tag{3.32}$$

$$\simeq n_p^Z n_n^{A-Z} \left(\frac{2\pi}{m_N T}\right)^{\frac{3}{2}A} 2^{-A} \exp\left[\left(Zm_p + (A-Z)m_n\right)/T\right], \tag{3.33}$$

where we have used Eq. (3.30) for neutrons and protons and approximated the masses of neutrons and protons to the atomic mass unit $m_N \equiv m_{^{12}C} \approx 931.5$ MeV, neglecting the small mass difference (~ 1.3 MeV) between protons and neutrons, in the second line. As a result, NSE abundance for some nuclear species n_A can be expressed as

$$n_A \simeq g_A A^{\frac{3}{2}} 2^{-A} \left(\frac{2\pi}{m_N T}\right)^{\frac{3(A-1)}{2}} n_p^Z n_n^{A-Z} \exp\left(\frac{B_A}{T}\right), \tag{3.34}$$

where B_A is the binding energy of the nuclear species, which is given by

$$B_A = Zm_p + (A-Z)m_n - m_A. \tag{3.35}$$

The binding energies of light elements B_A are summarized in Table 3.1. Since the number density of particles is diluted by the cosmic expansion and is proportional to $a(t)^{-3}$, it is convenient to express the abundance of nuclear elements in terms of comoving quantities, which is constant in the expanding Universe. We normalize the number density of nuclear elements with the mass abundance of baryons X_b,

$$\begin{aligned} X_b &\equiv m_N n_N \\ &= m_N(n_n + n_p + \sum_A A n_A), \end{aligned} \tag{3.36}$$

and label normalized quantities as X_A:

$$\begin{aligned} X_A &\equiv \frac{m_A n_A}{X_b} \\ &= \frac{A n_A}{n_N}, \end{aligned} \tag{3.37}$$

where n_n and n_p are respectively the number densities of free neutrons and free protons, and n_A is the number density of nuclear species A. The mass abundance of nuclear elements defined as Eq. (3.37) satisfies $\sum_A X_A = 1$ by definition. Using Eqs. (3.34) and (3.37), we find

$$X_A = \lambda(A) \left(\frac{T}{m_N}\right)^{\frac{3(A-1)}{2}} \eta_B^{A-1} X_p^Z X_n^{A-Z} \exp\left(\frac{B_A}{T}\right), \tag{3.38}$$

where $\lambda(A) \equiv g_A \zeta(3)^{A-1} \pi^{\frac{(1-A)}{2}} 2^{\frac{(3A-1)}{2}} A^{\frac{5}{2}}$ is a constant prefactor depending on the mass number A, and η_B is the baryon-to-photon ratio defined as

$$\eta_B \equiv \frac{n_N}{n_\gamma} \simeq 2.68 \times 10^{-8} \left(\Omega_B h^2\right), \tag{3.39}$$

where $\Omega_B \equiv \rho_B/\rho_c$, with the energy density of baryons ρ_B and the critical energy density of the Universe $\rho_c \equiv 3H^2/8\pi G$, is the density parameter of baryons. The value of η_B is known to be $\simeq 6.13 \times 10^{-10}$ from CMB observations [3]. Also, h is the reduced Hubble parameter defined by $H = 100h$ km/sec $\cdot$ Mpc^{-1}.

In order to discuss the production abundance in more detail, let us consider the system consisting of n, p, D, T, ^{3}He, and ^{4}He, neglecting heavier elements than ^{4}He. At high temperature ($\gtrsim 10$ MeV), NSE is attained for these nuclear species, and their mass abundances obey Eq. (3.38):

$$X_{\rm D} = 16.3 \left(\frac{T}{m_N}\right)^{3/2} \eta_B \exp\left(\frac{B_{\rm D}}{T}\right) X_n X_p, \tag{3.40}$$

$$X_{\rm T} = 57.4 \left(\frac{T}{m_N}\right)^{3} \eta_B^2 \exp\left(\frac{B_{\rm T}}{T}\right) X_n^2 X_p, \tag{3.41}$$

$$X_{^3{\rm He}} = 57.4 \left(\frac{T}{m_N}\right)^{3} \eta_B^2 \exp\left(\frac{B_{^3{\rm He}}}{T}\right) X_n X_p^2, \tag{3.42}$$

$$X_{^4{\rm He}} = 113 \left(\frac{T}{m_N}\right)^{9/2} \eta_B^3 \exp\left(\frac{B_{^4{\rm He}}}{T}\right) X_n^2 X_p^2. \tag{3.43}$$

and therefore

$$X_n + X_p + X_{\rm D} + X_{\rm T} + X_{^3{\rm He}} + X_{^4{\rm He}} = 1. \tag{3.44}$$

In the following, we firstly explain important nuclear reactions responsible for the production of light elements with the mass number $A < 4$.

As discussed before, three-body nuclear reactions decouple much earlier than the BBN epoch, and therefore they cannot contribute to the nucleosynthesis. Among two-body reactions, the following ones are especially important for the production of each nuclear species [30].

· Deuterium (D):

$$n + p \to {\rm D} + \gamma \tag{3.45}$$

· Mass-3 elements (T, ^{3}He):

$$\mathrm{D} + \mathrm{D} \rightarrow \mathrm{T} + p,\ {}^3\mathrm{He} + n \tag{3.46}$$
$${}^3\mathrm{He} + n \rightarrow \mathrm{T} + p \tag{3.47}$$
$$\mathrm{D} + p \rightarrow {}^3\mathrm{He} + \gamma \tag{3.48}$$

· Helium 4 (^{4}He):

$$\mathrm{T} + \mathrm{D} \rightarrow {}^4\mathrm{He} + n \tag{3.49}$$
$${}^3\mathrm{He} + \mathrm{D} \rightarrow {}^4\mathrm{He} + p \tag{3.50}$$

Then we discuss NSE abundances for a typical temperature in the following:

· At high temperature: $T \sim 10$ MeV, $t \sim 0.01$ sec

As we have seen in the previous subsection, if the temperature is at or above 10 MeV, all of the above elements are in NSE, and neutrons and protons have the same abundances, *i.e.* $X_n \simeq X_p \simeq 0.5$. Thus, for the baryon-to-photon ratio $\eta_B = 6 \times 10^{-10}$, mass abundances of light elements can be estimated by Eqs. (3.40)–(3.43); $X_{\mathrm{D}} \sim 10^{-11}, X_{\mathrm{T}} \sim 10^{-24}, X_{^3\mathrm{He}} \sim 10^{-24}$, and $X_{^4\mathrm{He}} \sim 10^{-34}$. As can be seen from these NSE values, an only tiny number of light elements are produced during high-temperature epochs.

· At around the freeze-out temperature of n/p ratio: $T \sim 1$ MeV, $t \sim 1$ sec

As estimated in Eq. (3.24) the freeze-out temperature of the neutron-to-proton ratio is $T_f \sim 1$ MeV and the freeze-out value is $(n/p)_f \sim 1/6$. Therefore, mass abundances of neutrons and protons are $X_n \simeq 1/6$ and $X_p \simeq 5/6$, respectively. Thus, for the baryon-to-photon ratio $\eta_B = 6 \times 10^{-10}$, mass abundances of light elements are $X_{\mathrm{D}} \sim 10^{-11}, X_{\mathrm{T}} \sim 10^{-24}, X_{^3\mathrm{He}} \sim 10^{-24}$, and $X_{^4\mathrm{He}} \sim 10^{-34}$. It would be surprising that the nucleosynthesis of light elements is still inert although the temperature is already lower than the binding energies of light elements B_A (see Table 3.1). This is due to the enormous amount of entropy in the Universe s compared to the baryon number density n_N, which can be seen from the observational value of the baryon-to-photon ratio $\eta_B \equiv \frac{n_N}{n_\gamma} \sim \frac{n_N}{s} \sim 10^{-10}$ the prefactors proportional to the power of η_B in Eqs. (3.40)–(3.43) prevent the light elements from being produced abundantly and delay the nucleosynthesis. In other words, a lot of photons contribute to the inverse reaction of $n + p \rightarrow \mathrm{D} + \gamma$ and immediately destroy D produced in the forward reaction. This kind of situations that delayed the formation of nuclear elements with $A \geq 3$ is called "*Deuterium bottleneck*".

· At low temperature: $T \sim 0.1$ MeV, $t \sim 100$ sec

When the temperature drops below 1 MeV, some of the nuclear species fall out of their NSE tracks as the creation- and destruction reactions gradually decouple. Specifically,

neutrons and protons finish interacting at around $T \simeq 0.8$ MeV, ^{4}He leaves from NSE at around $T \simeq 0.6$ MeV, the interaction between the mass-3 elements (T, ^{3}He) stops at around $T \simeq 0.08$ MeV, and the creation of mass-3 elements (T, ^{3}He) from D becomes ineffective at around $T \simeq 0.07$ MeV. Therefore, we cannot estimate the nuclear abundance by relying on the NSE condition in this epoch. In the case where nuclear elements fall out of the NSE tracks, but their total creation- and destruction (*i.e.* the forward and the inverse) rates are equal, the nuclear elements are still in the "*quasi-static equilibrium*" (QSE). The nuclear elements are actually in QSE after D becomes abundantly produced so that $X_D \simeq X_n \simeq X_p$, and after the most of D are converted into ^{4}He, which is most stable among light elements with $A < 12$. This happens at around $T \simeq 0.08$ MeV right after all nuclear elements fall out of the NSE tracks. Since all neutrons are consumed to synthesize ^{4}He which consists of two neutrons and protons, the final mass abundance of ^{4}He can be estimated as

$$X_{^4\mathrm{He}} = \frac{m_{^4\mathrm{He}} n_{^4\mathrm{He}}}{m_N n_N} \simeq \left.\frac{4m_N(n_n/2)}{m_N(n_p+n_n)}\right|_{T=T_{\mathrm{bbn}}} = \frac{2(n/p)_{\mathrm{bbn}}}{1+(n/p)_{\mathrm{bbn}}} \simeq 0.25, \tag{3.51}$$

where $(n/p)_{\mathrm{bbn}} \simeq 1/7$ is the SBBN value of the neutron-to-proton ratio just before rapid production of ^{4}He occurs, and $T_{\mathrm{bbn}} \simeq 0.08$ MeV is the temperature at that time. In the above, we have approximated $m_{^4\mathrm{He}} \simeq 4m_N$, neglecting the binding energy of ^{4}He.

The abundance of other nuclear species cannot be simply estimated as for ^{4}He. We need another way to analytically obtain their abundances. The nuclear abundances are in general followed by the equation:

$$\frac{dY_i}{dt} = \sum_{k,l} Y_k Y_l [kl] - \sum_j Y_i Y_j [ij], \tag{3.52}$$

where $Y_i \equiv X_i/A$, whereas $[ij]$ and $[kl]$ are destroying- and creating rates for i, respectively. After ^{4}He is rapidly produced at $T \sim 0.08$ MeV, the nuclear elements fall into QSE. Since the condition of QSE means that the left-hand side of Eq. (3.52) is vanishing, the abundance of a nuclear species i is governed by the following equation at this stage:

$$Y_i(T) = \frac{\sum_{k,l} Y_k Y_l [kl]}{\sum_j Y_j [ij]}. \tag{3.53}$$

Thus, once we obtain temperature-dependent destroying- and creating rates for nuclear species i, we can obtain a nuclear abundance Y_i as a function of the cosmic temperature T. The formula of the QSE abundance Eq. (3.53) holds until all of the destroying rates for i decouple. The final abundance of a nuclear species i, $Y_{i,\,\mathrm{final}}$, is determined by the freeze-out temperature of the decoupling T_f as follows:

$$\begin{aligned} Y_{i,\,\mathrm{final}} &= Y_i(T_f) \\ &= \frac{\sum_{k,l} Y_k\,(T_f)\, Y_l\,(T_f)\, [kl]\,(T_f)}{\sum_j Y_j\,(T_f)\, [ij]\,(T_f)}. \end{aligned} \tag{3.54}$$

${}^{A}Z$	T_f
H (D)	0.03 MeV
^{3}H (T)	0.009 MeV
^{3}He	0.03 MeV
^{4}He	0.06 MeV
^{7}Li	0.02 MeV
^{7}Be	0.02 MeV

Table 3.2: The freeze-out temperature T_f of each nuclear species ${}^{A}Z$ with the mass number A and the atomic number Z.

The freeze-out temperature of nuclear species is obtained in Ref. [30], and we summarize them in Table 3.2. The detailed analysis of the QSE abundance was performed in Ref. [31], and they obtained $Y_{\rm D} \simeq 0.7 \times 10^{-4}, Y_{\rm T} \simeq 0.37 \times 10^{-6}, Y_{^3{\rm He}} \simeq 0.2 \times 10^{-4}, Y_{^7{\rm Li}} \simeq 0.7 \times 10^{-10}$, and $Y_{^7{\rm Be}} \simeq 0.1 \times 10^{-10}$ for $\Omega_B h^2 = 0.01$ with the density parameter of baryons $\Omega_B \equiv \rho_B/\rho_c$ where ρ_B is the energy density of baryons and $\rho_c \equiv 3H^2/8\pi G$ is the critical density of the Universe. [3]

Numerical computation

In the previous subsection, we explain to what extent we can analytically understand the final abundances of light elements. Next, we focus on numerical computations of BBN for comparing its result with inferred values of light elements from astronomical observations.

Figure 3.5 shows the evolution of light element abundances in the SBBN. The results are obtained by numerically solving the Boltzmann equation for nuclear elements, Eq. (3.52), together with the Friedman equation, Eq. (2.6), and the conservation equation of energy and momentum, Eq. (2.7), with the Kawano BBN code [23]. As is obvious from Eq. (3.34), nuclear abundances depend on the value of the baryon-to-photon ratio η_B. Also, nuclear abundances are very sensitive to the freeze-out value of the neutron-to-photon ratio, and therefore to the neutron lifetime τ_n as described before. In Figure 3.5, these input parameters are fixed to be $\eta_B = 6.0 \times 10^{-10}$ and $\tau_n = 880$ sec, respectively. As for the nuclear abundances, in the figure they are expressed in terms of the number density of the nuclear species n_i divided by that of free protons n_p, which is related to Y_i by the relation:

$$Y_i = n_i/n_N = n_i/(n_n + n_p) = n_i/n_p. \tag{3.56}$$

[3] The density parameter of baryons is uniquely related to the baryon-to-photon ratio $\eta_B \equiv n_N/n_\gamma$ through the relation:

$$\eta_B \simeq 2.8 \times 10^{-8} \Omega_B h^2, \tag{3.55}$$

which can be applied after the electron annihilation as η_B is expected to be constant without any entropy injection. By using this relation, we can see that $\Omega_B h^2 = 0.01$ corresponds to $\eta_B \simeq 2.8 \times 10^{-10}$, which is slightly smaller than the Planck value $\Omega_B h^2 = 0.0224$ (*i.e.* $\eta_B \simeq 6.13 \times 10^{-10}$) [3].

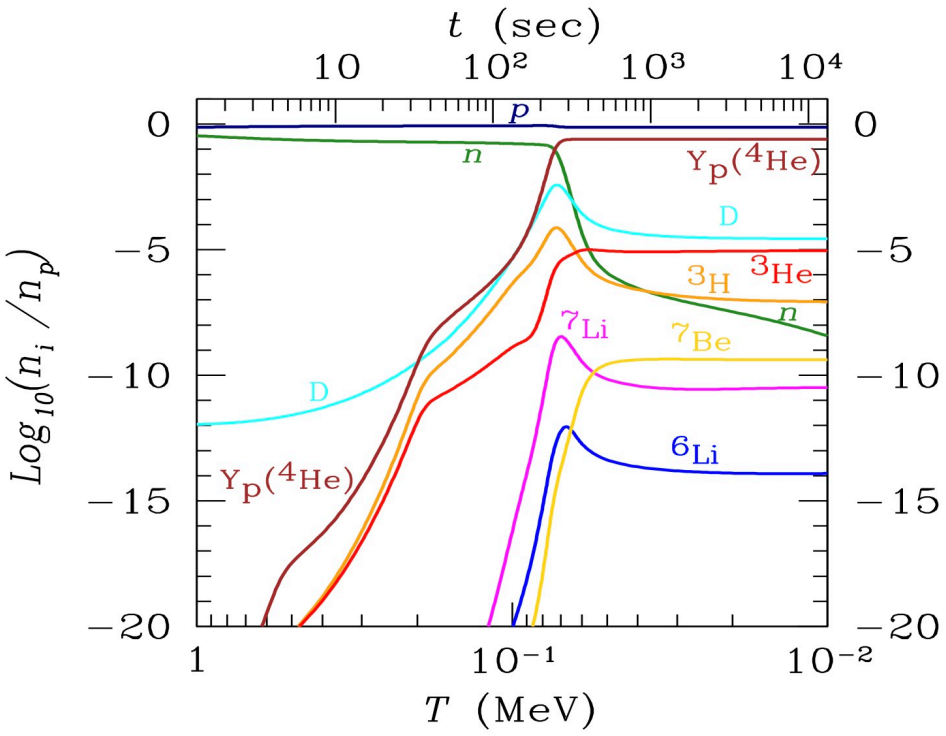

Figure 3.5: Evolution of light element abundances in the standard big-bang nucleosynthesis (SBBN). The baryon-to-photon ratio, the neutron lifetime, and the effective number of neutrino species are fixed to be $\eta_B = 6.0 \times 10^{-10}$, $\tau_n = 880$ sec, and $N_{\rm eff} = 3.046$, respectively. [Figure courtesy of K. Kohri.]

Also, we note that Y_p in the figure is not the abundance of protons, but the mass abundance of ^{4}He, *i.e.* $Y_p = m_{^4\mathrm{He}} n_{^4\mathrm{He}} / n_N$. It can be seen in Figure 3.5 that all elements are started to be created at around $T \sim 0.1$ MeV, where the deuterium bottleneck finally opens. Furthermore, it seems that the analytical estimation of light element abundances is true within an order of magnitude.

3.3 Observation of light elements

In the previous section, we discuss a theoretical prediction of light element abundances and explain analytical- and numerical estimation of them. In this section, we focus on an observational inference of primordial abundances of light elements. Since the main purpose of this thesis is to obtain an observational constraint on parameters of theoretical models, we only describe observed abundances of D, ^{4}He, which are generally used for a

comparison of theoretical predictions with observational determinations. [4]

3.3.1 Deuterium (D)

As a theoretical prediction of the deuterium abundance D/H ($\equiv n_{\rm D}/n_{\rm H}$) strongly depends on the baryon-to-photon ratio η_B in the BBN epoch, it has been used for a direct comparison between theoretical- and observational values to provide constraints on η_B or other parameters in the theoretical models. The determination of η_B from D/H has become available after the systematic uncertainty in the observed abundance of D/H significantly decreased by observing Lyman series absorption lines of neutral hydrogen and deuterium in quasar absorption systems at high redshift. Particularly, by selecting a handful of systems, Cooke et al. [39] significantly reduced the systematic uncertainties in the data, and their analysis provided a very accurate measurement of primordial abundance:

$$\left(\frac{\rm D}{\rm H}\right) = (2.53 \pm 0.04) \times 10^{-5} \quad (68\%\,\text{C.L.}). \tag{3.57}$$

Surprisingly, the uncertainty of D/H is only 2% at 1-σ level, and this enables us to make use of BBN as a powerful probe of physics in the early epoch. In a more recent analysis of Ref. [40], they took into account 13 measurements of D/H which focus on the absorption system at the redshift $z = 2.504$ towards Q1009+2956. Consequently, taking a weighted mean of the 13 analyses on D/H, they estimated the primordial value of D/H:

$$\left(\frac{\rm D}{\rm H}\right) = (2.545 \pm 0.025) \times 10^{-5} \quad (68\%\,\text{C.L.})\,, \tag{3.58}$$

which gives an accuracy of 1% level. In our studies explained in Chapters 5 and 6, we use this reported value of D/H to discuss observational constraints.

3.3.2 Helium 4 (^{4}He)

The ^{4}He abundance has long been used to constrain some non-standard physics/scenarios of cosmology or particle physics. This is because the ^{4}He abundance is very sensitive to

[4] As for the other elements, an observable amount of ^{3}He should be produced in the BBN epoch, but its primordial abundance is very difficult to infer because we cannot detect hyperfine emission lines from ^{3}He gas cloud at high redshift, which is expected to contain information of the primordial value. Also, authors in Ref. [33] claimed that they detected the ^{6}Li abundance, but it was later shown to be an artifact due to systematic errors in astrophysical origin [34–37]. As the reported abundance of ^{6}Li was much larger than the prediction of SBBN, an inconsistency between the theoretical- and the observed abundances of ^{6}Li was called the "Lithium-6 problem". Finally, there is a long-standing problem called the "Lithium-7 problem" in the primordial abundance of ^{7}Li that the theoretical prediction of the ^{7}Li abundance is almost three times greater than that inferred from observations (for a detailed recent review of the lithium probe, see [38]). Several possible solutions have been proposed in terms of particle physics, nuclear physics, and astronomy, but it has not solved yet. Since one generally refrains from using the ^{7}Li abundance to obtain constraints on some physics from BBN. Therefore, we do not discuss the ^{7}Li abundance, either.

the freeze-out value of the neutron-to-photon ratio and the freeze-out temperature of the interconverting processes between protons and neutrons, which are easy to be modified if we assume theories other than the standard big-bang cosmology, *viz.* the general relativity and the standard model of particle physics.

The primordial abundance of ^{4}He is determined by observing emission lines of H and ^{4}He from metal-poor stars in extra-galactic HII regions, where an ionized gas of hydrogen abundantly exists. Since ^{4}He is known to be produced by nuclear fusions in massive stars together with heavier elements, in order to infer the primordial abundance of ^{4}He produced in BBN, we must perform a regression of the ^{4}He abundance with respect to a metallicity of stars. However, the observational determination of the ^{4}He abundance has been annoyed with large systematic uncertainties relevant to the property of stars, which have prevented from obtaining an accuracy better than 1% level.

In Ref. [41], Y. Izotov et al. reported a new determination of the ^{4}He abundance by using the emission lines in an infrared band as well as a visible band obtained from observations of 45 extra-galactic HII regions. As a result, they obtained

$$Y_p = 0.2551 \pm 0.0022. \quad (68\%\,\text{C.L.})\,, \tag{3.59}$$

Recently, in the paper by E. Aver et al. [42], they have reanalyzed their original dataset by taking into account newly available observations of metal-poor stars with a near-infrared line λ10830 [41] and significantly reduced the uncertainties. Consequently, they obtained the regression:

$$Y_p = 0.2449 \pm 0.0040 + (78.9 \pm 43.3)\text{O/H} \quad (68\%\,\text{C.L.})\,, \tag{3.60}$$

where O/H is the oxygen abundance. Since the primordial abundance of ^{4}He can be obtained from regression to zero metallicity (*i.e.* O/H $\to 0$), they found

$$Y_p = 0.2449 \pm 0.0040 \quad (68\%\,\text{C.L.})\,, \tag{3.61}$$

which means the uncertainty is less than 2% at 68% C.L. In our studies, we adopt this reported value in Eq. (3.61).

3.4 Theoretical predictions and observed abundances

In the previous sections, we have seen how light element abundances are estimated in terms of theories and observations. In this section, we compare those results to get knowledge of implications and consequences.

Figure 3.6 shows the theoretical- and observed abundances of light elements as a function of the baryon-to-photon ratio η_B, which is the only free parameter of BBN. The figure tells us that the theoretical predictions and the observed abundances of D/H and Y_p (for $N_\nu = 3$) are well in agreement with each other, and the inferred value of η_B obtained from BBN is consistent with the independent constraint from CMB, $\eta_B = (6.11 \pm 0.08) \times 10^{-10}$

(2-σ C.L.). We note that $N_{\rm eff} = 3.046$ is the standard assumption of the big-bang cosmology, and cases of $N_\nu = 2$ and 4 are also shown for reference. The point is that the theoretical prediction of Y_p increases as η_B increases, while the opposite is true for D/H. The dependence of Y_p and D/H on η_B can be understood as follows. As can be seen from Eq. (3.40), the deuterium bottleneck opens earlier for large η_B. Thus, there remain more neutrons than for small η_B because fewer neutrons decay before the nucleosynthesis. Since the ^{4}He abundance is an increasing function of the n/p ratio, large η_B leads to large Y_p. As for D/H, the final abundance of D is determined by the freeze-out temperature of the destroying processes for D as explained in Subsection 3.2.3 (see Eq. (3.54)). The main processes responsible for the deuterium destruction are DD- and DT reactions in Eqs. (3.46) and (3.49). The reaction rates of these destroying processes are proportional to η_B, and more D are therefore burned into mass-3 (T, ^{3}He) or mass-4 (^{4}He) elements for large η_B. For this reason, there remains a smaller abundance of D for large η_B, and vice versa.

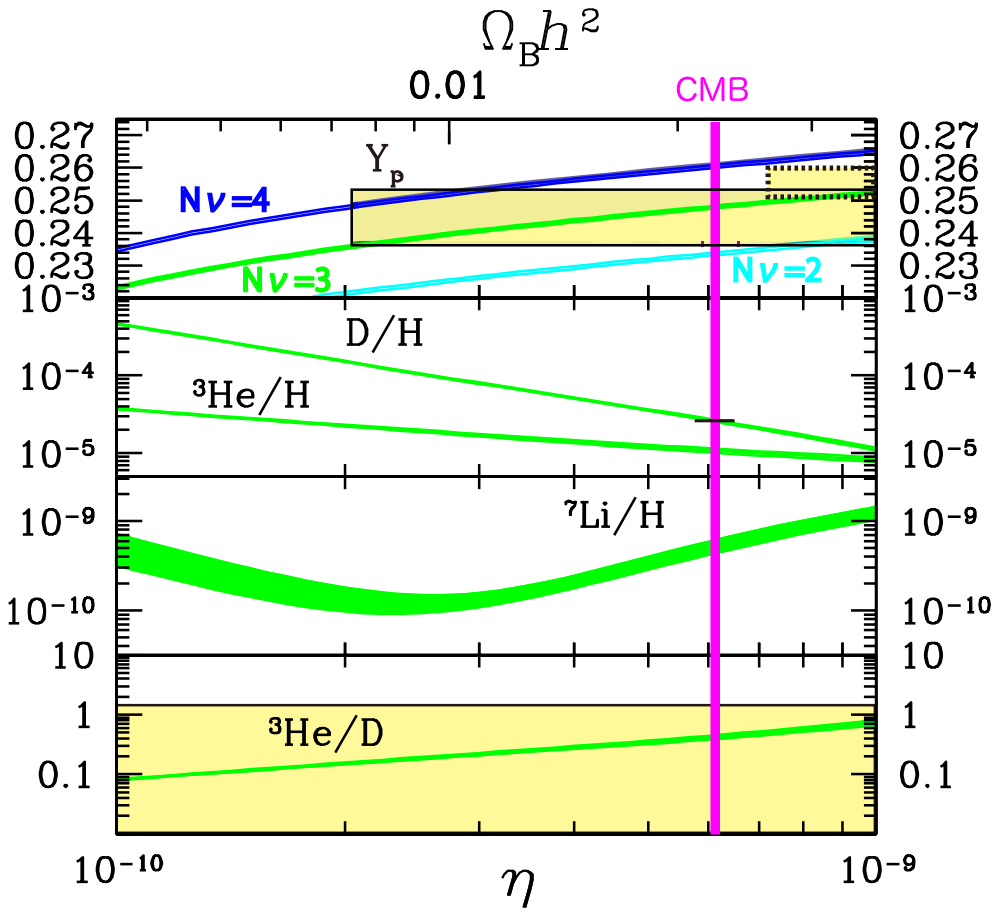

Figure 3.6: Theoretical predictions and observed abundances of light element abundances as functions of the baryon-to-photon ratio η_B and the density parameter of baryons Ω_B. The pink vertical band shows the CMB bound on the baryon-to-photon ratio at 2-σ level $\eta_B = (6.11 \pm 0.08) \times 10^{-10}$, reported in Ref. [43]. The yellow boxes are the observational values with 2-σ uncertainties. In the top panel, the boxes surrounded by the dashed- and solid lines are observational abundances of Y_p given in Eqs. (3.59) and (3.61), respectively. The theoretical abundances are plotted by the green bands. The ^{4}He abundance is depicted for three values of the effective number of neutrino species, namely $N_\nu = 2$, 3, and 4 (from the bottom to the top). [Figure courtesy of K. Kohri.]

Chapter 4

Neutrino oscillation

In this chapter, we review the formalism of neutrino oscillation for understanding its effect on observables in the early Universe.

Neutrino oscillation is a phenomenon that the flavor of neutrino changes to another flavor during its flight in a vacuum or in a medium. The theoretical study of neutrino oscillation was started in 1954 when B. Pontecorvo predicted the flavor transition between neutrinos and anti-neutrinos in analogy with the theory of oscillation between K_0 and $\overline{K_0}$ states [44]. After that, Z. Maki, M. Nakagawa, S. Sakata are inspired by the paper, and they proposed that different flavors of neutrinos periodically oscillate with each other if each flavor of neutrinos has different masses [45]. At the same time, R. Davis and other researchers in the HOMESTAKE experiment found that the observed flux of solar neutrinos (*i.e.* electron neutrinos) is much smaller than the theoretical prediction [46]. Similar results were also obtained by KamiokaNDE [47] and SNO [48] experiments, and the problem of neutrino flux ("solar neutrino problem") was verified. Therefore, many researchers made an effort to solve it in view of astrophysics or particle physics. It was not until 1998 that the theory of neutrino oscillation was confirmed. Researchers of Super-Kamiokande [49] experiment found that there is also a deficit in a flux of atmospheric neutrinos (*i.e.* μ-type neutrinos), and both problems of the solar and atmospheric neutrino fluxes can be simultaneously explained by the theory of neutrino oscillation [50].

Today, neutrinos are known to play an important role in a certain astrophysical environment or some epoch of the thermal history of the Universe. Thus, it would be nearly essential for those who are interested in these fields of research to take into account the effect of neutrino oscillation.

As is explained later in this chapter, a behavior of neutrino oscillation is known to be modified if neutrinos propagate in a matter. Therefore, we firstly explain neutrino oscillation in a vacuum in Section 4.1. Afterwards, we discuss the matter effects on neutrino oscillation in Section 4.2. Also, if we are interested in the effect of neutrino oscillation on thermodynamic variables of neutrinos in a statistical ensemble, we cannot straightforwardly apply the formalism in Sections 4.1 and 4.2. In such cases, we must rely on a density matrix formalism to simultaneously consider neutrino oscillation with neutrino

collisions. We explain the formalism in Section 4.3.

4.1 Neutrino oscillation in a vacuum

In this section, we briefly introduce the neutrino oscillation in a vacuum.

In the standard theory of particle physics, neutrino masses are assumed to be exactly zero, but this is not a symmetry requirement of $SU(3)\times SU(2)\times U(1)$. As described in the paper by Maki, Nakagawa, Sakata [45], if neutrinos actually have masses along with flavor mixings, their mass and flavor eigenstates can be mixed with each other, and neutrinos of flavor eigenstate α experience a transition into different flavor eigenstate $\beta(\neq\alpha)$ and vice versa. As explained in the above, neutrinos are experimentally known to in fact exhibit this kind of periodic behavior between different flavor eigenstates, and this phenomenon is called neutrino oscillation. In the following, we show how neutrino oscillation can be expressed on the basis of quantum mechanics, first assuming that there is no background particle in the system.

In the case where three types of neutrinos, namely electron neutrinos (ν_e), μ neutrinos (ν_μ), and τ neutrinos (ν_τ), have flavor mixings with each other, their flavor eigenstates can be expressed as superpositions of their mass eigenstates: [1]

$$\begin{pmatrix} |\nu_e\rangle \\ |\nu_\mu\rangle \\ |\nu_\tau\rangle \end{pmatrix} = U \begin{pmatrix} |\nu_1\rangle \\ |\nu_2\rangle \\ |\nu_3\rangle \end{pmatrix} \quad \text{or} \quad |\nu_\alpha\rangle = \sum_i U_{\alpha i}\, |\nu_i\rangle\,, \tag{4.1}$$

where $|\nu_i\rangle$ $(i=1,2,3)$ in the right-hand side are respectively mass eigenstates of neutrinos whose mass eigenvalues are m_1, m_2 and m_3, whereas $|\nu_\alpha\rangle$ $(\alpha = e,\mu,\tau)$ in the left-hand side are respectively flavor eigenstates of neutrinos which correspond to ν_e, ν_μ and ν_τ. Also, U is the flavor-mixing matrix of neutrinos, and it is often called PMNS matrix, where "PMNS" is an acronym for Pontecorvo, Maki, Nakagawa, and Sakata, who developed the theory of neutrino oscillation. The unitary matrix U is given by a product of rotation matrices in three dimensions (U_{23}, U_{13}, and U_{12}) and the CP matrix (U_{CP}), *i.e.*

$$U \;=\; U_{23}\, U_{13}\, U_{12}\, U_{CP}\,, \tag{4.2}$$

where each matrix in the right-hand side is normally parametrized as

$$U_{23} \equiv \begin{pmatrix} 1 & 0 & 0 \\ 0 & \cos\theta_{23} & \sin\theta_{23} \\ 0 & -\sin\theta_{23} & \cos\theta_{23} \end{pmatrix}\,, \tag{4.3}$$

$$U_{13} \equiv \begin{pmatrix} \cos\theta_{13} & 0 & e^{i\delta_{\rm D}}\sin\theta_{13} \\ 0 & 1 & 0 \\ -e^{-i\delta_{\rm D}}\sin\theta_{13} & 0 & \cos\theta_{13} \end{pmatrix}\,, \tag{4.4}$$

[1] In this section, we neglect a possibility that active neutrinos, involved in the standard model, have a flavor mixing with an extra flavor eigenstate, *i.e.* sterile neutrinos. That is, we only focus on the neutrino oscillation among three flavors of active neutrinos.

$$U_{12} \equiv \begin{pmatrix} \cos\theta_{12} & \sin\theta_{12} & 0 \\ -\sin\theta_{12} & \cos\theta_{12} & 0 \\ 0 & 0 & 1 \end{pmatrix} , \tag{4.5}$$

$$U_{CP} \equiv \begin{pmatrix} e^{i\alpha_1/2} & 0 & 0 \\ 0 & e^{i\alpha_2/2} & 0 \\ 0 & 0 & 1 \end{pmatrix} , \tag{4.6}$$

where θ_{12}, θ_{23} and θ_{13} are mixing angles in a vacuum giving flavor mixings between corresponding mass eigenstates, whereas $\delta_{\rm D}$ and $\alpha_{{\rm M},i}$ where $i = 1, 2$ are respectively the Dirac- and Majorana phases, which originate from the CP violation of the theory. Therefore, each component of the PMNS matrix $U_{\alpha i}$ can be written as

$$\begin{aligned} U &= \begin{pmatrix} U_{e1} & U_{e2} & U_{e3} \\ U_{\mu 1} & U_{\mu 2} & U_{\mu 3} \\ U_{\tau 1} & U_{\tau 2} & U_{\tau 3}, \end{pmatrix} \\ &= \begin{pmatrix} 1 & 0 & 0 \\ 0 & c_{23} & s_{23} \\ 0 & -s_{23} & c_{23} \end{pmatrix} \begin{pmatrix} c_{13} & 0 & s_{13}e^{-i\delta_{\rm D}} \\ 0 & 1 & 0 \\ -s_{13}e^{i\delta_{\rm D}} & 0 & c_{13} \end{pmatrix} \begin{pmatrix} c_{12} & s_{12} & 0 \\ -s_{12} & c_{12} & 0 \\ 0 & 0 & 1 \end{pmatrix} \begin{pmatrix} e^{i\alpha_1/2} & 0 & 0 \\ 0 & e^{i\alpha_2/2} & 0 \\ 0 & 0 & 1 \end{pmatrix} \\ &= \begin{pmatrix} c_{12}c_{13} & s_{12}c_{13} & s_{13}e^{-i\delta_{\rm D}} \\ -s_{12}c_{23} - c_{12}s_{23}s_{13}e^{i\delta_{\rm D}} & c_{12}c_{23} - s_{12}s_{23}s_{13}e^{i\delta_{\rm D}} & s_{23}c_{13} \\ s_{12}s_{23} - c_{12}c_{23}s_{13}e^{i\delta_{\rm D}} & -c_{12}s_{23} - s_{12}c_{23}s_{13}e^{i\delta_{\rm D}} & c_{23}c_{13} \end{pmatrix} \begin{pmatrix} e^{i\alpha_1/2} & 0 & 0 \\ 0 & e^{i\alpha_2/2} & 0 \\ 0 & 0 & 1 \end{pmatrix} , \end{aligned} \tag{4.7}$$

where we define $c_{ij} \equiv \cos\theta_{ij}$ and $s_{ij} \equiv \sin\theta_{ij}$. In Table 4.1, we summarize experimental values of oscillation parameters, namely $\delta m^2_{ij}, \theta_{ij}$, and $\delta_{\rm D}$.

For simplicity, we hereafter focus on the two-flavor neutrino mixing between ν_α and ν_β, where $\alpha \neq \beta$. In this case, the flavor- and mass eigenstates are related as follows:

$$|\nu_\alpha\rangle = \cos\theta\,|\nu_1\rangle + \sin\theta\,|\nu_2\rangle\,, \tag{4.8}$$

$$|\nu_\beta\rangle = -\sin\theta\,|\nu_1\rangle + \cos\theta\,|\nu_2\rangle\,, \tag{4.9}$$

where $|\nu_\alpha\rangle$ and $|\nu_\beta\rangle$ are the flavor eigenstates, whereas $|\nu_1\rangle$ and $|\nu_2\rangle$ are the mass eigenstates, respectively. Also, θ is the mixing angle between ν_α and ν_β. In this case, the flavor mixing matrix can be written as

$$U = \begin{pmatrix} \cos\theta & \sin\theta \\ -\sin\theta & \cos\theta \end{pmatrix} , \tag{4.10}$$

with which we can rewrite Eqs. (4.8) and (4.9) as

$$\begin{pmatrix} |\nu_\alpha\rangle \\ |\nu_\beta\rangle \end{pmatrix} = U \begin{pmatrix} |\nu_1\rangle \\ |\nu_2\rangle \end{pmatrix} . \tag{4.11}$$

Parameter	1-σ range
δm^2_{12}	$7.55^{+0.20}_{-0.16}$ eV^2
$\lvert\delta m^2_{31}\rvert$ (NO)	$(2.50 \pm 0.03) \times 10^{-3}$ eV^2
$\lvert\delta m^2_{31}\rvert$ (IO)	$2.42^{+0.03}_{-0.04} \times 10^{-3}$ eV^2
θ_{12}	$34.5^{+1.2}_{-1.0}$ °
$\sin^2\theta_{12}$	$3.20^{+0.20}_{-0.16}$
θ_{23} (NO)	$47.7^{+1.2}_{-1.7}$ °
$\sin^2\theta_{23}$ (NO)	$0.547^{+0.020}_{-0.030}$
θ_{23} (IO)	$47.9^{+1.0}_{-1.7}$ °
$\sin^2\theta_{23}$ (IO)	$0.551^{+0.018}_{-0.030}$
θ_{13} (NO)	$8.45^{+0.16}_{-0.14}$ °
$\sin^2\theta_{13}$ (NO)	$2.160^{+0.083}_{-0.069}$
θ_{13} (IO)	$8.53^{+0.14}_{-0.15}$ °
$\sin^2\theta_{13}$ (IO)	$2.220^{+0.074}_{-0.076}$
δ_{D}/π (NO)	$1.21^{+0.21}_{-0.15}$
δ_{D} (NO)	218^{+38}_{-27} °
δ_{D}/π (IO)	$1.56^{+0.13}_{-0.15}$
δ_{D} (IO)	281^{+23}_{-27} °

Table 4.1: Summary of neutrino oscillation parameters reported in Ref. [51].

The time evolution of the flavor eigenstate $|\nu_\alpha\rangle$ can be given as follows:

$$\begin{aligned}|\nu_\alpha\rangle(t) &= e^{-iHt}|\nu_\alpha\rangle\,(t=0)\\ &= \sum_i U_{\alpha i}e^{-iE_it}|\nu_i\rangle\\ &\sim e^{-ipt}\;U\begin{pmatrix} e^{\frac{-im_1^2t}{2p}} & 0\\ 0 & e^{\frac{-im_2^2t}{2p}}\end{pmatrix}U^\dagger\;|\nu_i\rangle\,.\end{aligned} \tag{4.12}$$

In the above, H is the free Hamilton of neutrinos, which satisfies $H|\nu_i\rangle = E_i|\nu_i\rangle = \sqrt{p^2+m_i^2}|\nu_i\rangle$ with E_i (m_i) the energy- (mass-) eigenvalue of $|\nu_i\rangle$. In the third line of Eq. (4.12), we assume that neutrinos are relativistic, $p >> m_i$, and used the approximation, $E_i \sim p + m_i^2/2p$. The expression of Eq. (4.12) is also true for the time evolution of $|\nu_\beta\rangle$. Thus, we can put them together into the matrix form as follows:

$$\begin{pmatrix}|\nu_\alpha\rangle\\ |\nu_\beta\rangle\end{pmatrix}(t) = \exp\left\{-i\left(p+\frac{m_1^2+m_2^2}{2p}t\right)\right\}\exp\left\{-i\frac{\delta m^2}{2p}t\right\}\begin{pmatrix}\cos2\theta & \sin2\theta\\ -\sin2\theta & \cos2\theta\end{pmatrix}\begin{pmatrix}|\nu_\alpha\rangle\\ |\nu_\beta\rangle\end{pmatrix}(t=0)\,, \tag{4.13}$$

where we have defined $\delta m^2 \equiv m_2^2 - m_1^2$. Taking a time derivative of the above equation, we find the evolution equation of flavor eigenstates:

$$i\frac{d}{dt}\begin{pmatrix}|\nu_\alpha\rangle\\ |\nu_\beta\rangle\end{pmatrix}(t) = \frac{\delta m^2}{2p}\begin{pmatrix}\cos2\theta & \sin2\theta\\ -\sin2\theta & \cos2\theta\end{pmatrix}\begin{pmatrix}|\nu_\alpha\rangle\\ |\nu_\beta\rangle\end{pmatrix}(t=0), \tag{4.14}$$

where we neglect the first exponential factor of the right-hand side of Eq. (4.13) since it is just a phase factor of neutrino wave functions.

From Eq. (4.13) we find the transition probability of neutrinos, $P(\nu_\alpha \to \nu_\beta)$:

$$\begin{aligned}P(\nu_\alpha\to\nu_\beta) &= |\langle\nu_\beta(t)|\nu_\alpha\rangle|^2\\ &= \sin^2 2\theta\sin^2\frac{\delta m^2}{2p}t.\end{aligned} \tag{4.15}$$

In the same way, we also find the survival probability of neutrinos, $P(\nu_\alpha \to \nu_\alpha)$:

$$\begin{aligned}P(\nu_\alpha\to\nu_\alpha) &= |\langle\nu_\alpha(t)|\nu_\alpha\rangle|^2\\ &= 1-\sin^2 2\theta\sin^2\frac{\delta m^2}{2p}t.\end{aligned} \tag{4.16}$$

As can be seen from Eqs. (4.15) and (4.16), a neutrino produced in a flavor eigenstate periodically changes its flavor during propagating through space. Moreover, we can also see from Eq. (4.15) that the transition probability is zero either if neutrinos are massless or if their masses are equal, *i.e.* $\delta m^2 = 0$. The transition- and survival probabilities are just described by the mixing angle θ if the oscillation length $L_\nu \equiv 4\pi p/\delta m^2$ is much shorter

than the typical distance or the time scale of the oscillation $\sim p/\delta m^2$ is much faster than that of the system:

$$\begin{aligned} P(\nu_\alpha \to \nu_\beta) &= \sin^2 2\theta \left\langle \sin^2 \frac{\delta m^2}{2p} t \right\rangle \\ &\sim \frac{1}{2} \sin^2 2\theta, \end{aligned} \tag{4.17}$$

$$\begin{aligned} P(\nu_\alpha \to \nu_\alpha) &= 1 - \sin^2 2\theta \left\langle \sin^2 \frac{\delta m^2}{2p} t \right\rangle \\ &\sim 1 - \frac{1}{2} \sin^2 2\theta, \end{aligned} \tag{4.18}$$

where $\langle \cdot \rangle$ is the time or thermal average, and we replaced $\langle \cdot \rangle$ part with its average, *i.e.* $\langle \sin^2 \frac{\delta m^2}{2p} t \rangle \to 1/2$.

So far, we assume that there is no background particle, and therefore neutrinos are freely propagating in the system. On the other hand, our objective is to understand the behavior of neutrino oscillation in the early Universe, where a huge amount of particles are present in the background. Therefore, we consider the matter effects in the next section.

4.2 Neutrino oscillation in a matter

In this section, we discuss the effects of background particles on neutrino oscillation. To make its effect clear, let us consider the simplified system consisting of ν_e, ν_μ, and electrons. We assume here that electrons are non-relativistic, and their spin directions are randomly distributed. In such a situation, all flavors of neutrinos interact with electrons through neutral-current interaction (right panel in Figure 3.1):

$$\nu_\alpha + e^- \to \nu_\alpha + e^- \quad \text{via } Z^0 \text{ boson}\,, \tag{4.19}$$

while ν_e additionally interacts through charged-current one (left panel in Figure 3.1):

$$\nu_e + e^- \to \nu_e + e^- \quad \text{via } W^\pm \text{ boson}\,. \tag{4.20}$$

As we have seen in Section 4.1, the transition probability only depends on the energy difference of neutrinos. Thus, it is only worth discussing the contribution of charged-current interactions of neutrinos, which makes a difference in the potentials of ν_e and ν_μ.

The interaction Hamiltonian for the charged-current process, $H_{\rm int}$, can be written as

$$\begin{aligned} H_{\rm int} &= \frac{G_F}{\sqrt{2}} \bar{\nu}_e \gamma^\mu (1-\gamma_5) e \bar{e} \gamma_\mu (1-\gamma_5) \nu_e \\ &= \sqrt{2} G_F n_e \nu_e^\dagger \nu_e, \end{aligned} \tag{4.21}$$

where γ_μ ($\mu = 1, 2, 3, 4$) is the Gamma matrix, and γ_5 ($\equiv i\gamma^0\gamma^1\gamma^2\gamma^3$) is the Chirality. In the above expression, we used the Fierz transformation and treated electrons as a thermal background. Also, a contribution responsible for the CP violation has been neglected for simplicity. Consequently, the time evolution of ν_e and ν_μ states can be given by

$$\begin{aligned} i\frac{d}{dt}\begin{pmatrix} |\nu_e\rangle \\ |\nu_\mu\rangle \end{pmatrix}(t) &= \left[\frac{\delta m^2}{2E}\begin{pmatrix} \cos 2\theta & \sin 2\theta \\ -\sin 2\theta & \cos 2\theta \end{pmatrix} + \sqrt{2}G_F n_e \begin{pmatrix} 1 & 0 \\ 0 & 0 \end{pmatrix}\right]\begin{pmatrix} |\nu_e\rangle \\ |\nu_\mu\rangle \end{pmatrix}(t=0) \\ &= \left[\frac{1}{2E}U_{\rm vac}M^2U_{\rm vac}^\dagger + \sqrt{2}G_F n_e \begin{pmatrix} 1 & 0 \\ 0 & 0 \end{pmatrix}\right]\begin{pmatrix} |\nu_e\rangle \\ |\nu_\mu\rangle \end{pmatrix}(t=0) \\ &= \frac{1}{2E}\left[U_{\rm vac}M^2U_{\rm vac}^\dagger + A\begin{pmatrix} 1 & 0 \\ 0 & 0 \end{pmatrix}\right]\begin{pmatrix} |\nu_e\rangle \\ |\nu_\mu\rangle \end{pmatrix}(t=0) \\ &\equiv H\begin{pmatrix} |\nu_e\rangle \\ |\nu_\mu\rangle \end{pmatrix}, \end{aligned} \tag{4.22}$$

where $A \equiv 2\sqrt{2}G_F n_e E$, and $U_{\rm vac}$ denotes the flavor mixing matrix in a vacuum. The second term in the bracket $[\cdot]$ arises from the charged-current process in Figure 3.1, which we are concerned with.

The effective mass difference in a medium is obtained by diagonalizing the neutrino Hamiltonian in Eq. (4.22). As a result, the effective mass difference in a medium $\delta m^2_M (= m^2_{M,2} - m^2_{M,1})$ can be written as

$$\delta m^2_M = \sqrt{(\delta m^2\cos 2\theta - A)^2 + (\delta m^2 \sin 2\theta)^2}\,, \tag{4.23}$$

whereas the effective mixing angle in a medium θ_M is determined so that it satisfies

$$\begin{pmatrix} |\nu_e\rangle_M \\ |\nu_\mu\rangle_M \end{pmatrix} = \begin{pmatrix} \cos\theta_M & \sin\theta_M \\ -\sin\theta_M & \cos\theta_M \end{pmatrix}\begin{pmatrix} |\nu_e\rangle \\ |\nu_\mu\rangle \end{pmatrix}, \tag{4.24}$$

where $|\nu_e\rangle_M$ and $|\nu_\mu\rangle_M$ are flavor eigenstates of ν_e and ν_μ in a medium, respectively. At last, we find

$$\cos 2\theta_M = \frac{\delta m^2\cos 2\theta - A}{\sqrt{(\delta m^2\cos 2\theta - A)^2 + (\delta m^2 \sin 2\theta)^2}}\,, \tag{4.25}$$

$$\sin 2\theta_M = \frac{\delta m^2\sin 2\theta}{\sqrt{(\delta m^2\cos 2\theta - A)^2 + (\delta m^2 \sin 2\theta)^2}}\,. \tag{4.26}$$

As is obvious from Eqs. (4.23) and (4.26), if there is no background particles and hence $A = 0$, the effective mass difference and mixing angle are equal to those in a vacuum, *i.e.* $\delta m^2_M = \delta m^2$ and $\theta_M = \theta$. In contrast, if the condition, $A = \delta m^2 \cos 2\theta$, is satisfied, the effective mixing angle takes its maximum value, *i.e.* $\sin 2\theta_M = 1$ ($\theta_M = \pi/4$), and the transition probability also becomes its maximum,

$$P(\nu_\alpha \to \nu_\beta) = \frac{1}{2}\sin^2 2\theta_M \to 1/2\ (= P_{\rm max}), \tag{4.27}$$

the last approximation holds if the oscillation time scale in a matter is much shorter than the typical time scale of the system.

The modification of the effective mass difference and mixing angle due to in-medium effects were first predicted by L. Wolfenstein in 1978 [52], followed by S. Mikheyev and A. Smirnov, who indicated a possibility of resonant neutrino oscillation [53]. This kind of the matter effects on neutrino oscillation is called "MSW (Mikheyev-Smirnov-Wolfenstein) effect" named after their names, and it is one of the most well-known phenomena in the field of neutrino physics. Similarly, the resonant oscillation is called "MSW resonance", and the theoretical prediction of this resonant oscillation has contributed to solving the solar neutrino problem, mentioned above. [2]

At this point, we are focusing on the flavor transition of one each neutrino. In contrast, in the case where neutrinos are in a thermal bath, and we are interested in the thermodynamic evolution of the system, it is not worth discussing the transition probability of neutrinos one by one. This is because there are a variety of neutrinos in a thermal bath characterized by *e.g.* different energy, birth time, or free streaming scale. For this reason, in the next section, we introduce the formalism which gives us a way to describe the neutrino oscillation effects on thermodynamic quantities.

4.3 Neutrino oscillation in statistical ensembles

In previous sections, we focus on the transition probability of neutrinos with particular energy E and oscillation phase $(\delta m^2/2p)t$. In contrast, if we are interested in neutrinos in a thermal bath, as in our studies in Chapters 5 and 6, we cannot directly apply the formalism in the previous sections as each neutrino has a different energy and oscillation phase. In such cases, it is mandatory to treat them as a statistical ensemble and consider the effect of neutrino oscillation on thermodynamic quantities. As we have seen in Subsection 2.2.3, thermodynamic evolution of particles can generally be described by the Boltzmann equation, Eq. (2.20). However, this equation is based on the classical theory, *i.e.* the general relativity, and it is therefore incompatible with the neutrino oscillation, which originates from the quantum nature of neutrinos. To simultaneously consider neutrino production by flavor transitions and neutrino collisions, we must rely on the density matrix formalism (see Refs. [55–57] for detailed derivations and more thorough discussions).

In this formalism, particle states are described by N-body density matrix $\varrho^{(n)}$, which has $N \times N$ elements. In contrast, in the system which we are interested in, the cosmic temperature is an MeV-scale, and a correlation between particles due to collisions can safely be ignored. Therefore the system can be well described by a direct sum of one-body

[2] Here, we assume the net density of neutrinos, $n_\nu - n_{\bar{\nu}}$, is so small that there is no matter effect due to the self-scattering of neutrinos, following the standard assumption on the lepton asymmetry of the Universe, *i.e.* $\eta_L \gtrsim 10^{-10}$. For a net density $\eta_L \gtrsim 10^{-7}$, such matter effects cannot be negligible (see *e.g.* [54]).

reduced density operators:

$$\varrho^{(n)}(k) = \sum_i \oplus \varrho_i(k) \oplus \bar{\varrho}_i(k) \oplus \varrho_\nu(k), \tag{4.28}$$

where ϱ_i and $\bar{\varrho}_i$ are one-body reduced density operators for particles other than neutrinos, and ϱ_ν is that for neutrinos and anti-neutrinos. The one-body reduced density matrix for neutrinos, ϱ_ν, can be expressed as $2N \times 2N$ matrix, where N is the number of neutrino species which has a flavor mixing. As in the system which we focus on, a correlation between neutrinos and anti-neutrinos is almost negligible as well, and the density matrix for neutrinos is almost block-diagonal in flavor space. In this case, the neutrino density matrix can be decomposed into two $N \times N$ submatrices; one is for neutrinos and the other for anti-neutrinos. In this thesis, we denote the density matrix for neutrinos by ϱ and that for anti-neutrinos by $\bar{\varrho}$. The diagonal component of the density matrix is the distribution function for each flavor of neutrinos, and the off-diagonal component is the correlation between different flavors of neutrinos. Then, an ij element of the density matrices for neutrinos and anti-neutrinos can respectively be expressed as $\varrho_{ij}(\mathbf{p}) = \left\langle a_i^\dagger(\mathbf{p}) a_j(\mathbf{p}) \right\rangle$ and $\bar{\varrho}_{ij}(\mathbf{p}) = \left\langle \bar{a}_i^\dagger(\mathbf{p}) \bar{a}_j(\mathbf{p}) \right\rangle$, where a_i and $a_i^\dagger$ are respectively the annihilation- and the creation operators for ν_i, and $\bar{a}_i$ and $\bar{a}_i^\dagger$ are those for $\bar{\nu}_i$.

The evolution of the density matrix is described by the extended version of the classical Boltzmann equation, which has a similar form to the Liouville-von-Neumann equation but with collision terms [55–57]. As only two-body scattering is relevant to the dynamics in the system with an MeV-scale temperature, up to the second-order in the weak interaction, or in the Fermi-coupling constant G_F, the equation can be expressed as:

$$iL[\varrho] = [\mathcal{H}, \varrho] + C[\varrho], \tag{4.29}$$

where $L[\varrho]$ in the left-hand side is the Liouville operator, which contains derivatives in time t, space $\boldsymbol{x}$, and momentum $\boldsymbol{p}$:

$$L[\cdot] = \partial_t[\cdot] + \dot{\boldsymbol{x}} \cdot \nabla_{\boldsymbol{x}}[\cdot] + \dot{\boldsymbol{p}} \cdot \nabla_{\boldsymbol{p}}[\cdot], \tag{4.30}$$

among which the space derivative is vanishing in the spatially homogeneous and isotropic system, as in the standard big-bang Universe. Also, the momentum derivative can be simplified due to the same reason as $\dot{\boldsymbol{p}} \cdot \nabla_{\boldsymbol{p}} \mapsto \dot{p}\, \partial_p$, where $p = |\boldsymbol{p}|$ is the absolute momentum, as there is no typical direction in the Universe. Moreover, as the momentum is gradually redshifted in the expanding Universe, it is proportional to a^{-1}, which leads to $\dot{p} = -pH$. Taken into account these conditions, the Liouville operator can be rewritten as:

$$L[\cdot] = \partial_t[\cdot] - Hp\, \partial_p[\cdot]\,. \tag{4.31}$$

As for the terms in the right-hand side of Eq. (4.29), $\mathcal{H}$ is the hamiltonian of neutrinos, which consists of two contributions:

$$\mathcal{H} = \mathcal{H}_{\rm vac} + \mathcal{H}_{\rm int}, \tag{4.32}$$

where the first term is the contribution relevant to the flavor mixing in a vacuum, whereas the second term originates from the coherent scattering of neutrinos with background particles, and it is proportional to the first order in the Fermi coupling. Also, the second term in the right-hand side, $C[\varrho]$, is the collision term for neutrinos, which describe the second-order effects in the Fermi coupling.

As is seen from the discussion so far, we assume:

1. the spatial inhomogeneity of the system can be ignored,
2. the density of the system is dilute so that a correlation between particles of different species can be neglected,
3. the energy scale of the system is low, and it is therefore enough to consider up to $\mathcal{O}(G_F^2)$ terms in the neutrino hamiltonian,

all of which seem to be valid in the epoch with the cosmic temperature $T << v\,(\sim G_F^{-1/2})$, where $v \sim \mathcal{O}(100)$ GeV is the typical energy scale described by the electroweak theory of the standard model of particle physics. The above assumptions are questionable in the extreme environments attained in *e.g.* supernovae explosions or neutron star mergers as the system is known to be highly inhomogeneous. For the discussion of such inhomogeneous effects, see Refs. [58–63].

In the following, we next look into each contribution in the neutrino hamiltonian and the collision term.

4.3.1 Vacuum term

This contribution originates from the mass difference and the mixing angle between distinct neutrino species. The expression is similar to the one in the previous section:

$$\mathcal{H}_{\rm vac} = \frac{U\mathcal{M}^2U^\dagger}{2E}, \tag{4.33}$$

where $\mathcal{M}$ is the mass matrix in mass basis, which can be expressed as $\mathcal{M}^2 = {\rm diag}(m_1^2, m_2^2, m_3^2)$ in the case of the three-flavor mixing, and it is related to the mass matrix in flavor basis M^2 as $\mathsf{M}^2 = U\mathcal{M}^2U^\dagger$. As can be seen from the expression, a behavior of neutrino oscillation in a vacuum is solely determined by neutrino energy E and phenomenological mixing parameters, the mass differences δm^2 and the mixing angles θ; *i.e.* all information of the system is included in the Hubble parameter H if no matter exists in the background. The vacuum term for anti-neutrinos $\bar{\mathcal{H}}_{\rm vac}$ is the same as Eq. (4.33), *i.e.* $\bar{\mathcal{H}}_{\rm vac} = \mathcal{H}_{\rm vac}$.

4.3.2 Matter term

As we discussed in the previous section, when neutrinos travel through a medium and scatter with background particles, their masses and mixings are effectively modified. This

is due to the forward scattering of neutrinos, which does not change their energy or momentum. The contribution to the neutrino self-energy is depicted in Figure 4.1. Since we are interested in the epoch with an MeV-scale temperature, the system mainly consists of photons, electrons, and neutrinos, which remain relativistic at this epoch. Therefore, for electron neutrinos l_α in the bubble diagram can be neutrinos of flavor α or electrons, and f in the tadpole diagram can be neutrinos of any flavor or electrons. For μ- and τ neutrinos the bubble diagram does not exist. The matter potential due to the forward scattering of neutrinos with electrons can therefore be written as [64]:

$$\mathcal{H}_{\mathrm{int},\,e} = \frac{\sqrt{2}G_F}{2}\left(1+4\sin^2\theta_W\right)\left(n_{e^-}-n_{e^+}\right) - \frac{8\sqrt{2}G_F p}{3m_W^2}\left(\rho_{e^-}+\rho_{e^+}\right), \tag{4.34}$$

for ν_e,

$$\mathcal{H}_{\mathrm{int},\,e} = -\frac{\sqrt{2}G_F}{2}\left(1-4\sin^2\theta_W\right)\left(n_{e^-}-n_{e^+}\right), \tag{4.35}$$

for ν_μ and ν_τ. In the above expression, θ_W is the weak mixing angle, while n_{e^-} (n_{e^+}) and ρ_{e^-} (ρ_{e^+}) are number- and energy densities of electrons and positrons, respectively. On the other hand, the matter potential due to the forward scattering of neutrinos themselves can be expressed as [56]:

$$\begin{aligned}\mathcal{H}_{\mathrm{int},\,\nu}(\mathbf{p}) = \sqrt{2}G_F\int d\mathbf{q}\left\{G_S\,\mathrm{Tr}\left(\left(\varrho(\mathbf{q})-\bar{\varrho}^*(\mathbf{q})\right)G_S\right)+G_S\left(\varrho(\mathbf{q})-\bar{\varrho}^*(\mathbf{q})\right)G_S\right\}\\ -\frac{8\sqrt{2}G_F p}{3m_Z^2}\int d\mathbf{q}qG_S\left(\varrho(\mathbf{q})+\bar{\varrho}^*(\mathbf{q})\right)G_S,\end{aligned} \tag{4.36}$$

where $q = |\boldsymbol{q}|$, and G_S is an $n\times n$ dimensionless matrix of neutral-current coupling constants, and it is equal to an identity matrix in the framework of the standard model of particle physics. To derive the above equation, we have assumed that the system is isotropic, and the effect of anisotropy, which is important in the supernovae explosion, can be ignored. In Eq. (4.36), the first term originates from the tadpole diagram, whereas the second term from the bubble diagram.

In the matter potentials induced by the neutrino-electron scattering, Eqs. (4.34)–(4.35), and the neutrino-neutrino scattering, Eq. (4.36), the asymmetric part can be neglected. This is because the baryon asymmetry of the Universe is known to be small $\sim\mathcal{O}(10^{-10})$ [29] and the asymmetry in the number densities of charged leptons, *i.e.* $n_{e^-}-n_{e^+}$, is expected to be the same order of magnitude as the baryon asymmetry for charge neutrality of the Universe. On the other hand, the asymmetry in the number densities of neutral leptons, *namely* neutrinos, is not very well constrained from observations, and an upper bound on the asymmetry is $\mathcal{O}(10^{-3}$–$10^{-2})$ depending on the flavor of neutrinos [65], which is much larger than the observed value of the baryon asymmetry. However, it is difficult to prepare for such large asymmetry of neutrinos in the framework of the standard model of particle physics, and there is no strong motivation to consider the cases where the asymmetric term in $\mathcal{H}_{\mathrm{int},\,\nu}$ ($\propto\varrho-\bar{\varrho}^*$) play an important role in the neutrino oscillation. Thus, throughout

this thesis we assume that all the asymmetric contributions of the matter potential can be ignored. In this case, for ν_e-ν_s mixing the matter potential, $\mathcal{H}_{\rm int}$, can be written as:

$$\mathcal{H}_{\rm int} = -\frac{8\sqrt{2}G_F p}{3m_Z^2}\left[\left(1-\sin^2\theta_W\right)^{-1}\left(\rho_{e^-}+\rho_{e^+}\right)G_e + \int d\mathbf{q}qG_S(\varrho(\mathbf{q})+\bar{\varrho}(\mathbf{q}))G_S\right], \quad (4.37)$$

where G_e is a diagonal matrix with one in the matrix element which corresponds to ν_e, and we have used the relation, $\cos\theta_W = m_W/m_Z$.

It should be worth noticing that if baryon asymmetry exist in the early Universe, there are extra contributions to the matter potential due to the tadpole diagram in Figure 4.1 [64]:

$$\mathcal{H}_{{\rm int},\,n} = -\frac{\sqrt{2}G_F}{2}\left(n_n - n_{\bar{n}}\right), \quad (4.38)$$

which originates from the asymmetry of the number densities of neutrons, and similarly

$$\mathcal{H}_{{\rm int},\,p} = \frac{\sqrt{2}G_F}{2}\left(1-4\sin^2\theta_W\right)\left(n_p - n_{\bar{p}}\right), \quad (4.39)$$

which originates from the asymmetry of the number densities of protons. These two contributions are not taken into account in this thesis since they are much smaller than the symmetric terms of $\mathcal{H}_{{\rm int},\,e}$ and $\mathcal{H}_{{\rm int},\,\nu}$ for the baryon asymmetry of $\mathcal{O}(10^{-10})$.

4.3.3 Collision term

As we have seen in the previous subsection, coherent forward scattering of neutrinos with background particles induce the matter potential in the neutrino hamiltonian, which brings about an interesting behavior of neutrino oscillation. These contributions are first order in the Fermi coupling constant. In the environment in which we are interested, *i.e.* in the early epoch of the Universe with an MeV-scale temperature, incoherent scattering of neutrinos is also important. As described earlier, only two-body reaction processes are relevant in this epoch, and it is therefore sufficient to consider contributions up to $\mathcal{O}(G_F^2)$ in the collision term. In this case, the general expression of the collision term can be written as:

$$\begin{aligned} C\left[\varrho_{ij}\right] = {} & \pi\mathcal{V}\left[k',l'|m',n'\right]\mathcal{V}[k,l|m,n]\;\delta_E^{(1)}\left(k',l'|m',n'\right) \\ & \left[\varrho_{n'l}\varrho_{m'k}\left(\delta_{mk'}-\varrho_{mk'}\right)\left(\delta_{il'}-\varrho_{il'}\right) - \varrho_{mk'}\varrho_{il'}\left(\delta_{km'}-\varrho_{km'}\right)\left(\delta_{n'l}-\varrho_{n'l}\right)\right]\delta_{nj} \\ & + \text{complex conjugate}, \end{aligned} \quad (4.40)$$

where $\delta_E^{(1)}$ is the 1D Dirac delta function, which corresponds to the energy conservation of particles in the initial- and final states, whereas δ_{ij} is the Kronecker delta function. Also, $\mathcal{V}$ contains the scattering matrix element, whose detailed expression is given in Chapter 5. In the expression, each label stands for momentum and a discrete index which characterizes individual particles, and a summation over the same indices is assumed.

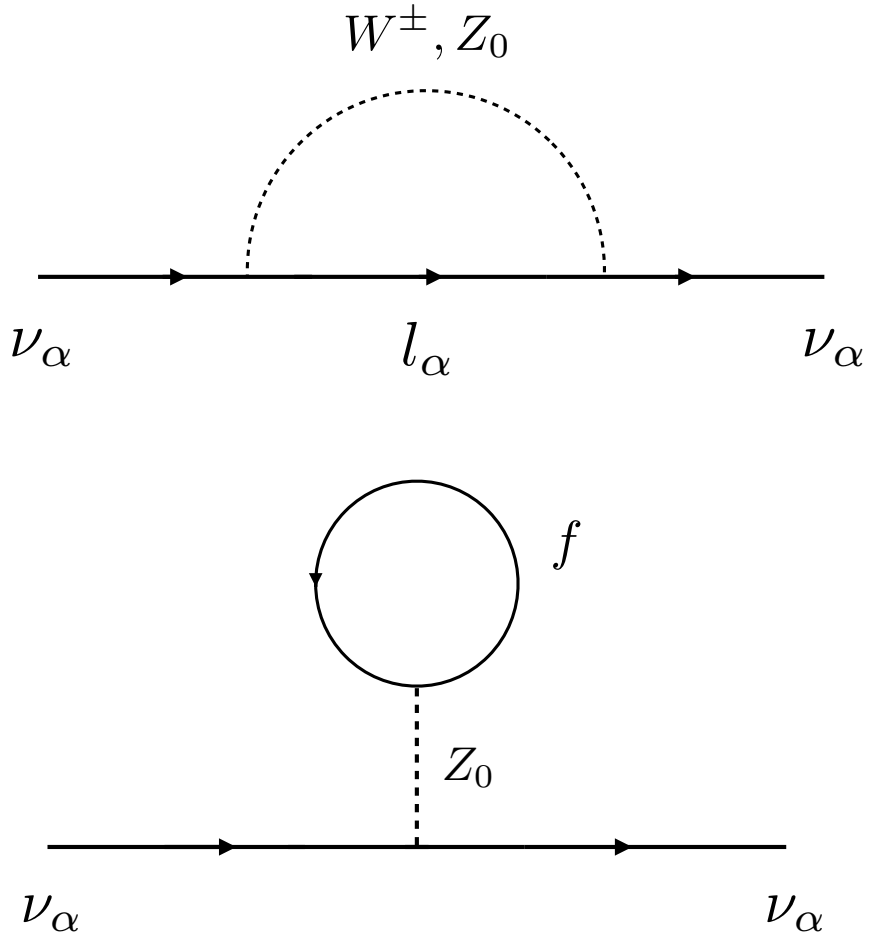

Figure 4.1: Feynman diagram for the lowest-order contribution to the forward scattering of neutrinos, which modifies the effective neutrino mass. In the upper panel, l_α in the bubble diagram is a lepton of the same flavor as the neutrinos in the initial- and final states. In the bottom panel, f in the tadpole diagram is a fermion coupling to the Z boson.

The part including the Kronecker delta function corresponds to Pauli blocking effects, but it is now in a matrix form. In Chapters 5 and 6 we consider all relevant processes for the collision term of neutrinos. In general, it is demanding to calculate Eq. (4.40) without any simplification, but in the case of neutrino oscillation between an active- and a sterile species of neutrinos the collision term is significantly simplified by neglecting Pauli blocking factors and electron masses and by assuming thermal distributions of background particles other than neutrinos:

$$C[\varrho] = R[\varrho] + D[\varrho], \tag{4.41}$$

where $R[\varrho]$ is the diagonal part of the collision term, which can be expressed as

$$R\left[\varrho_{ii}\right] = C_\alpha G_F^2 p T^4 \left(f_{\rm eq} - \varrho_{ii}\right), \tag{4.42}$$

whereas $D[\varrho]$ is the off-diagonal contribution of the collision term:

$$D\left[\varrho_{ij}\right] = -\frac{1}{2} C_\alpha G_F^2 p T^4 \varrho_{ij}, \tag{4.43}$$

where $i \neq j$, T is the cosmic temperature, and $f_{\rm eq} = 1/[\exp(p/T) + 1]$. Also, C_α is the coefficient of the collision term, $C_\alpha = 1.27$ for ν_e–ν_s mixing and $C_\alpha = 0.92$ for ν_μ–ν_s or ν_τ–ν_s mixing [66]. In particular, $R[\varrho]$ is responsible for repopulating neutrinos mixed with sterile neutrinos, while $D\left[\rho_{ij}\right]$ breaks the coherence of different flavors of neutrinos.

The simple expressions in Eqs. (4.42)–(4.43) cannot be used when neutrinos largely deviate from equilibrium, and for this reason we do not rely on such assumptions and calculate the collision term without any simplification in Chapters 5 and 6.

Chapter 5

MeV-scale reheating temperature and thermalization of active neutrinos [1]

Abstract: In this chapter, we investigate lower limits on the reheating temperature imposed by big-bang nucleosynthesis assuming both radiative and hadronic decays of such massive particles. For the first time, the effects of neutrino self-interactions and oscillations are taken into account in the neutrino thermalization calculations. By requiring consistency between theoretical and observational values of light element abundances, we find that the reheating temperature should conservatively be $T_{\rm RH} \gtrsim$ *1.8 MeV in the case of 100% radiative decay, and* $T_{\rm RH} \gtrsim$ *4–5 MeV in the case of 100% hadronic decays for particle masses in the range of 10 GeV to 100 TeV.*

5.1 Introduction

In the standard big-bang cosmology it is normally assumed that radiation components (photons, electrons/positrons, and neutrinos) were perfectly thermalized, and energy of radiation dominated the total energy density of the Universe well before the beginning of big-bang nucleosynthesis (BBN). In a modern picture of the early Universe, this radiation-dominated epoch is expected to be realized after the decay of a massive particle such as the inflaton, the particle associated with the inflaton field driving inflation, or another massive particle such as the curvaton. If such massive particles abundantly existed in the early Universe, their non-relativistic energy could dominate the total energy, and then an early matter-dominated epoch should have been realized before the radiation-dominated epoch. Therefore, particle production caused by their decays and subsequent entropy production (called reheating) dramatically modify the thermal history of the Universe. The Universe could experience the reheating more than once after inflation depending on the fundamental theory of particle physics. Since many theoretical models have been

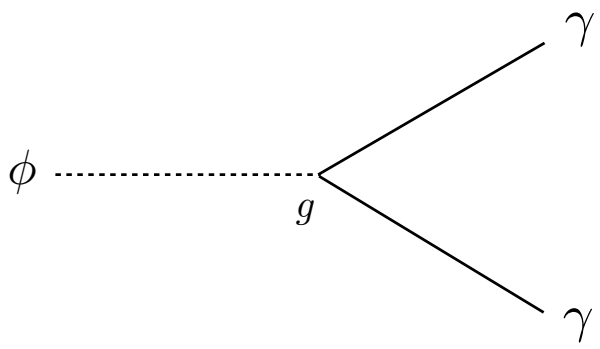

Figure 5.1: Feynman diagram for the decay of dilatons into two photons, $\phi \to \gamma + \gamma$. $g(\equiv m_\phi/M_{\rm Pl})$ is the coupling constant suppressed by the Planck mass.

proposed as a theory beyond the standard model of particle physics, it is required to have some ways to find the true theory of nature. One of the approaches is to investigate the possible value of "reheating temperature" which is defined by the cosmic temperature when the radiation-dominated epoch just started. This is because the reheating temperature is related to the property of the massive particles, and we can constrain the theories through the observational bound on the reheating temperature.

As for a candidate of inflaton field or curvaton field, a lot of unstable massive scalar fields, *e.g.* moduli, dilaton fields, are predicted in particle physics theories beyond the standard model such as supergravity or superstring theory. They tend to dominate the total energy of the Universe during their oscillation epochs. It is notable that they typically have masses at or above the weak scale and decay only through gravitational interaction. This means that they have long lifetimes of $\mathcal{O}(0.1)$ sec–$\mathcal{O}(10)$ sec, and the reheating temperature after their decay is expected to be $\mathcal{O}(1)$ MeV. For example, coupling between photons and dilatons, a scalar particle which appears in the superstring theory, can be written as $-\exp[-\phi/M_{\rm pl}]F_{\mu\nu}F^{\mu\nu}$, where $M_{\rm pl}$ is the Planck mass, ϕ is the dilaton field, and $F_{\mu\nu}$ is the field strength of photons. Since the exponential part of the coupling can be expanded as $\simeq 1 - \phi/M_{\rm pl}$, the coupling is suppressed by the Planck mass. For this coupling, the corresponding decay rate can be expressed as $m_\phi^3/M_{\rm pl}^2$ with m_ϕ the mass of dilatons. Thus, by defining $g \equiv m_\phi/M_{\rm pl}$ the decay process of ϕ can be represented as Figure 5.1, and the decay rate of ϕ is expressed as $g^2 m_\phi$. This kind of decays, whose rates are suppressed by the Planck mass, lead to the longevity of such particles.

Since neutrinos decoupled from the thermal plasma at around the cosmic temperature $T \sim \mathcal{O}(1)$ MeV, they would have suffered imperfect thermalization due to the late-time entropy production caused by their decay. Thus, we have a strong motivation to observationally test this kind of cosmological scenarios with decaying particles which induce the

MeV-scale reheating temperature.

The theory of BBN based on the standard big-bang cosmology, *i.e.* standard BBN, successfully explains observational light element abundances (see *e.g.* Ref. [29] and references therein), and the theory says that the light elements are synthesized at around $T \sim \mathcal{O}(0.01)$ MeV–$\mathcal{O}(0.1)$ MeV. As we shall see in Section 5.4, BBN is highly sensitive to the neutrino abundances. Therefore, we can examine the MeV-scale reheating scenarios by using BBN as a probe.

In Ref. [26], lower bounds on reheating temperature have been studied in terms of BBN for the first time. They have shown that an incomplete thermalization of neutrinos gives the most significant effect on BBN assuming that 100% of the long-lived massive particles decay into electromagnetic radiations such as photons or charged leptons. Because of competition between decreases and increases of the produced amount of ^{4}He by the imperfect thermalization of the neutrinos, we can constrain the reheating temperature. As a result, they have obtained a conservative lower bound on the reheating temperature $T_{\rm RH} > 0.5$ MeV–0.7 MeV (95% C.L.).

Afterwards, in Ref. [27], they discussed hadronic decays of massive particles, *i.e.* direct decays into quarks and/or gluons which immediately fragment into hadrons such as pions, kaons, or nucleons. The thermalization of radiations proceeds in the same way as in the case where 100% of the massive particles decay into electromagnetic radiations. This is because almost all of the kinetic energy of hadrons are transferred into radiation through Coulomb scattering with background electrons/positrons or inverse-Compton like scattering with background photons, and a neutral pion π^0 immediately decays into two photons. In the case of the hadronic decay, interconverting reactions between ambient protons and neutrons induced by emitted hadrons are extraordinarily important because they increase the neutron to proton ratio which is a key parameter of resultant abundances of light elements. As a result, they obtained a lower bound $T_{\rm RH} > 2.5$–4 MeV (95% C.L.) depending on the mass of the long-lived massive particles and their branching ratio into hadrons.

Subsequently, two- and three-flavor neutrino oscillations were respectively considered in the thermalization process of neutrinos in Refs. [67] and [68] where they obtained a lower bound $T_{\rm RH} > 2$ MeV (95% C.L.) and $T_{\rm RH} > 4.1$ MeV (95% C.L.) assuming radiative decay of the massive particles.

Some other cosmological probes other than BBN are also sensitive to neutrino abundances. Here we briefly refer to the recent papers which focused on this topic. In Ref. [27], they discussed possible effects of an incomplete thermalization of neutrinos on a temperature anisotropy and polarization of Cosmic Microwave Background (CMB) and a galaxy power spectrum of Large Scale Structure (LSS). Ref. [69] obtained a combined constraint $T_{\rm RH} > 4$ MeV (95% C.L.) by considering BBN, CMB (WMAP) and LSS (2dF Galaxy Redshift Survey).

After that, authors in Ref. [70] have updated the CMB and LSS data by using WMAP three-year data and SDSS luminous red galaxies data, and they obtained $T_{\rm RH} > 2$ MeV (95% C.L.). Similar analysis has been done in Ref. [71] by using WMAP five-year data

and SDSS luminous red galaxies data where they obtained $T_{\rm RH} > 2$ MeV (95% C.L.) from CMB only and $T_{\rm RH} > 3.2$ MeV (95% C.L.) from CMB by including external priors from SDSS red luminous galaxy survey and the constraint from the comic age. Besides, authors in Ref. [68] have reported a new constraint $T_{\rm RH} > 4.3$ MeV (95% C.L.) from CMB by using Planck 2015 data.

In this thesis, we extend the study of Ref. [27] by considering neutrino oscillation and neutrino self-interaction in the calculation of the neutrino thermalization. We assume both radiative and hadronic decays of the massive particles and give an updated bound on the reheating temperature set by BBN. This is the first study that considers effects of neutrino self-interactions on the neutrino thermalization to constrain the reheating temperature.

The structure of this chapter is as follows. In Section 5.2, we introduce the formalism of the neutrino thermalization assuming the MeV-scale reheating temperature. In Section 5.3, we show the results of neutrino thermalization in the reheating and describe how neutrino oscillation and neutrino self-interaction affect the thermalization process. The results of BBN are shown in Section 5.4 where we discuss the effects of both radiative and hadronic decays on light element abundances. Finally, we draw our conclusion in Section 5.5.

5.2 Reheating and neutrino thermalization

In this section, we describe the neutrino thermalization in the low-reheating-temperature Universe and introduce the key equations.

As described in the previous section, there are some candidate particles in theories going beyond the Standard Model of particle physics which are weakly interacting and decay at around BBN. Here, we call the long-lived massive particles just "massive particles" and label them X. We assume the energy density of the massive particles dominates those of other particles at an initial time and the Universe is completely matter-dominated before the massive particles start to decay. In this setting, the entropy production caused by the decay of X induces particle production via electromagnetic, weak, and strong interactions. As a result, photons and charged leptons are rapidly thermalized in the reheating via electromagnetic interactions, whereas the weakly interacting neutrinos are slowly created in the thermal bath of photons and charged leptons. [1] As neutrinos decouple from the thermal bath at around a temperature of $\mathcal{O}(1)$ MeV, neutrinos should not be fully thermalized if $T_{\rm RH} \sim \mathcal{O}(1)$ MeV. A degree of thermalization of neutrinos affects the light element abundances [26]. For this reason, it is especially important to accurately calculate

[1] In the case where the massive particles decay intro quarks and/or gluons, they fragment into mesons and baryons after the hadronization, and almost all the kinetic energy of hadrons are transferred into radiation due to the reason mentioned before. Therefore, contributions of secondary neutrinos produced by the decay of hadrons can be neglected. However, there is also another possibility that the massive particles directly decay into neutrinos, *e.g.* $X \to \nu_\alpha + \bar{\nu}_\alpha$ where $\alpha = e, \mu, \tau$ [69]. In this case, electromagnetic plasma is produced only from neutrinos via weak interaction, which gives totally different results of the neutrino thermalization and BBN. In this thesis we do not consider the possibility.

the thermalization of neutrinos in the reheating for $T_{\rm RH} \sim \mathcal{O}(1)$ MeV. Therefore, we next look into the dynamics of neutrino thermalization in the thermal plasma.

In the Universe with a temperature of $\mathcal{O}(1)$ MeV, electrons and positrons are the only charged leptons which are abundant in the system since the abundances of muons and tau leptons are strongly suppressed by Boltzmann factors. Therefore, neutrinos are mainly produced in the annihilation process of electrons and positrons, $e^- + e^+ \to \nu_\alpha + \bar{\nu}_\alpha$ where $\alpha = e, \mu, \tau$. Since electron neutrino (ν_e) is not only produced by the neutral-current weak interaction but also by the charged-current one, it tends to be produced more than μ neutrinos (ν_μ) and τ neutrinos (ν_τ) when all neutrinos are not fully thermalized. Consequently, neutrino oscillations play a role in equilibrating neutrino abundances in this case, and we have to simultaneously consider the neutrino production by collisions and flavor oscillations.

Our treatment of neutrino oscillation is consistent with that of Ref. [67]. That is, we adopt the effective two-flavor mixing scheme which is a good description for approximately including full three-flavor mixings when the collision rates of ν_μ and ν_τ are identical, and one mixing angle is predominantly important compared to others (see *e.g.* Ref. [54] for more details on the effective two-flavor mixing scheme). The former condition is well satisfied because of the absence of muons and tau leptons in the system with a temperature of $\mathcal{O}(1)$ MeV. On the other hand, the latter condition is only approximately satisfied since the reactor neutrino mixing θ_{13} is known to be non-negligible compared to other mixings, namely the solar neutrino mixing θ_{12} and the atmospheric neutrino mixing θ_{23} [51]. In later sections, however, we show that the effect of θ_{13} on BBN is very small compared to that of θ_{12} or neutrino self-interaction irrespective of the mass ordering of neutrinos. Therefore, the effective two-flavor mixing scheme (with the solar neutrino mixing) gives a good description of the full three-flavor mixings at least for the current purpose. In this scheme, we label the degenerate state of ν_μ and ν_τ as x neutrinos (ν_x) and consider the flavor mixing between ν_e and ν_x. Also, we label the other neutrino species which does not mix with other flavors as spectator neutrino ($\nu_{\rm sp}$) in this two-flavor treatment.

In general, neutrino states can be described by a one-particle irreducible density matrix $\varrho_{\boldsymbol{p}} \equiv \varrho(p,t)$ where $p \equiv |\boldsymbol{p}|$ is the absolute momentum. [2] Since we focus on the effective two-flavor mixing, the density matrix is expressed in terms of a 2×2 Hermitian matrix, and we label each element of the density matrix as

$$\varrho_{\boldsymbol{p}} = \begin{pmatrix} \rho_{ee} & \rho_{ex} \\ \rho_{ex}^* & \rho_{xx} \end{pmatrix} . \tag{5.1}$$

The diagonal part of the matrix corresponds to the distribution function of mixed neutrinos (namely ν_e and ν_x), that is, $\rho_{ee} = f_{\nu_e}$ and $\rho_{xx} = f_{\nu_x}$, while the off-diagonal elements represent the quantum coherence among neutrinos with different flavors. In this thesis, the chemical potentials of neutrinos are set to be zero. Under this assumption, the density

[2] Since we focus on the Universe with a temperature of $\mathcal{O}(1)$ MeV, we can neglect tiny neutrino masses which are known to be sub-eV scale [29]. In this case, the energy of neutrinos E is equal to its absolute momentum, *i.e.* $E = p$.

matrix of neutrinos is equal to that of anti-neutrinos, *i.e.* $\varrho_{\boldsymbol{p}} = \bar{\varrho}_{\boldsymbol{p}}$, and they have the same abundance. Therefore, it is not necessary to follow the time evolution of anti-neutrinos separately from that of the corresponding neutrinos.

We can obtain the time evolution of the neutrino density matrix by solving the momentum-dependent Quantum Kinetic Equation [56, 57] which is formally written as

$$\frac{d\varrho_{\boldsymbol{p}}}{dt} = \frac{\partial \varrho_{\boldsymbol{p}}}{\partial t} - H\, p \frac{\partial \varrho_{\boldsymbol{p}}}{\partial p} = -i\,[\mathcal{H}_{\boldsymbol{p}}, \varrho_{\boldsymbol{p}}] + C(\varrho_{\boldsymbol{p}})\,. \tag{5.2}$$

In the above equation, the term including the Hubble parameter H corresponds to the effect of the expansion of the Universe, and $C(\varrho_{\boldsymbol{p}})$ is the collision term of neutrinos expressed as

$$C(\varrho_{\boldsymbol{p}}) = \begin{pmatrix} R_{\nu_e} & -D\rho_{ex} \\ -D\rho_{ex}^* & R_{\nu_x} \end{pmatrix}\,, \tag{5.3}$$

where R_{ν_e} and R_{ν_x} are the production rates of ν_e and ν_x, respectively. Also, D is the collisional-damping rate which breaks the flavor coherence among different flavors of neutrinos. In this thesis, we adopt a simplified treatment of the damping effects discussed in Ref. [68] and neglect the additional contributions such as "damping-like terms" which appear in Ref. [57]. In this thesis, we consider the collisional processes $a(k) + b(p) \to c(k') + d(p')$ shown in Table. 5.1 including those of neutrino self-interaction. In this case, the expressions of the repopulation and the damping terms are [72],

$$\begin{aligned} R_{\nu_\alpha}(k) = 2\pi \int d\Pi_{k'} d\Pi_{p'} d\Pi_p\, \delta_E(kp|k'p') \\ \times \sum_i \mathcal{V}^2[\nu_\alpha(k), \bar{\nu}_\alpha(p)|i(k'), \bar{i}(p')]\,[f_i(E_{k'}) f_{\bar{i}}(E_{p'})(1 - f_{\nu_\alpha}(k))(1 - f_{\bar{\nu}_\alpha}(p)) \\ - f_{\nu_\alpha}(k) f_{\bar{\nu}_\alpha}(p)(1 - f_i(E_{k'}))(1 - f_{\bar{i}}(E_{p'}))] \\ + \sum_j \mathcal{V}^2[\nu_\alpha(k), j(p)|\nu_\alpha(k'), j(p')]\,[f_{\nu_\alpha}(k') f_j(E_{p'})(1 - f_{\nu_\alpha}(k))(1 - f_j(E_p)) \\ - f_{\nu_\alpha}(k) f_j(E_p)(1 - f_{\nu_\alpha}(k'))(1 - f_j(E_{p'}))]\,, \end{aligned} \tag{5.4}$$

$$\begin{aligned} D(k) = \pi \sum_\alpha \int d\Pi_{k'} d\Pi_{p'} d\Pi_p\, \delta_E(kp|k'p') \\ \times \sum_i \mathcal{V}^2[\nu_\alpha(k), \bar{\nu}_\alpha(p)|i(k'), \bar{i}(p')]\,[f_i(E_{k'}) f_{\bar{i}}(E_{p'})(1 - f_{\bar{\nu}_\alpha}(p)) \\ + f_{\bar{\nu}_\alpha}(p)(1 - f_{\bar{i}}(E_{p'}))(1 - f_i(E_{k'}))] \\ + \sum_j \mathcal{V}^2[\nu_\alpha(k), j(p)|\nu_\alpha(k'), j(p')]\,[f_{\nu_\alpha}(k') f_j(E_{p'})(1 - f_j(E_p)) \\ + f_j(E_p)(1 - f_j(E_{p'}))(1 - f_{\nu_\alpha}(k'))]\,, \end{aligned} \tag{5.5}$$

	Process ($\alpha \neq \beta$)	$S\,\lvert M\rvert^2$
I.	$e^- + e^+ \to \nu_\alpha + \bar{\nu}_\alpha$	$2^5\, G_{\rm F}^2\, [\,(2\sin^2\theta_W \pm 1)^2 (k\cdot p')(p\cdot k') + 4\sin^4\theta_W (k\cdot k')(p\cdot p')$ $+2\, m_e^2 \sin^2\theta_W (2\sin^2\theta_W \pm 1)(k\cdot p)\,]$
II.	$\nu_\alpha + e^+ \to \nu_\alpha + e^+$	$2^5\, G_{\rm F}^2\, [\,(2\sin^2\theta_W \pm 1)^2 (k\cdot k')(p\cdot p') + 4\sin^4\theta_W (k\cdot p)(k'\cdot p')$ $-2\, m_e^2 \sin^2\theta_W (2\sin^2\theta_W \pm 1)(k\cdot p')\,]$
III.	$\nu_\alpha + e^- \to \nu_\alpha + e^-$	$2^5\, G_{\rm F}^2\, [\,(2\sin^2\theta_W \pm 1)^2 (k\cdot p)(k'\cdot p') + 4\sin^4\theta_W (k\cdot k')(p\cdot p')$ $-2\, m_e^2 \sin^2\theta_W (2\sin^2\theta_W \pm 1)(k\cdot p')\,]$
IV.	$\nu_\alpha + \nu_\alpha \to \nu_\alpha + \nu_\alpha$	$2^6\, G_{\rm F}^2\, (k\cdot p)(k'\cdot p')$
V.	$\nu_\alpha + \nu_\beta \to \nu_\alpha + \nu_\beta$	$2^5\, G_{\rm F}^2\, (k\cdot p)(k'\cdot p')$
VI.	$\nu_\alpha + \overline{\nu}_\alpha \to \nu_\alpha + \overline{\nu}_\alpha$	$2^7\, G_{\rm F}^2\, (k\cdot p')(p\cdot k')$
VII.	$\nu_\alpha + \overline{\nu}_\beta \to \nu_\alpha + \overline{\nu}_\beta$	$2^5\, G_{\rm F}^2\, (k\cdot p')(p\cdot k')$
VIII.	$\nu_\alpha + \overline{\nu}_\alpha \to \nu_\beta + \overline{\nu}_\beta$	$2^5\, G_{\rm F}^2\, (k\cdot p')(p\cdot k')$

Table 5.1: Collision process $a(p) + b(k) \to c(p') + d(k')$ which contributes to the thermalization of neutrinos of each flavor ν_α, ν_β ($\alpha, \beta = e, \mu, \tau$ where $\alpha \neq \beta$). The process I is the production process of neutrinos due to electron annihilation, the processes II - III are the scattering processes between neutrinos and electrons, and the processes IV - VIII are the self-interaction processes among neutrinos. Here, θ_W is the Weinberg angle, $G_{\rm F}$ is the Fermi-coupling constant, S is the symmetry factor, and $|M|^2$ is the squared scattering matrix element. The positive sign in the expression is for ν_e and the minus sign for ν_μ or ν_τ (*i.e.* for ν_x and $\nu_{\rm sp}$). The expressions of the process I, II, IV, and V are also applied to the corresponding anti-neutrinos.

where $\alpha = e, x$, and k, p, k', and p' are absolute momenta of the particle a, b, c, and d, respectively. Also, $d\Pi_p \equiv \frac{d^3\boldsymbol{p}}{(2\pi)^3}$, and $\delta_E(kp|k'p') \equiv \delta^{(1)}(E_k + E_p - E_{k'} - E_{p'})$ is the 1D Dirac delta function corresponding to energy conservation for each process. The summation index i runs over electrons and all flavors of neutrinos other than ν_α (*i.e.* ν_β where $\beta \neq \alpha$), while j runs in addition over positrons, ν_α, and all flavors of anti-neutrinos. The expression of $\mathcal{V}^2$ is written as

$$\mathcal{V}^2[a(p), b(k)|c(p'), d(k')] = (2\pi)^3 \delta^{(3)}(k+p, k'+p') N_a^2 N_b^2 N_c^2 N_d^2 S|M|^2(a(p), b(k)|c(p'), d(k'))\,, \tag{5.6}$$

where $S|M|^2(a(p), b(k)|c(p'), d(k'))$ is the squared scattering matrix element for the processes in Table. 5.1 summed over initial and final spins, and symmetrized over identical particles in the initial and the final state. Also, $N_i \equiv \sqrt{1/2E_i}$ where E_i is the energy of particle i ($i = a, b, c, d$) and $\delta^{(3)}(k+p, k'+p') \equiv \delta^{(3)}(\boldsymbol{k}+\boldsymbol{p}-\boldsymbol{k}'-\boldsymbol{p}')$ is the 3D Dirac delta function corresponding to the momentum conservation. As for the processes in Table. 5.1, we analytically reduce the dimension of momentum integrals in the above expressions from nine to two and calculate the full collision terms without any simplifying assumptions in the same way as in Ref. [72].

In the expression of Eq. (5.2), $\mathcal{H}_{\boldsymbol{p}}$ is neutrino Hamiltonian which is expressed as

$$\mathcal{H}_{\boldsymbol{p}} = \mathcal{H}_{\boldsymbol{p},\,\mathrm{vac}} + \mathcal{H}_{\boldsymbol{p},\,\mathrm{mat}} = \frac{\mathsf{M}^2}{2p} - \frac{8\sqrt{2}\,G_{\mathrm{F}}p}{3}\left[\frac{\boldsymbol{E}_l}{m_W^2} + \frac{\boldsymbol{E}_\nu}{m_Z^2}\right] + \sqrt{2}\,G_{\mathrm{F}}\int d\Pi_{p'}(\varrho_{\boldsymbol{p}'} - \bar{\varrho}^*_{\boldsymbol{p}'})\,, \quad (5.7)$$

where G_{F} is the Fermi-coupling constant. Also, m_W and m_Z are the masses of W and Z bosons, respectively. In the above expression, the first term, $\mathcal{H}_{\boldsymbol{p},\,\mathrm{vac}}$, is the contribution which induces the vacuum oscillation where M is the mass matrix in flavor basis. The mass matrix M is related to the one in mass basis $\mathcal{M}$ as $\mathsf{M}^2 = U\mathcal{M}^2U^\dagger$ where U is the PMNS matrix. In the effective two-flavor mixing scheme,

$$\mathcal{M}^2 = \begin{pmatrix} m_1^2 & 0 \\ 0 & m_2^2 \end{pmatrix}\,,\; U = \begin{pmatrix} \cos\theta & \sin\theta \\ -\sin\theta & \cos\theta \end{pmatrix}\,, \quad (5.8)$$

where $\delta m^2 \equiv m_2^2 - m_1^2$ is the squared-mass difference and θ is the mixing angle in a vacuum between ν_e and ν_x. Also, the second term in the Hamiltonian, $\mathcal{H}_{\boldsymbol{p},\,\mathrm{mat}}$, corresponds to the matter potentials which arise from coherent scatterings between neutrinos and charged-leptons. In the term, $\boldsymbol{E}_l$ corresponds to the total energy density of charged leptons, while $\boldsymbol{E}_\nu$ to that of neutrinos:

$$\boldsymbol{E}_l = \begin{pmatrix} \rho_e & 0 \\ 0 & 0 \end{pmatrix}\,,\; \boldsymbol{E}_\nu = \int d\Pi_{p'}\,p'\,(\varrho_{\boldsymbol{p}'} + \bar{\varrho}^*_{\boldsymbol{p}'}) = \begin{pmatrix} \rho_{\nu_e} & \rho_{\nu_{ex}} \\ \rho^*_{\nu_{ex}} & \rho_{\nu_x} \end{pmatrix}\,, \quad (5.9)$$

where $\rho_e = \rho_{e^-} + \rho_{e^+}$ is the total energy density of electrons and positrons, while ρ_{ν_e} and ρ_{ν_x} are those of ν_e and ν_x, respectively. Also, we have defined $\rho_{\nu_{ex}} \equiv \int d\Pi_{p'}\,p'\,(\rho_{ex} + \bar{\rho}^*_{ex})$ and $\rho^*_{\nu_{ex}} \equiv \int d\Pi_{p'}\,p'\,(\rho^*_{ex} + \bar{\rho}_{ex})$. In the expression of $\boldsymbol{E}_l$, we have neglected the existence of muons or tau leptons due to their large masses. [3] The asymmetric part of $\mathcal{H}_{\boldsymbol{p},\,\mathrm{mat}}$ is often assumed to vanish when $\rho = \bar{\rho}$ for neutrinos and the number density of electrons and positrons are identical. For the diagonal part of the Hamiltonian this is true, however the off-diagonal part gets a contribution from the neutrinos as shown in Eq. (5.7) since $\varrho^*_{\boldsymbol{p}} \neq \varrho_{\boldsymbol{p}}$.

As for the oscillation parameters, we use the best fit values of the mass-squared differences and mixing angles reported in Ref. [51]: [4]

$$\delta m^2_{12} = 7.55 \times 10^{-5}\ \mathrm{eV}^2\,,\quad \sin^2\theta_{12} = 3.20 \times 10^{-1}\,, \quad (5.10)$$
$$\delta m^2_{13} = 2.50 \times 10^{-3}\ \mathrm{eV}^2\,,\quad \sin^2\theta_{13} = 2.160 \times 10^{-2}\ \ (\mathrm{NO})\,, \quad (5.11)$$
$$\delta m^2_{13} = -2.42 \times 10^{-3}\ \mathrm{eV}^2\,,\quad \sin^2\theta_{13} = 2.220 \times 10^{-2}\ \ (\mathrm{IO})\,, \quad (5.12)$$

[3] In the effective two-flavor mixing scheme, we need to treat both ν_μ and ν_τ in the same way. Therefore, we do not consider background muons or tau leptons whose contribution is very small compared to that of electrons.

[4] The atmospheric neutrino mixing $(\theta_{23}, \delta m^2_{23})$ is irrelevant to the oscillation between ν_e and ν_x in the effective two-flavor mixing scheme. Therefore, we do not use the value in this thesis.

where "NO" ("IO") means normal (inverted) mass ordering of neutrinos, respectively. For the numerical calculation, we rewrite the 2×2 density matrix with polarization vectors $(P_0, \boldsymbol{P})$:

$$\varrho_{\boldsymbol{p}} = \begin{pmatrix} \rho_{ee} & \rho_{ex} \\ \rho_{ex}^* & \rho_{xx} \end{pmatrix} = \frac{1}{2} \left[P_0(p)\, \sigma_0 + \boldsymbol{P}(p) \cdot \boldsymbol{\sigma} \right], \tag{5.13}$$

where $\sigma_0 = \mathbf{1}$ is the identity matrix and $\boldsymbol{\sigma} = (\sigma_x, \sigma_y, \sigma_z)$ are the Pauli matrices. With $\boldsymbol{P} = (P_x, P_y, P_z)$, distribution functions of mixed neutrinos can be written as

$$f_{\nu_e} = \frac{1}{2}(P_0 + P_z) \ , \ f_{\nu_x} = \frac{1}{2}(P_0 - P_z) \, . \tag{5.14}$$

Also, we can rewrite the expression of Eq. (5.2) as follows:

$$\dot{\boldsymbol{P}} = \overrightarrow{\mathcal{H}} \times \boldsymbol{P} - D \left(P_x \, \mathbf{x} + P_y \, \mathbf{y} \right) + \left(R_{\nu_e} - R_{\nu_x} \right) \mathbf{z} \, , \tag{5.15}$$

$$\dot{P}_0 = R_{\nu_e} + R_{\nu_x} \, , \tag{5.16}$$

which leads to

$$\dot{P}_{\nu_e} = \mathcal{H}_x \, P_y - \mathcal{H}_y \, P_x + 2 \, R_{\nu_e} \, , \tag{5.17}$$

$$\dot{P}_{\nu_x} = \mathcal{H}_y \, P_x - \mathcal{H}_x \, P_y + 2 \, R_{\nu_x} \, , \tag{5.18}$$

$$\dot{P}_x = \frac{1}{2} \, \mathcal{H}_y \left(P_{\nu_e} - P_{\nu_x} \right) - \mathcal{H}_z \, P_y - D \, P_x \, , \tag{5.19}$$

$$\dot{P}_y = \mathcal{H}_z \, P_x - \frac{1}{2} \, \mathcal{H}_x \left(P_{\nu_e} - P_{\nu_x} \right) - D \, P_y \, , \tag{5.20}$$

where $\mathbf{x}, \mathbf{y}$ and $\mathbf{z}$ are unit vectors, and we defined $P_{\nu_e} \equiv P_0 + P_z$ and $P_{\nu_x} \equiv P_0 - P_z$. Each component of the neutrino potential $\overrightarrow{\mathcal{H}}$, *i.e.* $\mathcal{H}_i = \mathrm{Tr} \left(\mathcal{H}_{\boldsymbol{p}} \, \sigma_i \right)$ where $i = x, y, z$, is written as

$$\mathcal{H}_x = \frac{\delta m^2}{2p} \sin 2\theta - \frac{16\sqrt{2} \, G_{\rm F} \, p}{3 \, m_Z^2} \int d\Pi_{p'} \, p' P_x \, , \tag{5.21}$$

$$\mathcal{H}_y = 2\sqrt{2} \, G_{\rm F} \int d\Pi_{p'} \, P_y \, , \tag{5.22}$$

$$\mathcal{H}_z = -\frac{\delta m^2}{2p} \cos 2\theta + \mathcal{H}_{\rm mat} \, . \tag{5.23}$$

The second term in $\mathcal{H}_z$ is the matter contribution which is explicitly written as

$$\mathcal{H}_{\rm mat} = -\frac{8\sqrt{2}}{3} G_{\rm F} \, p \left[\frac{\rho_e}{m_W^2} + \frac{\rho_{\nu_e} - \rho_{\nu_x}}{m_Z^2} \right] \tag{5.24}$$

$$= -\frac{4\sqrt{2}}{3 \, \pi^2} G_{\rm F} \, p \left[\frac{g_e}{m_W^2} \int_0^\infty dp' \, p'^2 \frac{E_e}{\exp(E_e/T_\gamma) + 1} + \frac{g_\nu}{m_Z^2} \int_0^\infty dp' \, p'^3 (f_{\nu_e} - f_{\nu_x}) \right] , \tag{5.25}$$

where T_γ is the photon temperature, and $E_e = \sqrt{p^2 + m_e^2}$ is the energy of electrons. Also, $g_e = 4$ is the statistical degree of freedom of electrons and $g_\nu = 2$ is that of neutrinos of each flavor.

With the matter potential $\mathcal{H}_{\rm mat}$, the mass-squared difference and the mixing angle in a vacuum are modified in a medium by MSW effect as follows [52, 53]:

$$\frac{\delta m_M^2}{2p} = \sqrt{\left(\frac{\delta m^2}{2p}\right)^2 \sin^2 2\theta + \left(-\frac{\delta m^2}{2p}\cos 2\theta + \mathcal{H}_{\rm mat}\right)^2} \ , \tag{5.26}$$

$$\sin^2 2\theta_M = \frac{\left(\frac{\delta m^2}{2p}\right)^2 \sin^2 2\theta}{\left(\frac{\delta m^2}{2p}\right)^2 \sin^2 2\theta + \left(-\frac{\delta m^2}{2p}\cos 2\theta + \mathcal{H}_{\rm mat}\right)^2} \ , \tag{5.27}$$

where δm_M^2 and θ_M are the in-medium mass-squared difference and the mixing angle, respectively. We note here that in Eqs. (5.26)–(5.27) we simplify the expressions by neglecting the small contributions of the off-diagonal part of the matter potential $\mathcal{H}_{\boldsymbol{p},\,\rm mat}$ in Eq. (5.7) (see Ref. [54] for the exact expressions of the MSW effect). As can be seen from Eqs. (5.26) and (5.27), the matter potential $|\mathcal{H}_{\rm mat}| \propto T_\gamma^5$ dominates the vacuum one $|\mathcal{H}_{\rm vac}| \equiv |-\frac{\delta m^2}{2p}\cos 2\theta| \propto T_\gamma^{-1}$, *i.e.* $|\mathcal{H}_{\rm mat}| >> |\mathcal{H}_{\rm vac}|$, at high temperature such as $T_\gamma > \mathcal{O}(10)$ MeV and $\theta_M \sim 0$ holds for most energy modes. [5] On the other hand, the opposite hierarchy, *i.e.* $|\mathcal{H}_{\rm vac}| >> |\mathcal{H}_{\rm mat}|$, holds at low temperature and the mixing parameters take the same values as those in a vacuum: $\theta_M \sim \theta$, $\delta m_M^2 \sim \delta m^2$. For neutrinos with momentum $p = \langle p \rangle \sim 3.15\, T_\gamma$ where $\langle \cdot \rangle$ means a thermal average, the level crossing between these potentials, *i.e.* $|\mathcal{H}_{\rm mat}| \sim |\mathcal{H}_{\rm vac}|$, occurs at the temperature $T_{\rm c}$

$$T_{\rm c} \ \sim \ G_{\rm F}^{-1/3}(\delta m^2 \cos 2\theta)^{1/6} \ \sim \ \begin{cases} 3 \text{ MeV} \left(\frac{\delta m_{12}^2}{2.5\times 10^{-3}\ \text{eV}^2}\right)^{1/6} \\ 5 \text{ MeV} \left(\frac{\delta m_{13}^2}{7.5\times 10^{-5}\ \text{eV}^2}\right)^{1/6} \end{cases} , \tag{5.28}$$

where, in the above evaluation, we have replaced p with $\langle p \rangle \sim 3.15\, T_\gamma$ and approximated $(\cos 2\theta)^{1/6} \ \sim \ 1$ which is well satisfied for θ_{12} and θ_{13}. Therefore, neutrino oscillation becomes effective at around a temperature of $\mathcal{O}(1)$ MeV for the solar neutrino mixing $(\theta_{12}, \delta m_{12})$ and the reactor neutrino mixing $(\theta_{13}, \delta m_{13})$, which is the reason for taking its effect on the neutrino thermalization into account.

On the other hand, since $\nu_{\rm sp}$ decouple from flavor mixings of neutrinos, the time evolution of this neutrino species is just given by the classical Boltzmann equation:

$$\frac{df_{\nu_{\rm sp}}}{dt} = \frac{\partial f_{\nu_{\rm sp}}}{\partial t} - H\, p \frac{\partial f_{\nu_{\rm sp}}}{\partial p} = C(f_{\nu_{\rm sp}}) \,, \tag{5.29}$$

where $f_{\nu_{\rm sp}}$ is the distribution function of $\nu_{\rm sp}$, and $C(f_{\nu_{\rm sp}})$ is the collision term whose expression is equal to that of ν_x, *i.e.* $C(f_{\nu_{\rm sp}}) = R_{\nu_x}$ (see Eq. (5.4)).

[5] We assume here that the neutrinos are thermalized with photons and have a temperature T_γ for simplicity.

To calculate the thermalization process of neutrinos in the expanding Universe, we also need to compute the energy conservation equation:

$$\frac{d\rho}{dt} = -3H(\rho + P)\,, \tag{5.30}$$

which can be expressed as the time evolution of the photon temperature T_γ:

$$\frac{dT_\gamma}{dt} = -\frac{-\Gamma_X \rho_X + 4H(\rho_\gamma + \rho_\nu) + 3H(\rho_e + P_e) + \frac{d\rho_\nu}{dt}}{\frac{\partial \rho_\gamma}{\partial T_\gamma}|_{a(t)} + \frac{\partial \rho_e}{\partial T_\gamma}|_{a(t)}}\,, \tag{5.31}$$

where $a(t)$ is the scale factor at the cosmic time t, Γ_X is the decay rate of the massive particles, whereas ρ and P are the total energy density and the total pressure, respectively:

$$\begin{aligned}
\rho &= \rho_\gamma + \rho_e + \rho_\nu + \rho_X \\
&= \frac{\pi^2}{15} T_\gamma^4 + \frac{g_e}{2\pi^2}\int_0^\infty dp'\, p'^2 \frac{E_e}{\exp(E_e/T_\gamma)+1} \\
&\qquad + \frac{g_\nu}{2\pi^2}\int_0^\infty dp'\, p'^3 (f_{\nu_e} + f_{\nu_x} + f_{\nu_{\rm sp}}) + \rho_X\,, \qquad (5.32) \\
P &= P_\gamma + P_e + P_\nu \\
&= \frac{\pi^2}{45} T_\gamma^4 + \frac{g_e}{6\pi^2}\int_0^\infty dp'\, \frac{p'^4}{E_e} \frac{1}{\exp(E_e/T_\gamma)+1} \\
&\qquad + \frac{g_\nu}{6\pi^2}\int_0^\infty dp'\, p'^3 (f_{\nu_e} + f_{\nu_x} + f_{\nu_{\rm sp}})\,. \qquad (5.33)
\end{aligned}$$

Here, $\rho_\gamma(P_\gamma)$, $\rho_e(P_e)$, $\rho_\nu(P_\nu)$ and ρ_X mean the energy density (pressure) of photons, electrons, neutrinos and the massive particles, respectively. The total energy density and the total pressure of neutrinos are a sum of three contributions: $\rho_\nu = \rho_{\nu_e} + \rho_{\nu_x} + \rho_{\nu_{\rm sp}}$, $P_\nu = P_{\nu_e} + P_{\nu_x} + P_{\nu_{\rm sp}}$. With the total energy density, the Hubble parameter H is obtained by solving the Friedmann equation:

$$H \equiv \frac{\dot{a}}{a} = \sqrt{\frac{8\pi G \rho}{3}}\,. \tag{5.34}$$

In the above expression, we can obtain the time evolution of ρ_X by solving the Boltzmann equation of the massive particles X:

$$\frac{d\rho_X}{dt} = -\Gamma_X \rho_X - 3H\rho_X\,, \tag{5.35}$$

which can be integrated analytically for non-relativistic particles X:

$$\frac{\rho_X}{s} = \frac{\rho_{X,0}}{s_0}\, e^{-\Gamma_X t}\,, \tag{5.36}$$

where $\rho_{X,0}$ and s_0 are respectively the initial energy- and entropy density of X, and $\rho_{X,0}$ is assumed to be much larger than those of other particles, *i.e.* $\rho_{X,0} >> (\rho_\gamma + \rho_e + \rho_\nu)_{t=0}$. In addition, Γ_X is related to $T_{\rm RH}$ through the Hubble parameter $H = H(T_{\rm RH})$ as follows:

$$\Gamma_X = 3H\,. \tag{5.37}$$

Since the energy density of the Universe is dominated by radiation components after most of the massive particles decayed and $T_\gamma \sim T_{\rm RH}$ is realized, we can approximately write the Hubble parameter as

$$H = \sqrt{\frac{g^*\pi^2}{90}}\frac{T_{\rm RH}^2}{m_{\rm pl}}\,, \tag{5.38}$$

where $m_{\rm pl} \sim 2.435\times10^{18}$ GeV is the reduced Planck mass, and $g^* = 10.75$ is the relativistic degrees of freedom in the Universe with a temperature of $\mathcal{O}(1)$ MeV. Hence, the relation between $T_{\rm RH}$ and the decay rate of X is approximately written as

$$T_{\rm RH} \sim 0.7\left(\frac{\Gamma_X}{\rm sec^{-1}}\right)^{1/2}\ {\rm MeV}\,. \tag{5.39}$$

From the above expression, we can see that $T_{\rm RH} \sim \mathcal{O}(1)$ MeV corresponds to the lifetime of the massive particles $\tau_X = \Gamma_X^{-1} \sim \mathcal{O}(1)$ sec. [6] It should be worth noticing that the reheating temperature defined by Eq. (5.39) is just a rough estimate of the cosmic temperature when the reheating is completed. Therefore, the definition of the reheating temperature includes a systematic error at or below the level of $\mathcal{O}(1)$ %. On the other hand, this error is irrelevant to the observational constraint in terms of the decay rate of X, Γ_X, or the lifetime of X, τ_X, as these parameters are 'directly' related to the final result of BBN.

To obtain the neutrino distribution functions and a degree of the neutrino thermalization in the reheating, we simultaneously solve the Eqs. (5.17), (5.18), (5.19), (5.20), (5.29), (5.31), (5.34) and (5.36) from the initial time $t = 10^{-4}$ sec to the final time $t = 10^7$ sec corresponding to the cosmic time well before and after BBN, respectively. We find that the final results are independent of the choice of the initial time as long as the initial temperature of electromagnetic particles is much higher than $T_{\rm RH}$. Besides, we divide the energy range of neutrinos into 100 bins and calculate the kinetic equation for each bin. This means that we must simultaneously compute more than 400 equations in the code. Furthermore, we set the maximum- and the minimum values of the neutrino energies depending on the value of the reheating temperature, but we guarantee that the maximum- and minimum values respectively satisfy the relations $p_{\rm max} > 30\ T_\gamma$ and $p_{\rm min} < 10^{-2}\ T_\gamma$ at all times for numerical convergence. As for the initial energy density of the massive particle ρ_X, we assume that the massive particle X has an initial energy density 1000 times larger than the total energy density of radiations, $\rho_{\rm rad} = \rho_\gamma + \rho_e + \rho_\nu$. This choice of ρ_X gives convergent results of the neutrino thermalization. We have checked a numerical accuracy

[6] Since the actual value of g^* depends on the value of $T_{\rm RH}$, Eq. (5.37) just gives a rough estimate of when the radiation-dominated epoch is realized.

of $\mathcal{O}(10^{-2})\%$ level for each input parameter mentioned above, which is much smaller than the theoretical- and observational errors in the light element abundances. Therefore, numerical results should be accurate enough to guarantee a precision of $\mathcal{O}(0.1)\%$ level for the lower bound on the reheating temperature.

To calculate neutrino thermalization processes, we use a modified version of the LASAGNA code [73, 74] which is, in the original version, a solver of ordinary differential equations for calculating sterile neutrino production in the early Universe. The LASAGNA code contains three types of ODE solvers. Two of them are based on the fourth-order explicit- and implicit Runge-Kutta methods, and the other is based on the implicit method which depends on the numerical differential formulae (ndf) of order 1–5, developed by Shampine [75] (see Refs. [73, 74] for more details). This time, we use the ndf solver because the solver is suitable for integrating stiff ODEs and it is numerically efficient.

In the next section, we show our numerical results of the neutrino thermalization and BBN in the low-reheating-temperature Universe.

5.3 Results: neutrino thermalization in the reheating

In this section, we show our numerical results of neutrino thermalization. To express the time evolution of the neutrino thermalization, we define the effective number of neutrino species $N_{\rm eff}$:

$$N_{\rm eff} = N_{{\rm eff},\,\nu_e} + N_{{\rm eff},\,\nu_x} + N_{{\rm eff},\,\nu_{\rm sp}} = \sum_{\alpha\,=\,e,\,x,\,{\rm sp}} \rho_{\nu_\alpha}/\rho_{\nu_{\alpha,\,{\rm std}}}\,, \tag{5.40}$$

where $N_{{\rm eff},\,\nu_\alpha}$ is the contribution for each neutrino species, and $\rho_{\nu_{\alpha,\,{\rm std}}}$ is the energy density of each neutrino species in the standard big-bang cosmology. [7] The value of $N_{\rm eff}$ is almost equal to the actual number of neutrino species when all neutrinos are fully thermalized.

Figure 5.2 shows the relation between $T_{\rm RH}$ and $N_{\rm eff}$ for the cases with and without neutrino self-interaction. As shown in Figure 5.2, the value of $N_{\rm eff}$ increases as $T_{\rm RH}$ becomes large, and the value is almost equal to 3.046 above $T_{\rm RH} \gtrsim 10$ MeV which is the canonical value in the standard big-bang cosmology with large $T_{\rm RH}$ [76, 77]. The above threshold value of $T_{\rm RH}$ arises from the fact that weak reaction processes which are responsible for the neutrino thermalization decouple at around a temperature $T_{\rm dec}$ given by $\Gamma_{\rm weak}/H \sim G_F^2 T_{\rm dec}^5/(T_{\rm dec}^2/m_{\rm pl}) \sim 1$, *i.e.* $T_{\rm dec} \sim (G_F^2 m_{\rm pl})^{-\frac{1}{3}} \sim \mathcal{O}(1)$ MeV where $\Gamma_{\rm weak}$ is the thermal reaction rate of weakly-interacting particles. Therefore, if $T_{\rm RH}$ is larger than $T_{\rm dec}$, neutrinos have enough time to be fully thermalized before decoupling. Also, it can be seen from Figure 5.2 that both neutrino oscillation and neutrino self-interaction increase the value of $N_{\rm eff}$. This is because the production rate of ν_e is larger than that of ν_x ($R_{\nu_e} > R_{\nu_x}$), and thereby neutrino oscillation increases the total production rate of neutrinos $R_{\nu,\,{\rm tot}}$ ($\equiv R_{\nu_e} + R_{\nu_x}$). To understand this effect more quantitatively, let us assume that all neutrino

[7] The energy density of ν_e is slightly larger than those of ν_x and $\nu_{\rm sp}$ after electron annihilation due to the larger reaction rate of ν_e with electrons. Therefore, we discriminate among $\rho_{\nu_{\alpha,\,{\rm std}}}$ with different flavors.

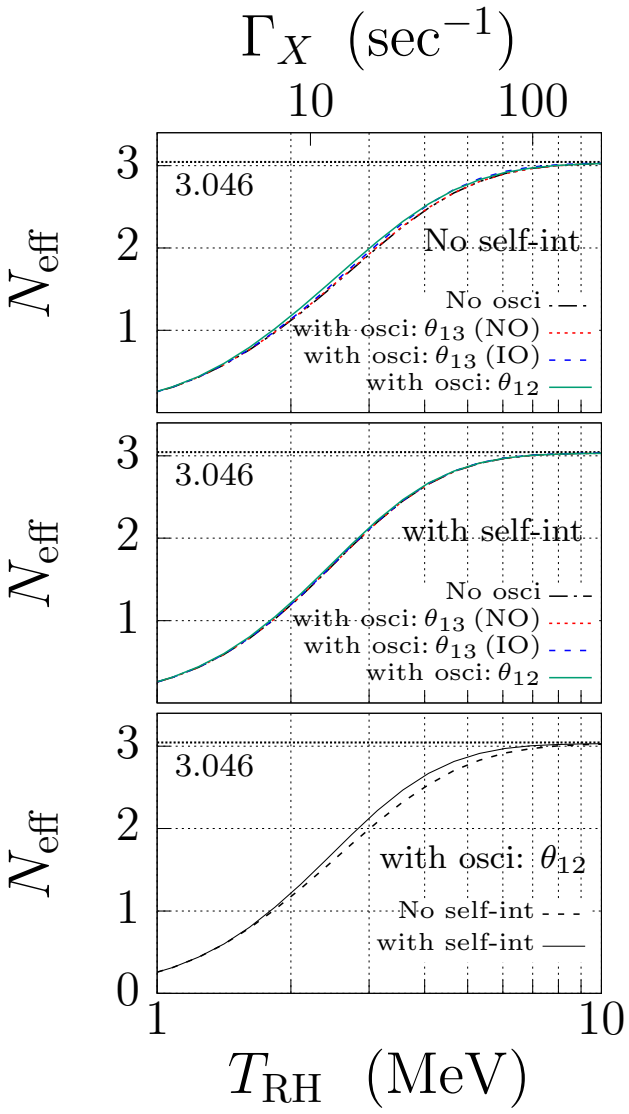

Figure 5.2: Relations between $T_{\rm RH}$ and $N_{\rm eff}$. The top- and middle panels respectively show the effect of neutrino oscillation in the case without and with neutrino self-interaction, while the bottom one shows the effect of neutrino self-interaction in the case with $(\delta m^2_{12}, \theta_{12})$. The canonical value $N_{\rm eff} = 3.046$ [76] is also plotted with the black dotted horizontal line.

species are almost thermalized. In this case, we can approximate the production rates of ν_e and ν_x as [78]

$$R_{\nu_e} \sim C_e G_F^2 T_\gamma^5 (f_{\rm eq} - f_{\nu_e}) \,, \tag{5.41}$$

$$R_{\nu_x} \sim C_x G_F^2 T_\gamma^5 (f_{\rm eq} - f_{\nu_x}) \,, \tag{5.42}$$

where $f_{\rm eq}$ is the Fermi-Dirac distribution $f_{\rm eq} = 1/(1 + \exp(p/T_\gamma))$, and f_{ν_e} and f_{ν_x}

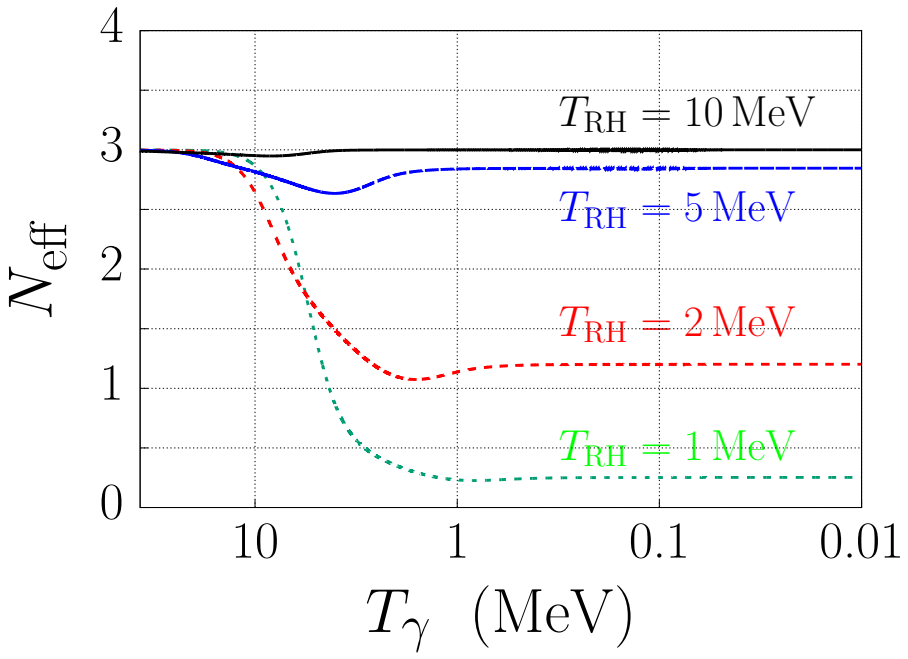

Figure 5.3: Time evolution of $N_{\rm eff}$ for each value of $T_{\rm RH}$. The black solid line is for $T_{\rm RH} = 10$ MeV, the blue long-dashed line is for $T_{\rm RH} = 5$ MeV, the red middle-dashed line is for $T_{\rm RH} = 2$ MeV, and the green short-dashed line is for $T_{\rm RH} = 1$ MeV. Neutrino oscillation with $(\delta m^2_{12}, \theta_{12})$ and neutrino self-interaction are considered in the calculation.

are distribution functions of ν_e and ν_x, respectively. Also, $C_e \sim 1.27$ is the collision coefficient for ν_e and $C_x \sim 0.92$ is that for ν_x [79]. By denoting the effect of neutrino oscillation at a certain time by $\Delta f \equiv f_\nu|_{\rm with\,osci} - f_\nu|_{\rm no\,osci} \equiv -\Delta f_{\nu_e} = \Delta f_{\nu_x}$, we can evaluate the effect of neutrino oscillation on the total production rate of neutrinos $\Delta R_{\nu,\,\rm tot} \equiv R_{\nu,\,\rm tot}|_{\rm with\,osci} - R_{\nu,\,\rm tot}|_{\rm no\,osci} = (R_{\nu_e}|_{\rm with\,osci} + R_{\nu_x}|_{\rm with\,osci}) - (R_{\nu_e}|_{\rm no\,osci} + R_{\nu_x}|_{\rm no\,osci}) = (R_{\nu_e}|_{\rm with\,osci} - R_{\nu_e}|_{\rm no\,osci}) + (R_{\nu_x}|_{\rm with\,osci} - R_{\nu_x}|_{\rm no\,osci}) \equiv \Delta R_{\nu_e} + \Delta R_{\nu_x}$ as follows:

$$\begin{aligned} \Delta R_{\nu,\,\rm tot} &= \Delta R_{\nu_e} + \Delta R_{\nu_x} \\ &\sim G_F^2 T_\gamma^5 (-C_e \Delta f_{\nu_e} - C_x \Delta f_{\nu_x}) \\ &= G_F^2 T_\gamma^5 (C_e - C_x) \Delta f \,. \end{aligned} \tag{5.43}$$

As we can see from the expression, the quantity $\Delta R_{\nu,\,\rm tot}$ is larger than zero when $\Delta f = f_{\nu_e} - f_{\nu_x} > 0$ which holds if the reheating temperature is sufficiently low for neutrinos to be fully thermalized and thereby $f_{\nu_e} > f_{\nu_x}$. Consequently, we can see that neutrino oscillation increases the total production rate of neutrinos unless all neutrinos are completely thermalized. Neutrino self-interaction plays a role similar to neutrino oscillation. That is, they equilibrate abundances of neutrinos among themselves and enhance the thermalization of neutrinos in the same way as neutrino oscillation.

We can also see from Figure 5.2 that the effect of θ_{13} is much smaller than that of θ_{12} or neutrino self-interaction. This is true independent of the neutrino mass ordering. The relative differences of effects among different mixings can be understood as follows: If the vacuum term ($\mathcal{H}_{\rm vac}$) dominates other matter terms ($\mathcal{H}_{\rm mat}$) and neutrino oscillation occur adiabatically, the effective transition rate of neutrinos from one flavor to another (*i.e.* $\nu_\alpha \to \nu_\beta$ where $\alpha \neq \beta$) due to neutrino oscillation can be written as [80]

$$\Gamma_{\rm trans} = \frac{1}{4} \sin 2\theta \, \Gamma_{\rm coll} \,, \tag{5.44}$$

where $\Gamma_{\rm coll}$ is the collision rate of neutrinos. Therefore, the value of the mixing angle solely determines how large oscillation happens in this case. As we can see from Eqs. (5.10)-(5.12), the value of $\sin^2 \theta_{12}$ is almost ten times larger than that of $\sin^2 \theta_{13}$. That is the reason that the effect of θ_{12} on the neutrino thermalization is larger than θ_{13} in the case of normal mass ordering. In the case of inverted mass ordering, neutrino oscillation proceeds via MSW resonance, and non-adiabatic effects can be important. As for this point, authors in Ref. [54] evaluated the adiabaticity of the MSW resonance and concluded that the non-adiabatic effects are negligible. Therefore, an efficient oscillation should occur when a large population of neutrinos goes through the resonance even if we adopt the reactor neutrino mixing θ_{13}. Since the MSW resonance happens at around a temperature of $T_c \sim 5$ MeV for neutrino with $p = \langle p \rangle \sim 3.15\, T_\gamma$, we can expect larger oscillation effects in the case of θ_{13} (IO) at $T_{\rm RH} < T_c$, which in fact can be seen in Figure 5.2.

Figure 5.4 shows the time evolution of $N_{\rm eff}$, and Figure 5.4 is the same as Figure 5.3, but for the contribution for each neutrino species $N_{{\rm eff},\nu_\alpha}$ ($\alpha = e$, x, sp). Since the final abundance of neutrinos does not depend on the condition before reheating, we assume that neutrinos have thermal spectra (*i.e.* Fermi-Dirac distributions) at the initial time. We can see from Figure 5.3 that the value of $N_{\rm eff}$ decreases until $T_{\rm RH}$ is realized. This is due to the entropy production from decays of the massive particles. The value of $N_{\rm eff}$ then increases at $T_\gamma < T_{\rm RH}$ until neutrinos are decoupled from other particles at around a few MeV. This corresponds to the upturn behavior in the evolution of $N_{\rm eff}$. Besides, we can see from the evolution of $N_{{\rm eff},\nu_\alpha}$ in Figure 5.4 that neutrino oscillation becomes effective at around a temperature of a few MeV, whereas neutrino self-interaction becomes effective at higher temperature. The former is because, as we have discussed in the previous section, neutrino oscillation with the solar neutrino mixing $(\delta m^2_{12}, \theta_{12})$ is effective when the photon temperature is lower than $T_c \sim 3$ MeV. The latter is due to the reason that the reaction rates of neutrino self-interactions monotonically increase with the photon temperature.

The role of neutrino oscillation and neutrino self-interaction is shown in Figure 5.5, where we plot final energy spectra of neutrinos for the cases with and without neutrino oscillation or neutrino self-interaction. The energy spectra are evaluated at $T_\gamma \sim 10^{-2}$ MeV which corresponds to the epoch well after electron annihilation. In the case of $T_{\rm RH} = 2$ MeV, both of these effects decrease the difference in neutrino abundances. On the other hand, if $T_{\rm RH}$ is large enough (*e.g.* $T_{\rm RH} = 10$ MeV), neutrinos are almost completely thermalized well before decoupling. Therefore, neutrino oscillation or neutrino self-interaction plays no role in the final abundance of neutrinos.

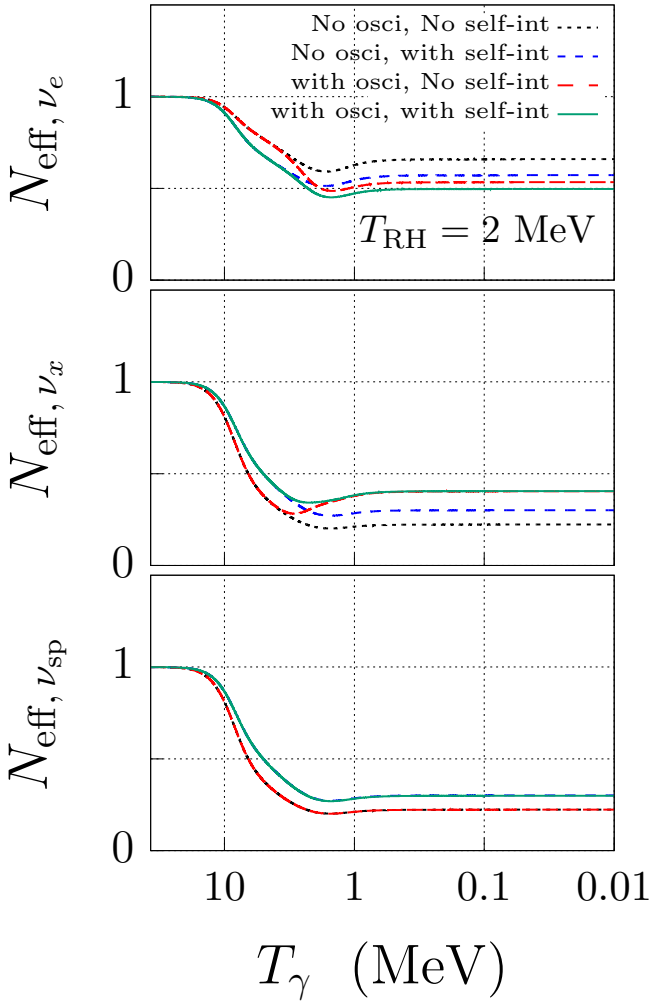

Figure 5.4: Time evolution of $N_{\mathrm{eff},\,\nu_\alpha}$ for $T_{\rm RH} = 2$ MeV. $N_{\mathrm{eff},\,\nu_e}$ (top panel) is for ν_e, $N_{\mathrm{eff},\,\nu_x}$ (middle panel) is for ν_x and $N_{\mathrm{eff},\,\nu_{\rm sp}}$ (bottom panel) is for $\nu_{\rm sp}$. In the red long-dashed and green solid lines, neutrino oscillation with $(\delta m^2_{12}, \theta_{12})$ is taken into account, and neutrino self-interaction is considered in the blue middle-dashed and green solid lines. In the figure of $N_{\mathrm{eff},\,\nu_{\rm sp}}$, the black short-dashed (blue middle-dashed) and red long-dashed (green solid) lines are overlapping.

Figure 5.6 shows the dependence of the mean energy of ν_e, ν_x and $\nu_{\rm sp}$(*i.e.* $\rho_{\nu_\alpha}/n_{\nu_\alpha}$) on $T_{\rm RH}$. The quantity $R_{\rm dist}$ on the vertical axis was introduced to measure the distortion in the final energy spectrum of neutrinos in Ref. [27], and it is defined as

$$R_{\rm dist} = \frac{1}{3.15\, T_{\nu,\,\rm eff}} \frac{\rho_\nu}{n_\nu}\,, \tag{5.45}$$

where $T_{\nu,\,\rm eff}$ is the effective temperature of neutrinos $T_{\nu,\,\rm eff} = [\frac{4\pi^2}{3\zeta(3)} n_\nu]^{1/3}$. As we can see

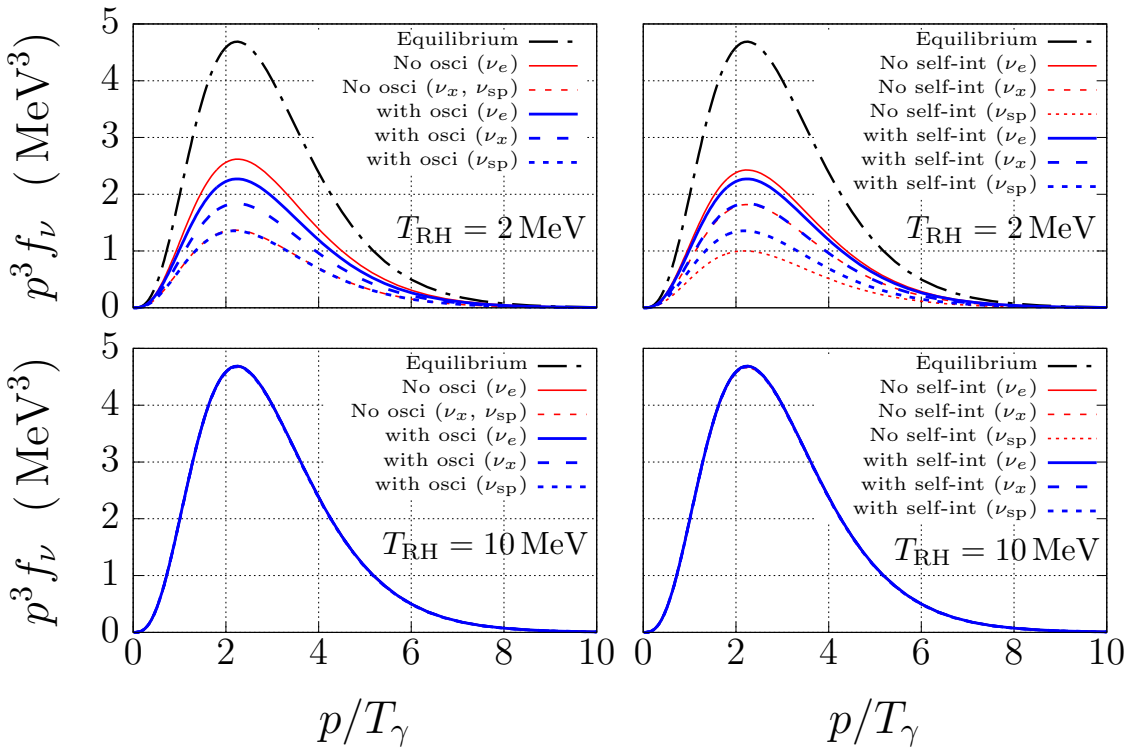

Figure 5.5: Final energy spectra of neutrinos. The horizontal axis is the neutrino energy p divided by the photon temperature T_γ. The vertical axis is the differential energy spectrum of neutrinos. In the figure, neutrino self-interaction is considered in the left column, whereas neutrino oscillation with $(\delta m^2_{12}, \theta_{12})$ is considered in the right column. We consider $(\delta m^2_{12}, \theta_{12})$ in the case with neutrino oscillation in the left column. The thermal spectrum is plotted with the black dot-dashed line. In the top-left panel, the thin red short-dashed and blue thick short-dashed lines are overlapping, while the red thin long-dashed and blue thick long-bashed lines are overlapping in the top-right panel. Also, all plots are almost overlapping in the case of $T_{\rm RH} = 10$ MeV.

from this definition, $R_{\rm dist} = 1$ corresponds to the thermal spectrum, and $R_{\rm dist} > 1$ indicates larger mean energy. It can be seen from Figure 5.6 that the value of $R_{\rm dist}$ increases as $T_{\rm RH}$ becomes smaller. This is because neutrinos are only produced from the annihilation of electrons $e^- + e^+ \to \nu_\alpha + \bar{\nu}_\alpha$, and neutrinos in the final state therefore have energy larger than twice the electron mass. Thus, if neutrinos are mainly produced when the electron mass is not negligible, and the equilibration process $e^\pm + \nu_\alpha \to e^\pm + \nu_\alpha$ is not effective as in the case of $T_{\rm RH} \lesssim \mathcal{O}(1)$ MeV, $R_{\rm dist}$ becomes larger than unity. Also, since ν_e scatter with electrons stronger than ν_x and $\nu_{\rm sp}$ due to the charged-current interaction, the energy distribution of ν_e is closer to the thermal spectrum. That is the reason that the relation $R_{{\rm dist},\nu_{\rm e}} < R_{{\rm dist},\nu_x}$, $R_{{\rm dist},\nu_{\rm e}} < R_{{\rm dist},\nu_{\rm sp}}$ holds for a sufficiently small $T_{\rm RH}$. Furthermore, we can see from Figure 5.6 that both neutrino oscillation and neutrino self-interaction increase

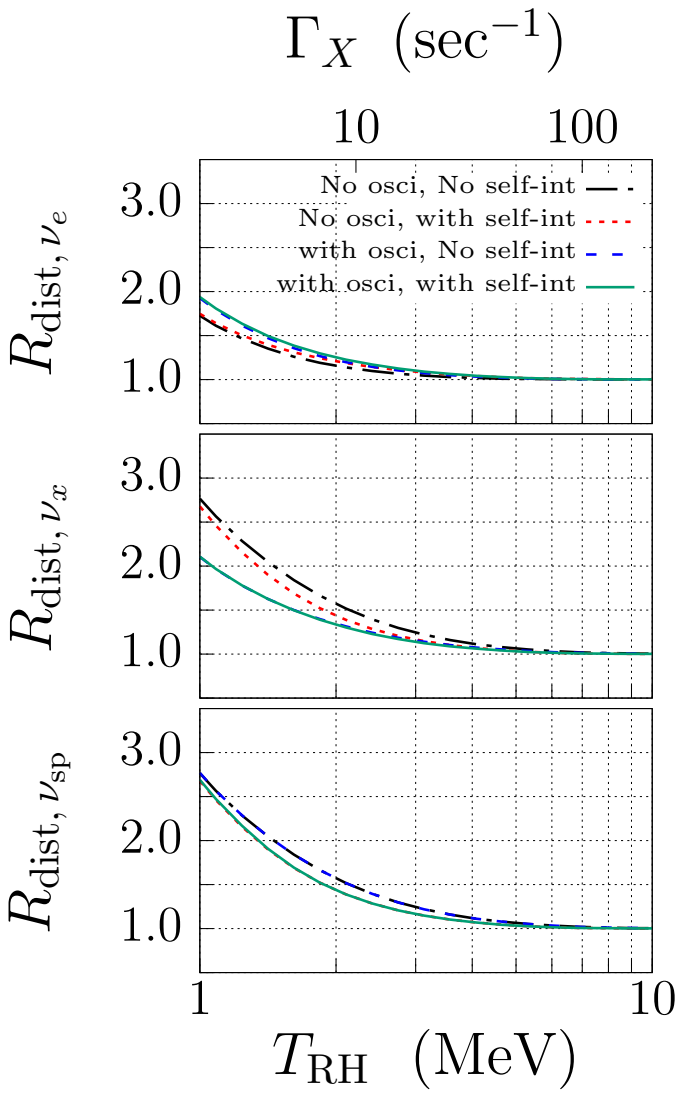

Figure 5.6: Dependence of the mean energy of ν_e (top panel), ν_x (middle panel) and $\nu_{\rm sp}$ (bottom panel) on $T_{\rm RH}$. The vertical axis is the distortion parameter $R_{\rm dist}$ for each neutrino species. $R_{\rm dist} = 1$ corresponds to the thermal spectrum. In the middle panel, the blue long-dashed and green solid lines are overlapping. Also, in the bottom panel, the black dot-dashed (red short-dashed) and blue long-dashed (green solid) lines are overlapping. We consider $(\delta m^2_{12}, \theta_{12})$ in the case with neutrino oscillation.

$R_{{\rm dist},\,\nu_e}$, while decrease $R_{{\rm dist},\,\nu_x}$. This is because neutrino oscillation and neutrino self-interaction equilibrate the neutrino abundances of different flavors as shown in Figure 5.5. The reason is as follows: If the final distribution function of neutrinos is changed by a factor of κ (*i.e.* $f_\nu \mapsto \kappa f_\nu$ where $\kappa < 1$ for ν_e and $\kappa > 1$ for ν_x) due to neutrino oscillation

or neutrino self-interaction, then the distortion parameter should be also modified by

$$\widetilde{R}_{\rm dist}/R_{\rm dist} = \frac{\kappa\rho_\nu/\kappa n_\nu}{3.15(\kappa^{1/3}T_{\nu,\,\rm eff})}\left(\frac{\rho_\nu/n_\nu}{3.15T_{\nu,\,\rm eff}}\right)^{-1} = \kappa^{-1/3}\,, \tag{5.46}$$

where $\widetilde{R}_{\rm dist}$ and $R_{\rm dist}$ are distortion parameters for the cases with and without effects of neutrino oscillation or neutrino self-interaction, respectively. Therefore, these effects increase $R_{{\rm dist},\,\nu_{\rm e}}$ and decrease $R_{{\rm dist},\,\nu_x}$ as long as neutrino oscillation or neutrino self-interaction is effective. Moreover, since the reaction rate of neutrino self-interaction strongly depends on the number density of neutrinos, its effect on $R_{\rm dist}$ becomes small more rapidly than neutrino oscillation as $T_{\rm RH}$ decreases. These effects on $R_{\rm dist}$ can be estimated by comparing neutrino distribution functions in Figure 5.5 and is consistent with the results in Figure 5.6. On the other hand, since $\nu_{\rm sp}$ does not mix with another flavor of neutrinos, they are only affected by neutrino self-interaction.

In the next section, we discuss the light element abundances created in the process of BBN taking our computed neutrino thermalization into account.

5.4 Big Bang Nucleosynthesis

As mentioned in Section 5.2, incomplete thermalization of neutrinos affects the dynamics of the standard BBN. In this section, we explain the role of neutrinos in the production of light elements and show our results of BBN obtained by assuming $T_{\rm RH} \sim \mathcal{O}(1)$ MeV.

5.4.1 Formulation of BBN

We have seen in the previous section that the late-time entropy production due to decays of X induces the incomplete thermalization of neutrinos before decoupling. Since neutrinos take part in the weak reaction processes,

$$n \leftrightarrow p + e^- + \bar{\nu}_e\,, \tag{5.47a}$$

$$e^+ + n \leftrightarrow p + \bar{\nu}_e\,, \tag{5.47b}$$

$$\nu_e + n \leftrightarrow p + e^-\,, \tag{5.47c}$$

which interchange ambient neutrons and protons with each other, non-thermal spectra of neutrinos significantly change the freeze-out value of the neutron-to-proton ratio $(n/p)_f \equiv (n_n/n_p)_{T=T_f}$ where n_n and n_p are the number density of neutrons and protons, respectively, whereas T_f is the freeze-out temperature of the processes (5.47a)–(5.47c). As described later in this section, the theoretical values of light element abundances are very sensitive to the neutron-to-proton ratio before BBN. Therefore, theoretical predictions of the standard BBN should be modified in the Universe with small $T_{\rm RH}$. Since the predictions of standard BBN is well consistent with the observational values, we can constrain $T_{\rm RH}$ by requiring

that the late-time entropy production does not spoil the current success of the standard BBN.

In the case where the massive particles have a hadronic branching ratio, there are additional neutron-proton interchanging processes other than (5.47a)–(5.47c) via strong interactions caused by injected hadrons $N + H \leftrightarrow N' + H'$ where N and N' are nucleons, and H and H' are mesons or baryons. If the hadronic branching ratio is large enough, the hadronic processes dominantly affect the neutron-to-proton ratio, which results in different light element abundances compared to the case of 100% radiative decays of the massive particles [27]. In the current study, we consider the hadronic processes involving pions ($\pi^{\pm}$) and nucleons (n, $\bar{n}$, p, $\bar{p}$) which are injected from hadronic decays of the massive particles. The energetic hadrons produced in the decay of the massive particles are instantaneously stopped by Coulomb scattering with background electrons/positrons or inverse-Compton like scattering with background photons [81–83]. Therefore, the hadrons affecting neutron-proton inter-conversions are thermalized, and we can use thermal cross-sections for the calculation. As for the hadronic cross-sections, we adopt those given in Table.1 of Ref. [81] for the mean values and assume 30% experimental error in each cross-section for conservative treatment (see also Refs. [27, 84]).

To follow the evolution of light element abundances, we solve the Boltzmann equations of light elements using the Kawano code [23]. Since some of the nuclear reaction rates in the code are already outdated, we replace them with the latest ones (see Ref. [85] for more information). Also, we rewrite some equations in the code to allow for the late-time entropy production accompanied by the decays of X. Moreover, since the free neutron decay (*i.e.* the forward process of (5.47a)) continues even after the other weak processes of (5.47a)–(5.47c) decoupled at $T_\gamma \sim T_f$, the value of the neutron-to-proton ratio just before BBN depends on the lifetime of neutrons (see *e.g.* [28]). In the current study, we use the value of the neutron lifetime τ_n reported in Ref. [29]:

$$\tau_n = 880.2 \pm 1.0 \text{ sec} \quad (68\% \text{ C.L.}) \ . \tag{5.48}$$

As for the observational values of light elements, we adopt the primordial mass fraction of helium ^{4}He, Y_p, reported in Ref. [42]:

$$Y_p = 0.2449 \pm 0.0040 \quad (68\% \text{ C.L.}) \, , \tag{5.49}$$

whereas for the observational value of primordial abundance of deuterium D, we adopt the latest value reported in Ref. [40]:

$$\text{D/H} = (2.545 \pm 0.025) \times 10^{-5} \quad (68\% \text{ C.L.}) \, . \tag{5.50}$$

5.4.2 Results of BBN: Radiative decay

First we show the results of radiative decay, *i.e.* the hadronic branching ratio Br = 0. In this case, photons and charged leptons emitted from the decay of X are instantaneously

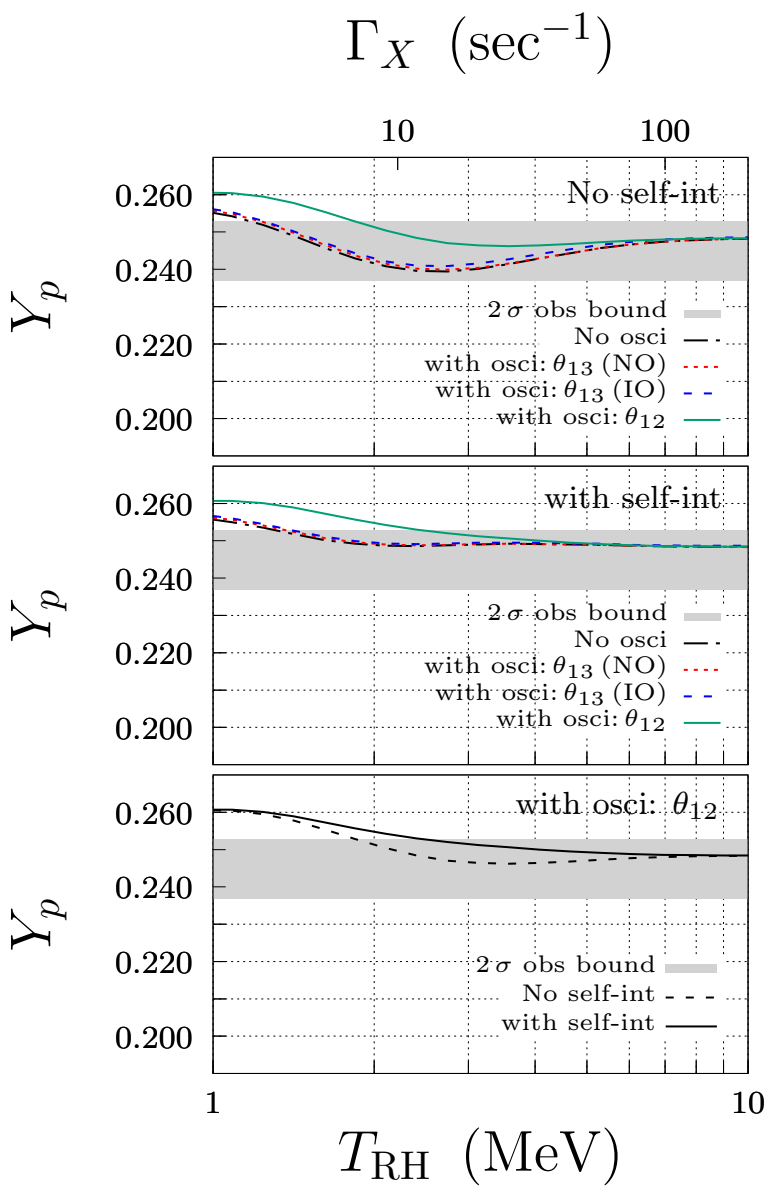

Figure 5.7: Relations between $T_{\rm RH}$ and Y_p in the case of 100% radiative decays of X. We adopt $\eta_B = 6.13 \times 10^{-10}$ in the figure. The top- and middle panels show the effect of neutrino oscillation for the cases without and with neutrino self-interaction, respectively. The black dot-dashed line is for the case without neutrino oscillation, the red short-dashed line is for the case with θ_{13} (NO), the blue long-dashed line is for the case with θ_{13} (IO), and the green solid line is for the case with θ_{12}. The bottom panel shows the effect of neutrino self-interaction when we consider neutrino oscillation with $(\delta m^2_{12}, \theta_{12})$. The black dashed- and solid lines are for the cases without and with neutrino self-interaction, respectively. The gray-shaded region corresponds to the 2-σ observational bound.

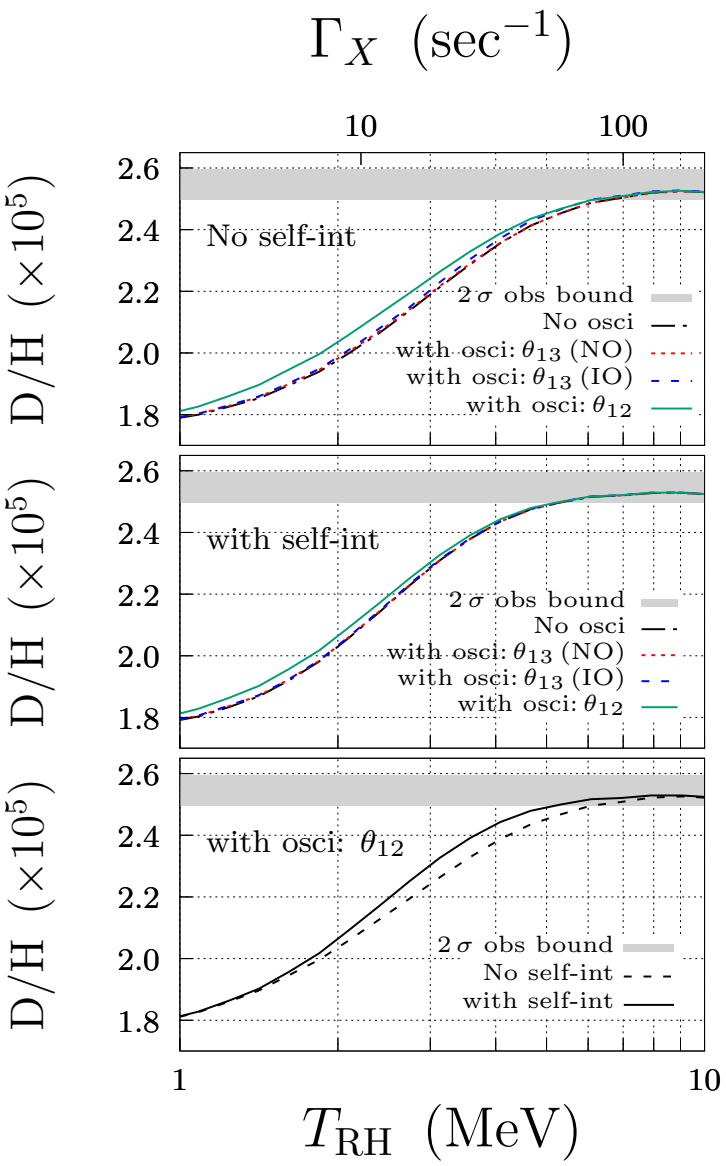

Figure 5.8: Same as Figure 5.7, but for D/H.

thermalized via the electromagnetic force, and results of neutrino thermalization and BBN are independent of the mass of X, m_X. In Figure 5.7 and Figure 5.8, the relation between $T_{\rm RH}$ and D/H and Y_p are shown, respectively. We assume 100% radiative decays of the massive particles in these figures. The baryon-to-photon ratio η_B is the only free parameter in the standard BBN. In the low-reheating-temperature Universe, a baryon number is diluted by the entropy production due to the decays of the massive particles, and hence η_B is decreased by many orders of magnitude. Therefore, we set the large initial value of η_B so that the final value of η_B is consistent with observations of light elements. To plot

Figure 5.7 and Figure 5.8, we fix the final value of η_B to the median value reported by Planck collaboration [3]:

$$\eta_B = 6.13 \times 10^{-10} \,. \tag{5.51}$$

Since almost all neutrons are processed into ^{4}He which is the most stable among light elements, the primordial mass fraction of ^{4}He can be written as $Y_p \equiv \rho_{^4\mathrm{He}}/\rho_B \sim 2/\{1 + (n/p)^{-1}_{\mathrm{BBN}}\} \sim 0.25$, where $(n/p)_{\mathrm{BBN}} \equiv (n/p)_f \, e^{-t/\tau_n}$ is the neutron-to-proton ratio just before deuterium bottleneck opens (*i.e.* $T_\gamma \sim 0.08$ MeV and $t \sim 200$ sec), and the last approximation holds in the standard big-bang cosmology where $(n/p)_{\mathrm{BBN}} \sim 1/7$ [28]. Therefore, the value of $(n/p)_{\mathrm{BBN}}$ almost entirely determines the final abundance of ^{4}He. As for the final abundance of D, the value of N_{eff} is also important because it is related to the Hubble parameter (see Eqs. (5.32), (5.34) and (5.40)) and determines when each light element departs from the nuclear statistical equilibrium [30, 31]. [8] Furthermore, as we can see from Figure 5.7 and Figure 5.8, the influences of neutrino oscillation and self-interaction on light element abundances are similar, and both of these effects increase Y_p and D/H. To understand the numerical results on light element abundances, next we focus on the dynamics of the freeze-out of the neutron-to-proton ratio.

Since nucleons are always non-relativistic, $(n/p)_f$ can be expressed with the freeze-out temperature if T_{RH} is MeV scale as $(n/p)_f \sim \exp(-Q/T_f)$ where $Q \equiv m_n - m_p \sim 1.3$ MeV is the mass difference of nucleons. We note that T_f is determined by the relative values of the neutron-proton inter-converting weak reaction rates Γ_{np} and the Hubble parameter H and is roughly given by $\Gamma_{np}(T_f)/H(T_f) \sim 1$. In the low-reheating-temperature Universe, the total energy density is smaller than that in the standard big-bang cosmology under the same photon temperature due to the incomplete thermalization of neutrinos. [9] Therefore, the expansion rate of the Universe is also small in the scenario, and this effect delays the decoupling of the processes (5.47a)–(5.47c) and thereby decreases $(n/p)_f$.

The influence is not only in the Hubble parameter H but also in the reaction rates Γ_{np}.

[8] We can intuitively understand the dependence of the D abundance on the expansion rate of the Universe in the BBN epoch by focusing on the binding energy of D and ^{4}He, *i.e.* $B_{\mathrm{D}} \sim 2.22$ MeV and $B_{^4\mathrm{He}} \sim 28.3$ MeV, and the freeze-out temperature of the destroying reactions of D. Since the binding energy of ^{4}He is much larger than that of D, D should burn into ^{4}He (via mass-3 elements, T and ^{3}He) as long as the destroying reactions of D such as DD and DT fusions are effective. For this reason, a small value of N_{eff} (or equivalently a small expansion rate H), attained in the low reheating temperature cases, delays a decoupling of the destroying reactions, and hence a smaller abundance of D remains unburnt. That is the reason that a large expansion rate in the BBN epoch leads to a large abundance of D and vice versa.

[9] We recall the reader that T_γ determines when light element abundances are to be created since the reaction process $p + n \to D + \gamma$ responsible for the deuterium production is the first step of BBN, and its backward reaction rate depends on T_γ. For this reason, the values of Γ_{np} and H should not be characterized by the cosmic time but rather by T_γ. That is the reason that a larger value of $N_{\mathrm{eff}} \propto \rho_\nu/\rho_\gamma$ leads to a larger expansion rate of the Universe at the epoch of BBN.

Specifically, the reaction rate of the processes (5.47a)–(5.47c) can be written as [27]

$$\begin{aligned}
\Gamma_{n\to pe^-\bar{\nu}_e} &= K\int_0^{Q-m_e} dp' \left[\sqrt{(p'-Q)^2-m_e^2}(Q-p')\frac{p'^2}{1+e^{(p'-Q)/T_\gamma}}\left(1-f_{\nu_e}(p')\right)\right], \\
\Gamma_{ne^+\to p\bar{\nu}_e} &= K\int_{Q+m_e}^{\infty} dp' \left[\sqrt{(p'-Q)^2-m_e^2}(p'-Q)\frac{p'^2}{e^{(p_{\nu_e}-Q)/T_\gamma}+1}\left(1-f_{\nu_e}(p')\right)\right], \\
\Gamma_{n\nu_e\to pe^-} &= K\int_0^{\infty} dp' \left[\sqrt{(p'+Q)^2-m_e^2}(p'+Q)\frac{p'^2}{1+e^{-(p'+Q)/T_\gamma}}f_{\nu_e}(p')\right], \\
\Gamma_{pe^-\bar{\nu}_e\to n} &= K\int_0^{Q-m_e} dp' \left[\sqrt{(p'-Q)^2-m_e^2}(Q-p')\frac{p'^2}{e^{-(p_{\nu_e}-Q)/T_\gamma}+1}f_{\nu_e}(p')\right], \\
\Gamma_{pe^-\to n\nu_e} &= K\int_0^{\infty} dp' \left[\sqrt{(p'+Q)^2-m_e^2}(Q+p')\frac{p'^2}{e^{(p_{\nu_e}+Q)/T_\gamma}+1}\left(1-f_{\nu_e}(p')\right)\right], \\
\Gamma_{p\bar{\nu}_e\to ne^+} &= K\int_{Q+m_e}^{\infty} dp' \left[\sqrt{(p'-Q)^2-m_e^2}(Q-p')\frac{p'^2}{1+e^{-(p_{\nu_e}-Q)/T_\gamma}}f_{\nu_e}(p')\right],
\end{aligned}$$

where m_e is the electron mass, and $K \sim (1.636\tau_n)^{-1}$ is a normalization factor whose value is determined by the neutron lifetime τ_n. Of these reaction rates, some depend on f_{ν_e} and others on $1-f_{\nu_e}$. In the low-reheating-temperature Universe, the neutrino abundance of each flavor is smaller than the case of the standard big-bang cosmology. Therefore, by denoting the reduction of f_{ν_e} due to the incomplete thermalization of neutrinos by Δf_{ν_e}, the following relation holds for sufficiently small $T_{\rm RH}$ ($< T_{\rm dec} \sim \mathcal{O}(1)$ MeV):

$$\left|\frac{\Delta f_{\nu_e}}{(1-f_{\nu_e})}\right| \ll \left|\frac{\Delta f_{\nu_e}}{f_{\nu_e}}\right| \qquad \text{for} \quad f_{\nu_e} \ll 0.5\,. \tag{5.52}$$

As a result, with such a small value of $T_{\rm RH}$, the total reaction rate $\Gamma_{np} \equiv \Gamma_{n\to pe^-\bar{\nu}_e} + \Gamma_{ne^+\to p\bar{\nu}_e} + \Gamma_{n\nu_e\to pe^-} + \Gamma_{pe^-\bar{\nu}_e} + \Gamma_{pe^-\to n\nu_e} + \Gamma_{p\bar{\nu}_e\to ne^+}$ becomes smaller than that of the standard big-bang cosmology as written in Ref. [27]. Therefore, this effect accelerates the decoupling of the processes (5.47a)–(5.47c) and thereby increases $(n/p)_f$. Consequently, the relative magnitude of these two opposite contributions determines the net effect of incomplete thermalization of neutrinos on $(n/p)_f$.

As described in the previous section, neutrino oscillation and self-interaction slightly enhance the neutrino thermalization and increase the total energy density of neutrinos and hence $N_{\rm eff}$. As a result, the Hubble expansion rate increases due to these effects. Additionally, since the ν_e abundance is decreased by the conversion $\nu_e \to \nu_x$, and only ν_e take part in the reaction processes (5.47a)–(5.47c), Γ_{np} decreases by considering these effect. Therefore, neutrino oscillation and self-interaction always play a role in delaying the freeze-out of neutron-to-proton ratio and increasing T_f and $(n/p)_f$, which leads to larger values of Y_p and D/H.

As is the case for $N_{\rm eff}$ (see Figure 5.2), we can also see from Figure 5.7 and Figure 5.8 that the impact of the solar neutrino mixing $(\delta m^2_{12}, \theta_{12})$ is much larger than that of the

reactor neutrino mixing $(\delta m^2_{13}, \theta_{13})$ independent of the neutrino mass ordering. Therefore, the effective two-flavor mixing with $(\delta m^2_{12}, \theta_{12})$ gives a good approximation to the full three-flavor neutrino mixings. For this reason, we hereafter only consider $(\delta m^2_{12}, \theta_{12})$ in the case with neutrino oscillation.

To obtain the observational constraint on $T_{\rm RH}$, we perform a Monte-Carlo calculation of BBN and χ^2 analysis at each point on the grids of η_B and $T_{\rm RH}$ assuming observational values for Y_p (Ref. [42]) and D/H (Ref. [40]). [10] In the Monte-Carlo calculation, we assume that the reaction rates in the standard BBN, the hadronic reaction rates and the neutron lifetime follow Gaussian distribution and propagate their reported errors to obtain theoretical uncertainties on the light element abundances. Since an allowed region is defined by a parameter space where theoretical abundances of light elements explain each observational value, we give the lower bound on $T_{\rm RH}$ combining χ^2 values of both D/H and Y_p: [11]

$$\chi^2_{{\rm D/H}+Y_p} \equiv \chi^2_{\rm D/H} + \chi^2_{Y_p} = \frac{\{({\rm D/H})_{\rm th}(\eta_B, T_{\rm RH}) - ({\rm D/H})_{\rm obs}\}^2}{\sigma^2_{{\rm D,\,th}}(\eta_B, T_{\rm RH}) + \sigma^2_{{\rm D,\,obs}}} + \frac{\{Y_{p,\,{\rm th}}(\eta_B, T_{\rm RH}) - Y_{p,\,{\rm obs}}\}^2}{\sigma^2_{Y_p,\,{\rm th}}(\eta_B, T_{\rm RH}) + \sigma^2_{Y_p,\,{\rm obs}}}\,, \tag{5.53}$$

where $\chi^2_{\rm D/H}$ and $\chi^2_{Y_p}$ are χ^2 values of D/H and Y_p, respectively. Also, $\sigma_{i,\,{\rm th}}$ and $\sigma_{i,\,{\rm obs}}$ where $i = {\rm D/H}$ and Y_p are respectively the theoretical and observational 1-σ variance of each light element abundance.

Figure 5.9 shows the allowed region in the plane of η_B and $T_{\rm RH}$ in the case of the 100% radiative decays. In the current study, we assume that $\chi^2_{\rm D/H}$ and $\chi^2_{Y_p}$ follow Gaussian distribution. In this case, we can find the lower bound at 95% C.L. on $T_{\rm RH}$ by requiring $\chi^2_{{\rm D/H}+Y_p}(\eta_B, T_{\rm RH}) < 5.991$:

$$T_{\rm RH} \gtrsim 1.8\ {\rm MeV}\,, \tag{5.54}$$

in the case with both neutrino oscillation and self-interaction. As can be seen from Figure 5.2, the value of the reheating temperature $T_{\rm RH}$ is uniquely related to that of the effective number of neutrino species $N_{\rm eff}$ in the scenario that we are considering. [12] Thus,

[10] As written in *e.g.* [69,86], it is technically incorrect to adopt the CMB bound $\eta_B = (6.13 \pm 0.04) \times 10^{-10}$ reported by the Planck collaboration [3] as a prior of BBN because the recombination process depends on the values of $N_{\rm eff}$ and Y_p, and there are correlations between η_B and these quantities. In other words, CMB is not independent of the neutrino thermalization and BBN. In Ref. [3], they adopt the canonical value $N_{\rm eff} = 3.046$ [76] and Y_p calculated by assuming the standard BBN, which are not necessarily realized in the low-reheating-temperature Universe.

[11] There remains a long-standing problem in the standard BBN that the theoretical prediction of the ^{7}Li abundance is approximately three times larger than that of the observational value if we input the value of the baryon-to-photon ratio from CMB into the calculation of BBN (see *e.g.* [29]). Therefore, we refrain from using the ^{7}Li abundance to constrain $T_{\rm RH}$ in the current study.

[12] The value of the effective number of neutrino species $N_{\rm eff}$ depends on the cosmological scenario. For example, if we consider possibilities of dark radiations, neutrino decays, or entropy production by some exotic particles, its value tend to be largely modified. Therefore, the value of $N_{\rm eff}$ is 'degenerate' between different cosmological scenarios, and therefore we cannot clarify the true story of nature by just discussing

Eq. (5.54) leads to the possible minimum value of $N_{\rm eff}$ at 95% C.L.:

$$N_{\rm eff} \gtrsim 1.0. \tag{5.55}$$

The lower bound on $N_{\rm eff}$ is notably smaller than the 2-σ bound obtained from the standard big-bang nucleosynthesis, $N_{\rm eff} > 2.26$ [88].

Also, we depict in Figure 5.10 the comparison between cases with and without neutrino oscillation or neutrino self-interaction. As can be seen from Figure 5.10, we find $T_{\rm RH} \gtrsim 1.5$ MeV in the case with neutrino oscillation and without self-interaction, whereas $T_{\rm RH} \gtrsim 0.6$ MeV in the case without neutrino oscillation and with neutrino self-interaction. The BBN bound in the case with neutrino oscillation or self-interaction is tighter than that in the case without them. This is because, as we can see from Figure 5.8, neutrino oscillation and self-interaction increase the value of Y_p, and the discrepancy between theoretical and observational values becomes large compared to the case without these effects.

5.4.3 Results of BBN: Hadronic decay

As described above, if the massive particles have a branching ratio into hadrons, the constraint on $T_{\rm RH}$ imposed by BBN can be modified compared to when the decays of X are fully radiative (*i.e.* Br = 0). The effects of hadronic decays on light element abundances are shown in Figure 5.11 where we plot the dependence of D and ^{4}He abundances on $T_{\rm RH}$ for each value of m_X and Br. The case of Br = 0 in the figure corresponds to 100% radiative decays of X which is plotted for reference. In the figure, we assume that the massive particles have a non-negligible branching ratio into $u\,\bar{u}$ quark pairs to calculate the number of hadrons produced in the decays of X with Pythia 8.2 code. [13] The systematic error in the result of the Pythia code is expected to be much smaller than those in the hadronic reaction rates. Thus, errors in the number of emitted hadrons should safely be ignored.

Figure 5.11 shows that both the ^{4}He and D abundances increases due to the hadronic decay effects. The reason is as follows. First, there exist more target protons than target neutrons in the system for $T \lesssim 10$ MeV. This is because the neutron-proton ratio follows $n/p \simeq \exp(-Q/T)$ as long as the neutron-proton exchange reactions through weak interaction keep them in equilibrium, and n/p is therefore smaller than unity in this epoch. Second, injected hadrons such as pions and kaons extraordinarily exchange ambient protons with neutrons through strong interaction via, *e.g.*

$$p + \pi^- \to n + \pi^0,$$
$$n + \pi^+ \to p + \pi^0.$$

the value of $N_{\rm eff}$. We need another information, e.g. distribution functions of neutrinos, which are possibly revealed by future direct detection experiments of neutrinos such as PTOLEMY [87].

[13] We have checked that the BBN bound does not depend on the quark flavor emitted from the massive particles if the mass of the massive particles is much larger than the total mass of emitted quarks (*i.e.* $m_X >> m_{q_\alpha}$ where m_{q_α} is the quark mass of particular flavor α).

We note that the neutral pion π^0 produced in the processes immediately decays into two photons and does not cause the corresponding inverse processes in this epoch. For these reasons, the injected hadrons induce a net flow from p to n. This gives an out of equilibrium abundances of neutron and proton and leads to a larger n/p ratio (see [27, 81] for more detailed discussions). As a result, the ^{4}He and D abundances, which increase with $(n/p)_{\rm f}$, get larger than those of the standard BBN. Besides, it can be seen from Figure 5.11 that the effect of hadronic decays is large for a large Br or a small m_X. Comparing the cases of $m_X = 100$ TeV, Br = 0.001 (red thin dashed) and $m_X = 10$ GeV, Br = 1 (blue thick solid) in Figure 5.11, we can see that the discrepancy of D/H or Y_p between these cases is of the same order or much larger than that of the 2-σ observational error if $T_{\rm RH}$ is a few MeV.

To understand the reason, we define the comoving variable for the initial abundance of the massive particles $Y_X = n_X/s$ where n_X is the number density of the massive particles X, and s is the total entropy density of the Universe. If we assume that X dominates the total energy at the initial time and most of it is transferred to radiation components before the reheating is completed, we can write the initial value of Y_X as follows:

$$Y_X = \frac{n_X}{s} \sim \frac{(\frac{\pi^2}{30}\, g^*\, T_{\rm RH}^4)/m_X}{\frac{2\pi^2}{45}\, g_s^*\, T_{\rm RH}^3} \sim \frac{3}{4}\frac{T_{\rm RH}}{m_X}\,, \tag{5.56}$$

where g^* and g_s^* are relativistic degrees of freedom defined by energy and entropy density respectively. In the standard big-bang cosmology, $g^* \sim g_s^*$ holds before electron-positron annihilation sets in. As we can see from the above expression, Y_X gets larger for smaller m_X. Besides, the number of hadrons emitted from the decays of X is almost proportional to $m_X^{0.4}$ (see Ref. [83]), and therefore the total number of hadrons emitted from X is almost proportional to $m_X^{-0.6}$. Since the energetic hadrons instantaneously lose their energy and are thermalized with background particles before inter-converting ambient neutrons and protons, the number of emitted hadrons determine the magnitude of the hadronic-decay effect on BBN. Therefore, the influence of hadronic decays on BBN should be stronger for smaller m_X.

To show the effects of neutrino oscillation and neutrino self-interaction on the light element abundances in the case of hadronic decays, we plot in Figure 5.12 the dependence of Y_p and D/H on $T_{\rm RH}$ for (m_X, Br) = (10 GeV, 1.0) and (100 TeV, 0.001) where we expect large and small effects of hadronic decays, respectively. As we can see from Figure 5.12, if $T_{\rm RH}$ is a few MeV, neutrino oscillation and neutrino self-interaction affect light element abundances at the level of $\mathcal{O}(10)$% for D/H and $\mathcal{O}(1)$% for Y_p when $m_X = 10$ GeV and Br = 1.0, whereas the correction is $\mathcal{O}(10)$% for both cases of D and Y_p when $m_X = 100$ TeV and Br = 0.001. Since we give the observational bound on $T_{\rm RH}$ by summing up the χ^2 values of D/H and Y_p, the constraint on $T_{\rm RH}$ should be changed by $\mathcal{O}(1)$% when $m_X = 10$ GeV and Br = 1.0 and by $\mathcal{O}(10)$% when $m_X = 100$ TeV and Br = 0.001.

We show in Figure 5.13 the allowed region in the same plane as Figure 5.9, but in the case when hadronic decays are included. In the figure, we show four representative cases of (m_X, Br) = (10 GeV, 1.0), (10 GeV, 0.001), (100 TeV, 1.0) and (100 TeV, 0.001).

A possible minimum value of the reheating temperature $T_{\rm RH,\,min}$ in terms of BBN is shown in Figure 5.14 as a function of m_X. We can see from the figure that the BBN bound is tighter in the case of a small m_X or a large Br. Codnsequently, we obtain the lower bound on $T_{\rm RH}$ at 95% C.L.:

$$T_{\rm RH} \gtrsim 4.1 - 4.9 \text{ MeV} \quad \text{for} \quad m_X = 10 \text{ GeV} - 100 \text{ TeV}\,, \tag{5.57}$$

when the hadronic branching ratio Br = 1.0, whereas

$$T_{\rm RH} \gtrsim 2.1 - 3.7 \text{ MeV} \quad \text{for} \quad m_X = 10 \text{ GeV} - 100 \text{ TeV}\,, \tag{5.58}$$

when Br = 0.001 in the case with both neutrino oscillation and neutrino self-interaction. In the same as 100% radiative decay cases, these bounds on $T_{\rm RH}$ can be rewritten as lower bounds on $N_{\rm eff}$ at 95% C.L.:

$$N_{\rm eff} \gtrsim 2.7 - 2.9 \quad \text{for} \quad m_X = 10 \text{ GeV} - 100 \text{ TeV}\,, \tag{5.59}$$

when the hadronic branching ratio Br = 1.0, whereas

$$N_{\rm eff} \gtrsim 1.3 - 2.5 \quad \text{for} \quad m_X = 10 \text{ GeV} - 100 \text{ TeV}\,, \tag{5.60}$$

when the hadronic branching ratio Br = 0.001. As can be seen from the above constraints, the lower bound on $N_{\rm eff}$ can be more severe than the standard BBN bound for the hadronic decay cases depending on the choice of m_X and Br. Since there is no other motivated scenarios where neutrinos are diluted compared to photons, a possible detection of the effective number of neutrino species smaller than three in future observations should be a clear evidence of the low reheating temperature. Also, it should also be useful to detect the cosmic neutrino background (CνB) and reveal the energy distribution of neutrinos for verifying the MeV-scale reheating scenario as neutrinos obtain unique non-thermal spectra depending on the value of $T_{\rm RH}$. In this way, the future direct detection program of CνB such as the PTOLEMY experiment will be able to examine this scenario [87].

In this study, we also find that neutrino oscillation and neutrino self-interaction can change the value of $T_{\rm RH,\,min}$ at the level of $\mathcal{O}(1)$% for most of the range of m_X in the case of hadronic decays.

5.5 Conclusion of Chapter 5

In this chapter, we have investigated the possibility that the reheating temperature of the Universe is $\mathcal{O}(1)$ MeV motivated by long-lived massive particles which often appear in the particle physics theory beyond the standard model and induce a late-time entropy production by their decays. In this scenario, neutrinos are not necessarily thermalized well before the beginning of BBN. Hence, the expansion rate of the Universe and weak reaction processes are significantly altered, which changes the freezeout value of the neutron to

proton ratio. We have calculated the thermalization of neutrinos including the effects of both neutrino oscillation and neutrino self-interaction (Figures 5.2–5.4) and obtained a lower bound on the reheating temperature $T_{\rm RH} \gtrsim 1.8$ MeV (95% C.L.) (Figure 5.9) in the case of 100% radiative decay.

On the other hand, if the massive particles also decay into hadrons, there is an additional effect on BBN via inter-conversion of ambient neutron and proton through the scatterings of the hadrons. In this case, the constraint becomes tighter than that of 100% radiative decay (Figure 5.11). Then, we obtained the lower bound $T_{\rm RH} \gtrsim 2$ MeV–5 MeV (95% C.L.) depending on the masses of the massive particles (10 GeV–100 TeV) and the hadronic branching ratio of the decay (Figures 5.13–5.14).

In this study, we also found that neutrino oscillation and neutrino self-interaction increase the efficiency of neutrino thermalization (Figures 5.2 and 5.4) and decrease the exchange rate between neutrons and protons, thereby enhancing the theoretically expected abundances of helium, Y_p (Figure 5.7), and deuterium, D/H (Figure 5.8). These effects increase the minimum value of the reheating temperature at the level of $\mathcal{O}(10)$% in the case of 100% radiative decays (Figure 5.9) and $\mathcal{O}(1)$% in most cases of hadronic decays (Figure 5.12).

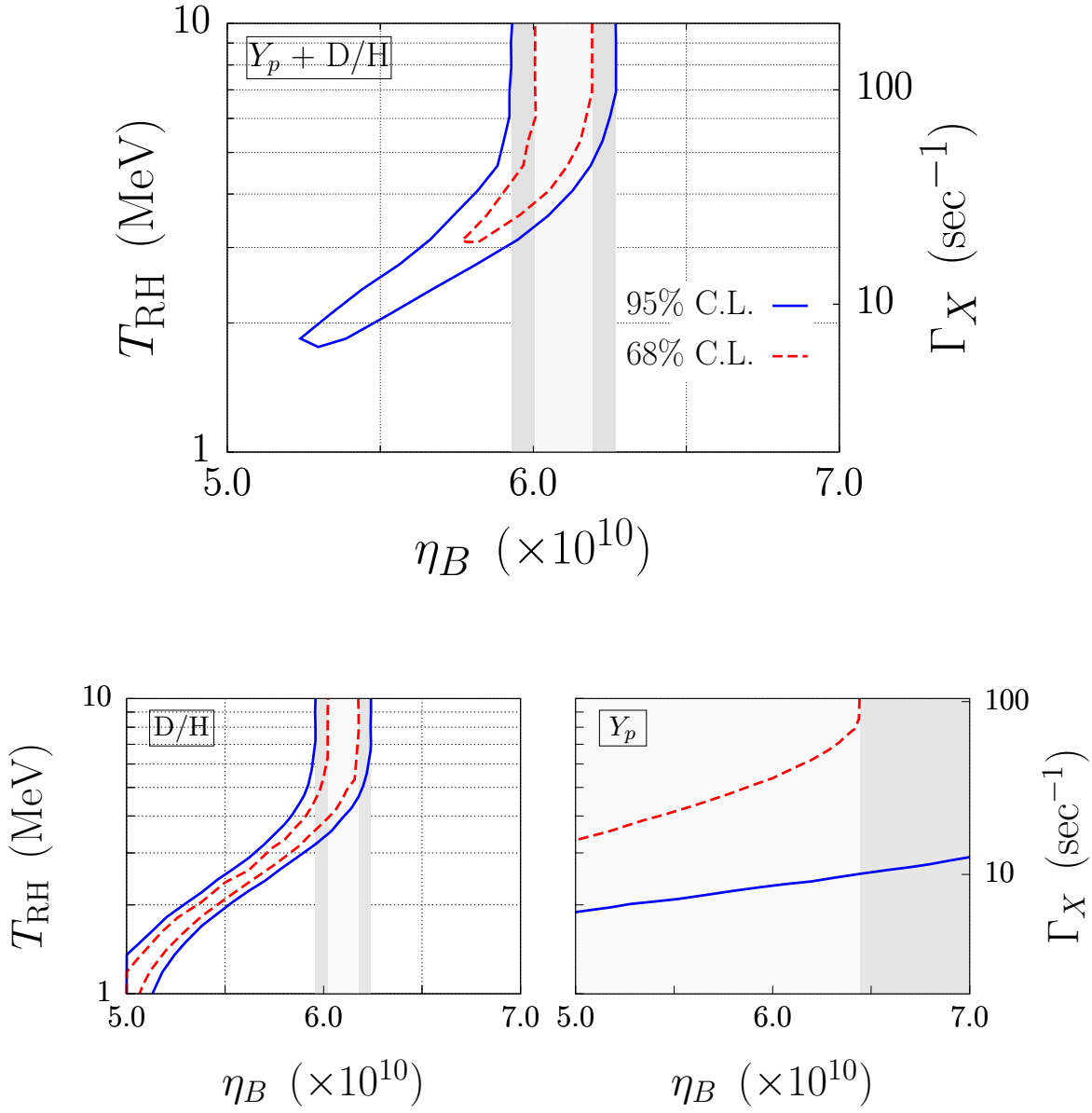

Figure 5.9: Allowed region in the (η_B, $T_{\rm RH}$) plane in the case of 100% radiative decays of X. The 95% (68%) C.L. contour is plotted with the blue solid (red dashed) line. The outside of the small region surrounded by the blue solid (red dashed) line is excluded at 95% (68%) C.L. The constraint on η_B at 95% C.L. (68% C.L.) in the case of the standard BBN is also shown as the dark (light) shaded region. The top panel shows the allowed region in terms of both Y_p and D/H, whereas the bottom-left and bottom-right panels show those of D/H and Y_p, respectively. Neutrino oscillation and neutrino self-interaction are considered in the calculation.

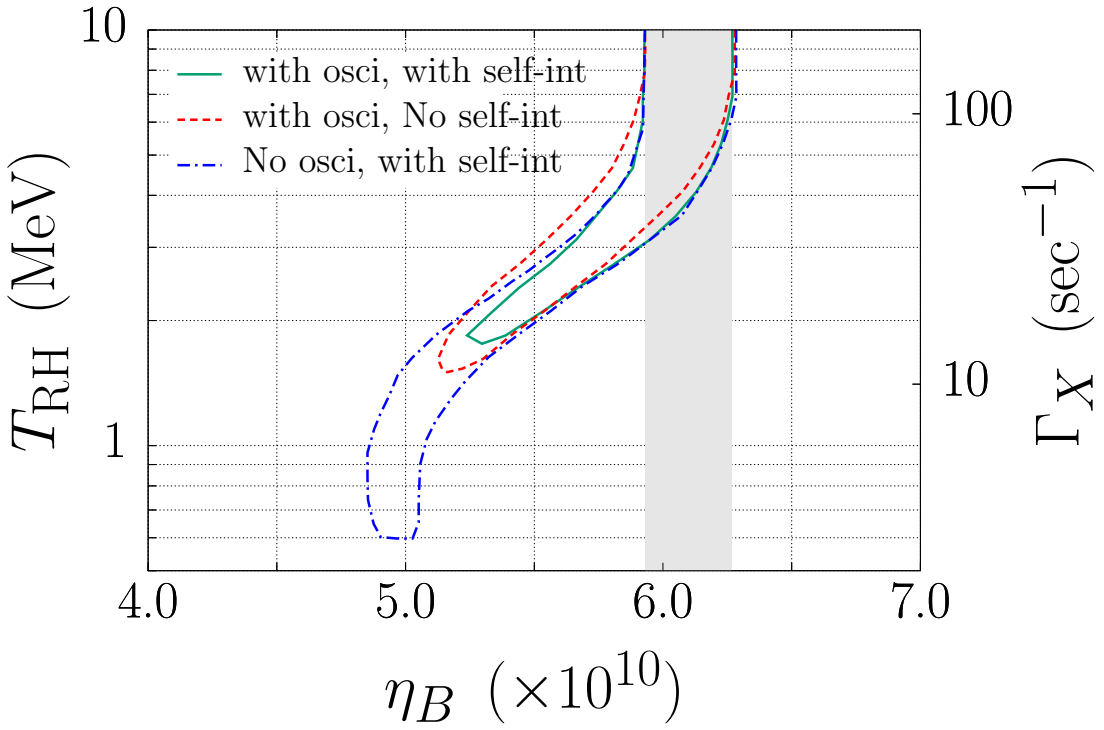

Figure 5.10: Comparison of allowed regions in the (η_B, $T_{\rm RH}$) plane in the cases with or without neutrino oscillation and self-interaction. The outside of the small region surrounded by the contour is excluded at 95% C.L. in each case. The constraint on η_B at 95% C.L. in the case of the standard BBN is also shown as the gray-shaded region. We assume 100% radiative decays of X. The 95% contour with the green solid line is for the case with both neutrino oscillation and self-interaction, one with the red long-dashed line is for the case only with neutrino oscillation, and one with the short-dashed line is for the case only with neutrino self-interaction.

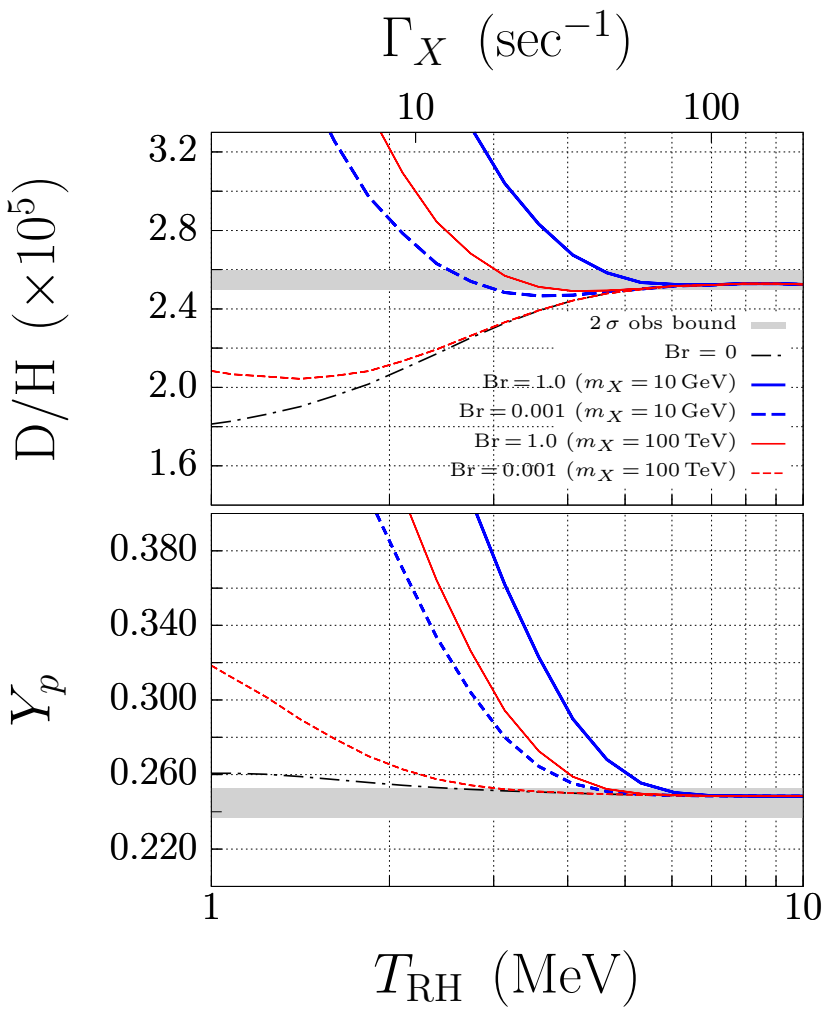

Figure 5.11: D/H and Y_p as a function of $T_{\rm RH}$ in the case with hadronic decays of X. The blue thick solid- and dashed lines are for the case of $m_X = 10$ GeV, while the red thin solid- and dashed lines are for the case of $m_X = 100$ TeV. Also, the blue- and red solid lines are for the case of Br $= 1$, while the blue- and red dashed lines are for the case of Br $= 0.001$. For comparison, we also plot the case of Br $= 0$ with the black dot-dashed line. In the figure, we consider both neutrino oscillation and self-interaction.

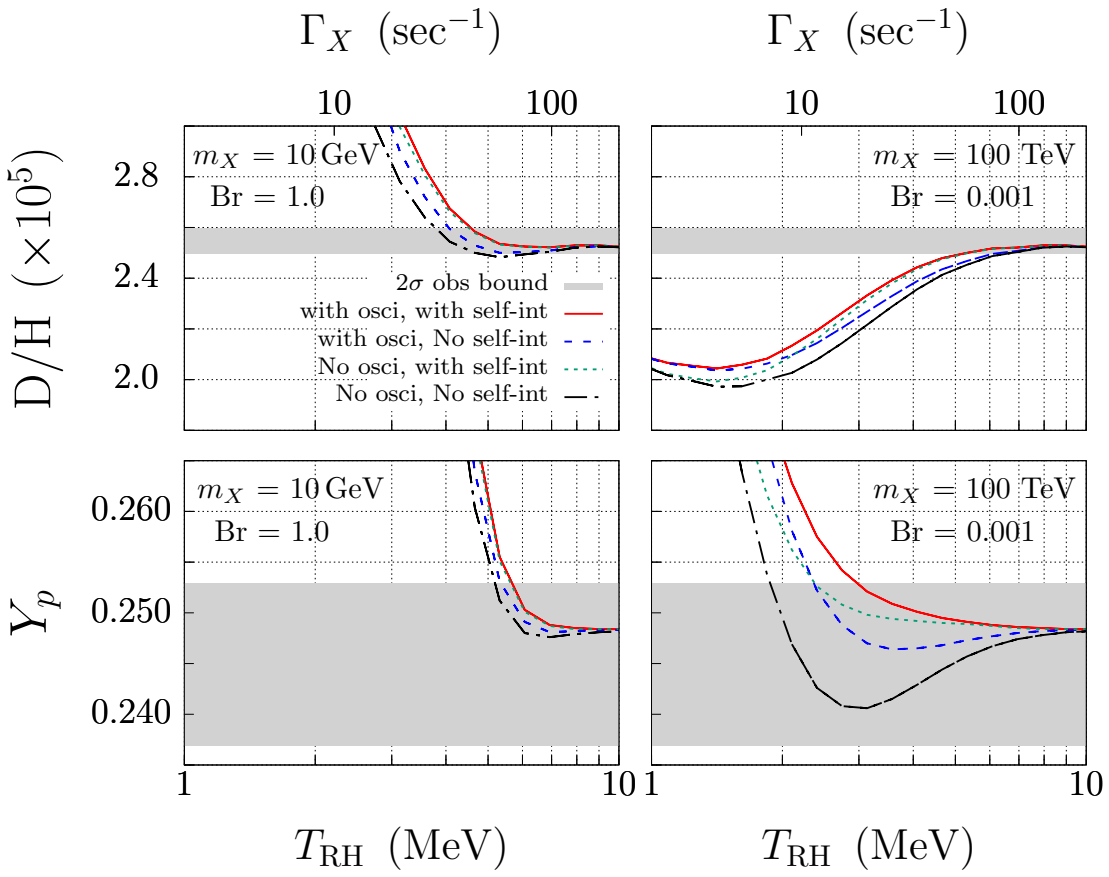

Figure 5.12: Effects of neutrino oscillation and self-interaction on D/H and Y_p in the case with hadronic decays of X. We adopt $\eta_B = 6.13 \times 10^{-10}$ in the figure. The red solid- and blue long-dashed lines are for the case with neutrino oscillation, while the green short-dashed and black dot-dashed lines are for the case with neutrino self-interaction.

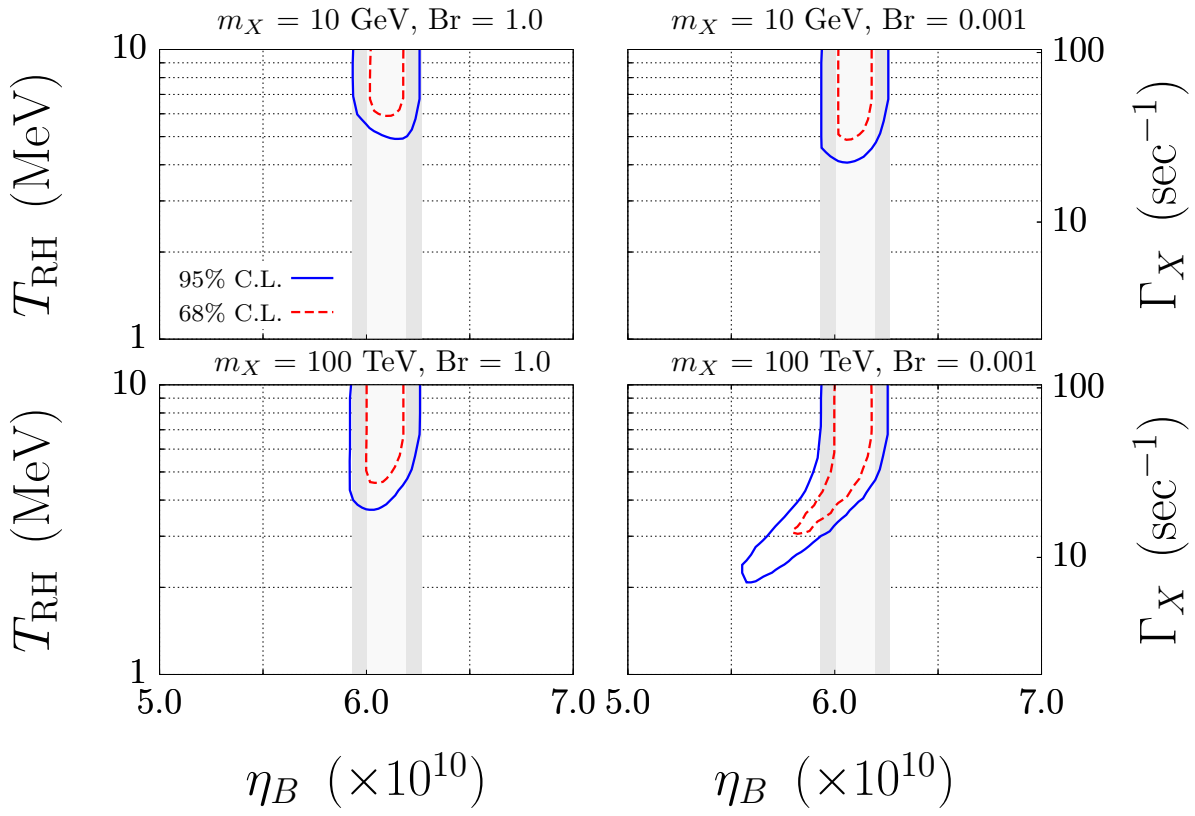

Figure 5.13: Same as Figure 5.9, but for the case of hadronic decays of the massive particles. The outside of the small region surrounded by the blue solid (red dashed) line is excluded at 95% (68%) C.L. The constraint on η_B at 95% (68%) C.L. in the case of the standard BBN is also shown as the dark (light) shaded region.

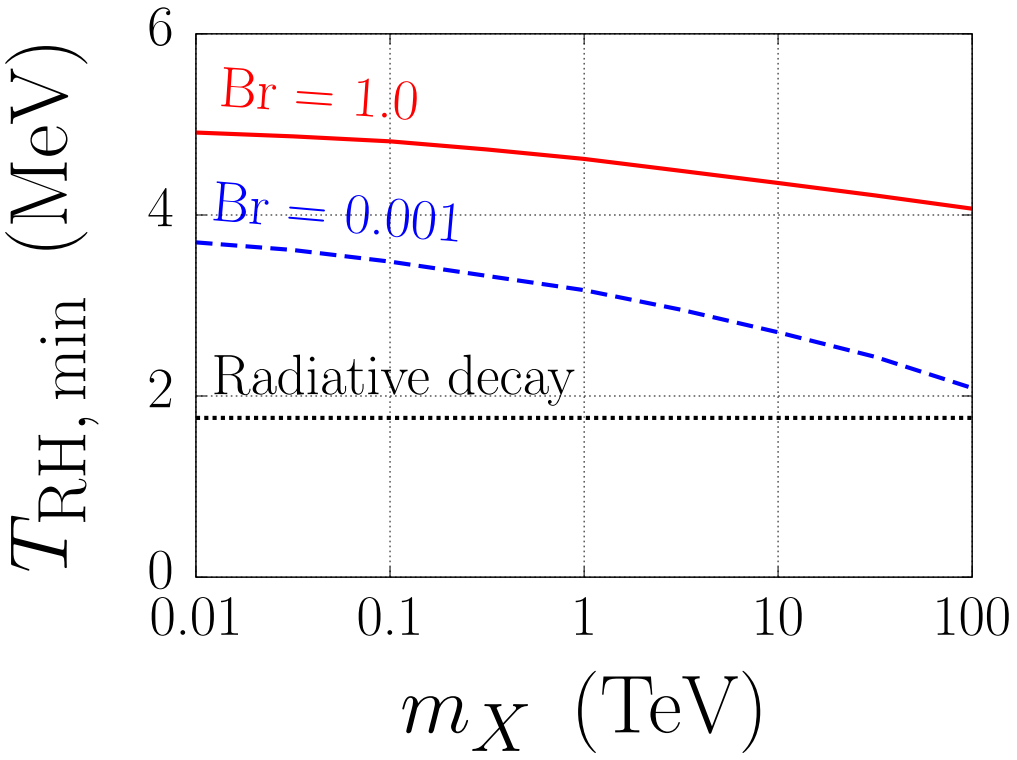

Figure 5.14: Lower bound on the reheating temperature $T_{\mathrm{RH,\,min}}$ at 95% C.L. as a function of m_X in the case with both neutrino oscillation and neutrino self-interaction. We plot the results in the cases of Br = 0.001 (blue dashed) and 1.0 (red solid). The case of 100% radiative decay is also plotted with the black dashed line.

Chapter 6

MeV-scale reheating temperature and thermalization of sterile neutrinos [2]

Abstract: In this chapter, we investigate the possible existence of sterile neutrinos with a various range of masses in terms of cosmology by assuming an MeV-scale reheating temperature. By numerically calculating sterile neutrino production via neutrino oscillation, we find that the existence of light sterile neutrinos inferred from short-baseline neutrino oscillation experiments becomes consistent with observational results of big-bang nucleosynthesis (BBN) if the reheating temperature is $\mathcal{O}(1)$ MeV.

6.1 Introduction

Since the LSND collaboration has reported a 3.8-σ anomaly in their results in the 1990s [89], various experimental projects have been proposed to investigate its physical origin. The anomaly was later confirmed by the MiniBooNE collaboration in both neutrino and anti-neutrino modes [90], and they recently verified a consistent anomaly in its updated version of the experiment [91]. In addition to the above accelerator neutrino oscillation experiments, similar anomalies have been found in other types of experiments, *e.g.* reactor neutrino experiments such as Daya Bay [92] and Double Chooz [93] or Gallium experiments such as SAGE [94–96] and GALLEX [97–99]. One of the most plausible solutions to the anomaly is the existence of light sterile neutrinos with its mass of eV-scale which has a flavor mixing with active neutrinos. In order to verify or exclude the possibility, many future experimental programs have been planned, *e.g.* SBN experiment hosted by Fermi laboratory [100] and JSNS^2 experiment hosted by KEK [101]. Recently, IceCube collaboration investigated the existence of the light sterile neutrinos by searching for a resonant conversion from sterile- to active neutrinos. As a result, they obtained a strong constraint on the light sterile neutrinos, excluding a wide parameter region indicated by the short-

baseline neutrino anomaly [102]. Moreover, the existence of such light sterile neutrinos is strongly disfavored by other disappearance experiments such as MINOS/MINOS+ [103] and NOνA [104]. Also, as shown in Ref. [105], a combined constraint from reactor neutrino experiments (Daya Bay [106], Bugey-3 [107], and PROSPECT [108]) partially exclude the possible parameter values of the eV-scale sterile neutrinos inferred from the appearance experiments. Therefore, there is an unacceptable contradiction between appearance- and disappearance experiments, and the origin of the anomaly is still under debate (see Ref. [105] for the current experimental status of sterile neutrinos).

If such light sterile neutrinos exist and have an appreciable mixing with active neutrinos, they would be abundantly produced through neutrino oscillation in the early Universe and affect the consequences of big-bang nucleosynthesis (BBN) and cosmic microwave background (CMB). In Refs. [73, 86], they calculated the production of light sterile neutrinos in the early Universe and shown that the light sterile neutrinos inferred from the anomaly are completely thermalized before the beginning of BBN and CMB, which means that the existence of the light sterile neutrino is strongly excluded from BBN and CMB. However, this contradiction between cosmology and the possible existence of the sterile neutrino can be solved by assuming large chemical potentials of active neutrino [73, 109–111], self-interaction among sterile neutrinos [112, 113] or non-standard interaction of sterile neutrinos [114–117].

In this study we focus on another solution to the problem that the thermalization of the sterile neutrinos is suppressed by the low reheating temperature. This possibility has been investigated in Refs. [105, 118–122]. In Refs. [118, 119, 122], they studied the production of sterile neutrinos assuming an MeV-scale reheating temperature. In the thermalization calculation of sterile neutrinos, they estimated the sterile neutrino abundance produced via non-resonant active-sterile neutrino oscillation by using simple analytical formula (see Eq. (4) in Ref. [118]). They assumed that the sterile neutrino production via vacuum oscillation starts when the reheating is completed, which is not true as indicated in Ref. [121]. In reality, a large part of active- and sterile neutrinos are produced in the reheating, *i.e.*, *before* the reheating temperature is attained, and therefore in-medium effects cannot be neglected in the thermalization calculation of sterile neutrinos for a sterile neutrino mass of $\mathcal{O}(1)$ eV and the reheating temperature is $\mathcal{O}(1)$ MeV. Also, they simplified their discussions by assumming that the reheating temperature is 5 MeV, leading to more severe constraints on sterile neutrinos than in reality obtained without fixing the value of the reheating temperature. As a result, they obtained a rough picture of to what extent BBN and CMB have a sensitivity to sterile neutrinos by discussing a contribution of sterile neutrinos on the effective number of neutrino species $N_{\rm eff}$. After that, authors in Ref. [121] revisited the sterile neutrino production in the MeV-scale reheating scenario by calculating the semi-classical Boltzmann equation with effective collision terms and provided a more detailed analysis on the thermalization of active- and sterile neutrinos. However, as described in *e.g.* Refs. [78, 123], it is necessary to calculate the original kinetic equation, instead of the semi-classical Boltzmann equation, to accurately follow the sterile neutrino thermalization unless the off-diagonal components of the collision term for

neutrinos (*i.e.* collisional damping term) dominate those of the neutrino hamiltonian. In addition, Ref. [121] did not provide an exact constraint in the parameter space of sterile neutrinos from cosmology.

In this study, we revisit the sterile neutrino thermalization in the Universe with an MeV-scale reheating temperature and refine the cosmological constraint on the sterile neutrinos obtained in Ref. [105, 118–120, 122], by performing a detailed computation of BBN. The main purpose of this study is to provide robust and accurate constraints on the eV-scale mass sterile neutrinos, motivated by the short-baseline neutrino anomaly.

The structure of this chapter is as follows: In Section 6.2, we introduce cosmological scenarios with late-time entropy production which induces the MeV-scale reheating temperature and explain our formulation for calculating the production of active- and sterile neutrinos. In Section 6.3, we show our numerical results of the thermalization calculations of neutrinos, and afterwards we discuss our results of the computation of BBN in Section 6.4. Finally, Section 6.6 is devoted to conclusions.

6.2 Sterile neutrino production in the reheating

In this section, we explain the dynamics of cosmological scenarios with late-time entropy production, which results in the MeV-scale reheating temperature and introduce key equations for calculating sterile neutrino production in the reheating.

In this scenario, we assume the existence of a long-lived scalar particle, which we label as X in this thesis. A candidate of the scalar particle is inflaton or other exotic particles which appear in particle physics theories beyond the standard model such as gravitino, flaton or dilaton. If such particles are abundantly produced in the early Universe, these particles would dominate the energy density of the Universe and create an early matter-dominated epoch before the ordinary radiation-dominated epoch. In this case, decays of the scalar particles induce a large entropy production and subsequent dramatic particle production of the standard model particles. Therefore, if sterile neutrinos $\nu_{\rm s}$ couple to active neutrinos, *viz.* electron neutrinos (ν_e), μ neutrinos (ν_μ), and τ neutrinos (ν_τ), via flavor mixing, sterile neutrinos are also produced from active neutrinos via neutrino oscillation in the reheating. As we describe in the later section, light element abundances created in BBN highly depend on the neutrino abundance. Therefore, it is important to accurately calculate production abundances and final energy spectra of active- and sterile neutrinos created before the onset of BBN. In what follows, we describe the fundamental equations which are necessary to follow active- and sterile neutrino thermalization in the reheating.

If the reheating temperature is below QCD scale $\sim \mathcal{O}(100)$ MeV, and the radiation-dominated epoch therefore realizes after the hadronization, neutrinos are solely produced in the annihilation process of charged leptons $l + \bar{l} \to \nu_\alpha + \bar{\nu}_\alpha$ ($\alpha = e, \mu, \tau$) where l and $\bar{l}$ are charged leptons and corresponding anti-particles, respectively. These processes proceed via weak interaction while photons and charge leptons are rapidly created in the

thermal plasma via electromagnetic interaction. Therefore, sterile neutrinos are also slowly produced from active neutrino via flavor mixings in the reheating. For this reason, in order to follow the time evolution of sterile neutrinos, we need to simultaneously compute the production of active neutrinos by collisions and sterile neutrino thermalization via neutrino oscillation. [1] An analytical estimation of the sterile neutrino abundance produced by non-resonant oscillation between active- and sterile neutrinos was provided in Ref. [124], where they obtained that a production rate of sterile neutrino has a sharp peak at temperature $T_{\rm max}$:

$$T_{\rm max} \sim 13\,{\rm MeV}\left(\frac{m_{\rm s}}{1\,{\rm eV}}\right)^{1/3}, \tag{6.1}$$

where $m_{\rm s}$ is the mass of sterile neutrinos. Hence, if the reheating temperature is below $T_{\rm max}$, sterile neutrino abundance is strongly suppressed compared to that obtained in the standard big-bang cosmology. That is the reason that the low-reheating-temperature scenario could solve the above-mentioned contradictions between the existence of sterile neutrinos and cosmology.

The states of active- and sterile neutrinos are expressed as a one-body-irreducible density matrix, written as a $N_f \times N_f$ Hermitian matrix where N_f is the number of neutrino flavors mixed. In this study, we assume that only one of the three flavors of active neutrinos has a flavor mixing with sterile neutrinos, which is often called the 1+1 mixing scheme. Under the assumption, two flavors of active neutrinos are irrelevant to the neutrino oscillation and the sterile neutrino production. We call the neutrino species which mixes with sterile neutrinos active-mixed neutrino $\nu_{\rm a}$ in contrast to other decoupled species, active-spectator neutrinos $\nu_{\rm sp}$. Since it is natural for all flavors of active neutrinos to have a flavor mixing with sterile neutrinos, this treatment is approximately true if one of the three mixings between active- and sterile neutrinos dominates the others. Otherwise, this treatment is just an assumption for simplicity. In the following, we first introduce a formalism assuming that electron neutrinos (ν_e) have a flavor mixing with sterile neutrinos ($\nu_{\rm s}$). In this case, other active species, namely μ neutrinos (ν_μ) and τ neutrinos (ν_τ), decouple from the neutrino oscillation and the sterile neutrino production.

6.2.1 Formalism: ν_e–$\nu_{\rm s}$ mixing

We assume here that only ν_e have a flavor mixing with $\nu_{\rm s}$. In this case, the states of spectator neutrinos, namely ν_μ and ν_τ, are degenerate, and it is unnecessary to separately calculate dynamical equations for each. This is because the cosmic temperature is always below $\mathcal{O}(1)$ MeV after the reheating for $T_{\rm RH} \sim \mathcal{O}(1)$ MeV, and muons and τ leptons are therefore absent from the thermal bath of the Universe due to their large masses. In the following, quantities of the spectator neutrinos are multiplied by a factor of two for summing up contributions of ν_μ and ν_τ.

[1] We do not consider exotic interactions among active- or sterile neutrinos. Hence, the sterile neutrinos are solely produced via active-sterile neutrino oscillations.

Since we assume the 1+1 mixing, the density matrix of neutrinos with energy E can be expressed as a 2×2 matrix:

$$\varrho_{\boldsymbol{p}}(t) \equiv \varrho(E,t) = \begin{pmatrix} \varrho_{\rm aa} & \varrho_{\rm as} \\ \varrho^*_{\rm as} & \varrho_{\rm ss} \end{pmatrix} , \tag{6.2}$$

where the energy of active- and sterile neutrinos E can be replaced with their absolute momentum p, *i.e.* $E \to p \equiv |\boldsymbol{p}|$ with $\boldsymbol{p}$ the three-momentum of neutrinos. This is because masses of active neutrinos are known to be sub-eV scale [29] and negligible in a thermal bath of $T \sim \mathcal{O}(1)$ MeV. Also, we restrict ourselves to the mass range of sterile neutrinos below 10 keV so that they are always relativistic before their production effectively finishes at around a temperature of the neutrino decoupling $T \sim T_{\rm dec}$. [2] In Eq. (6.2), the diagonal elements of the density matrix corresponds to the distribution functions of active- and sterile neutrinos, *i.e.* $\varrho_{\rm aa} = f_{\rm a}$ and $\varrho_{\rm ss} = f_{\rm s}$ while the off-diagonal elements correspond to a quantum coherence between them.

The time evolution of the density matrix is described by the momentum-dependent quantum kinetic equation, which is derived from Liouville-Von-Neumann Equation for the N-body density matrix. It can formally be written as [56, 57]

$$\frac{d\varrho_{\boldsymbol{p}}(t)}{dt} = \left(\frac{\partial}{\partial t} - H\, p \frac{\partial}{\partial p} \right) \varrho_{\boldsymbol{p}}(t) = -i\,[\mathcal{H}_\nu, \varrho_{\boldsymbol{p}}(t)] + C[\varrho_{\boldsymbol{p}}(t), t] \,, \tag{6.3}$$

where $C[\varrho_{\boldsymbol{p}}(t), t]$ is the collision term for the active-mixed neutrinos, H is the Hubble parameter, and $\mathcal{H}_\nu$ in the commutator is the neutrino Hamiltonian.

In this study, we assume for simplicity that neutrino chemical potentials are zero, $\mu_{\nu_\alpha} \equiv 0$. [3] Hence, the effect of μ_{ν_α} does not affect the thermalization of sterile neutrinos. In such a case, it is unnecessary to follow the time evolution of anti-neutrinos separately from corresponding neutrinos, and the neutrino Hamiltonian consists of two contributions:

$$\mathcal{H}_\nu = \frac{\mathsf{M}^2}{2p} - \frac{8\sqrt{2}\,G_{\rm F} p}{3} \left[\frac{\boldsymbol{E}_{\rm CC}}{m_W^2} + \frac{\boldsymbol{E}_{\rm NC}}{m_Z^2} \right] , \tag{6.4}$$

where G_F is the Fermi coupling constant, and m_W (m_Z) is the mass of W (Z) boson. The first term in the right-hand side of Eq. (6.4) is responsible for the neutrino oscillation in a vacuum, and M is the mass matrix in flavor basis, which is related to the one in mass basis $\mathcal{M}$ as $\mathsf{M}^2 = U\mathcal{M}^2U^\dagger$ where U is the flavor-mixing matrix. Since we assume the 1+1 mixing, we have

$$\mathcal{M}^2 = \begin{pmatrix} m_1^2 & 0 \\ 0 & m_2^2 \end{pmatrix} \,,\; U = \begin{pmatrix} \cos\theta & -\sin\theta \\ \sin\theta & \cos\theta \end{pmatrix} , \tag{6.5}$$

[2] This limitation is mandatory because non-relativistic neutrinos do not oscillate into another flavor [125], and we cannot rely on the kinetic equation for neutrinos (Eq. (6.3)) in such cases.

[3] This is a reasonable assumption because an additional term in the neutrino hamiltonian, which arises from non-zero values of μ_{ν_α}, can be negligible compared to others if we assume $\mu_{\nu_\alpha} \sim \mathcal{O}(10^{-10})$, as is naturally attained in the standard mechanism of baryogenesis via sphaleron processes. The effect of the neutrino chemical potentials on the production of sterile neutrinos has been closely studied in *e.g.* Refs. [73, 110, 111, 126].

where m_1 and $m_2\,(>m_1)$ are respectively the mass eigenvalues relevant to the active mixed- and sterile neutrinos, and θ is the vacuum mixing angle between them. Given the expression of the flavor-mixing matrix U, we can write the relation between the mass- and the flavor eigenstates of neutrinos as

$$|\nu_{\rm a}\rangle = \cos\theta\,|\nu_1\rangle - \sin\theta\,|\nu_2\rangle\,, \tag{6.6}$$
$$|\nu_{\rm s}\rangle = \sin\theta\,|\nu_1\rangle + \cos\theta\,|\nu_2\rangle\,, \tag{6.7}$$

where $|\nu_{\rm a}\rangle$ and $|\nu_{\rm s}\rangle$ are flavor eigenstates of active- and sterile neutrinos while $|\nu_1\rangle$ and $|\nu_2\rangle$ are the mass eigenstates of lighter- and heavier states, respectively.

On the other hand, the second- and third terms in the right-hand side of Eq. (6.4) are matter effects induced by the coherent scatterings of active-mixed neutrinos with electrons $\nu_{\rm a} + e^{\pm} \to \nu_{\rm a} + e^{\pm}$, which modify the relation between the mass- and the flavor eigenstates of neutrinos. Especially, the second (third) term of Eq. (6.4) arises from charged- (neutral-) current weak interactions of $\nu_{\rm a}$ $(=\nu_e)$ with electrons, and $\boldsymbol{E}_{\rm CC} \equiv {\rm diag}(\rho_e, 0)$ and $\boldsymbol{E}_{\rm NC} \equiv {\rm diag}(\rho_{\nu_{\rm a}}, 0)$ where ρ_e and $\rho_{\nu_{\rm a}}$ are the energy densities of electrons and active-mixed neutrinos, respectively. [4]

As for the collision term for the active-mixed neutrinos in Eq. (6.3), $C[\varrho_{\boldsymbol{p}}(t), t]$, we take into account the processes summarized in Table 5.1 in Chapter 5; namely, the production of active neutrinos from electron annihilation, neutrino-electron scatterings, and neutrino self-interactions. The expression of the collision term can be written as

$$C[\varrho_{\boldsymbol{p}}(t), t] = \begin{pmatrix} R_{\nu_{\rm a}} & -D\varrho_{\rm as} \\ -D\varrho^*_{\rm as} & 0 \end{pmatrix}\,, \tag{6.8}$$

where $R_{\nu_{\rm a}}$ is the production rate of active-mixed neutrinos, and D is the collisional-damping factor, which gives decoherence between states of $\nu_{\rm a}$ and $\nu_{\rm s}$. The expressions of $R_{\nu_{\rm a}}$ and D can be written as Eqs. (5.4) and (5.5) in Chapter 5, respectively.

For numerical convenience, we expand the density matrix with Pauli matrices and rewrite the kinetic equation into scalar equations:

$$\varrho_{\boldsymbol{p}}(t) = \begin{pmatrix} \varrho_{\rm aa} & \varrho_{\rm as} \\ \varrho^*_{\rm as} & \varrho_{\rm ss} \end{pmatrix} = \frac{1}{2}\left[\, P_0\,\sigma_0 + \boldsymbol{P}\,\cdot\boldsymbol{\sigma}\,\right]. \tag{6.9}$$

where P_0 and $\boldsymbol{P} = (P_x, P_y, P_z)$ are expansion coefficients, which are called polarization vectors. In the above expression, $\sigma_0 = \mathbf{1}$ is the identity matrix, and $\boldsymbol{\sigma} = (\sigma_x, \sigma_y, \sigma_z)$ are the Pauli matrices. Since the diagonal components of the density matrix correspond to the distribution functions for active mixed- and sterile neutrinos, we have

$$f_{\nu_{\rm a}} = \frac{1}{2}(P_0 + P_z)\ ,\ f_{\nu_{\rm s}} = \frac{1}{2}(P_0 - P_z)\,. \tag{6.10}$$

[4] Since abundances of muons and τ leptons are much smaller than that of electrons, *i.e.* $\rho_x << \rho_e$ where $x = \mu, \tau$, in a thermal bath of $T \sim \mathcal{O}(1)$ MeV due to Boltzmann suppression, we do not consider contributions of muons or τ leptons.

The expression of the quantum kinetic equation (Eq. (6.3)) can be rewritten with polarization vectors as follows:

$$\dot{\boldsymbol{P}} = \overrightarrow{\mathcal{H}} \times \boldsymbol{P} - D\,(P_x\,\mathbf{x} + P_y\,\mathbf{y}) + \dot{P}_0\,\mathbf{z}\,, \tag{6.11}$$

$$\dot{P}_0 = R_{\nu_{\rm a}}\,, \tag{6.12}$$

which we further rewrite into

$$\dot{P}_{\nu_{\rm a}} = \mathcal{H}_x\,P_y + R_{\nu_{\rm a}}\,, \tag{6.13}$$

$$\dot{P}_{\nu_{\rm s}} = -\mathcal{H}_x\,P_y\,, \tag{6.14}$$

$$\dot{P}_x = -\mathcal{H}_z\,P_y - D\,P_x\,, \tag{6.15}$$

$$\dot{P}_y = \mathcal{H}_z\,P_x - \frac{1}{2}\,\mathcal{H}_x\,(P_{\nu_{\rm a}} - P_{\nu_{\rm s}}) - D\,P_y\,, \tag{6.16}$$

where we have defined $P_{\nu_a} \equiv P_0 + P_z$ and $P_{\nu_{\rm s}} \equiv P_0 - P_z$. Furthermore, the neutrino hamiltonian $\mathcal{H}_\nu$ given by Eq. (6.4) is rewritten in terms of polarization vectors as $\overrightarrow{\mathcal{H}} = (\mathcal{H}_x, \mathcal{H}_y, \mathcal{H}_z)$ where

$$\mathcal{H}_x = \frac{\delta m^2}{2p}\sin 2\theta\,, \tag{6.17}$$

$$\mathcal{H}_y = 0\,, \tag{6.18}$$

$$\mathcal{H}_z = -\frac{\delta m^2}{2p}\cos 2\theta + \mathcal{H}_{\rm mat}\,. \tag{6.19}$$

In the above expression, $\delta m^2 \equiv m_2^2 - m_1^2$ $(m_2 > m_1)$ is the squared-mass difference between the mass eigenstates, and $\mathcal{H}_{\rm mat}$ is the matter potential, whose expression can be written as

$$\begin{aligned}\mathcal{H}_{\rm mat} &= -\frac{8\sqrt{2}}{3}G_{\rm F}\,p\left[\frac{\rho_e}{m_W^2} + \frac{\rho_{\nu_{\rm a}}}{m_Z^2}\right] \\ &= -\frac{4\sqrt{2}}{3\,\pi^2}G_{\rm F}\,p\left[\frac{g_e}{m_W^2}\int_0^\infty dp'\,p'^2\frac{E_e}{\exp(E_e/T_\gamma)+1} + \frac{g_\nu}{m_Z^2}\int_0^\infty dp'\,p'^3 f_{\nu_{\rm a}}\right].\end{aligned} \tag{6.20}$$

In the above expression, T_γ is the photon temperature, and $E_e = \sqrt{p^2 + m_e^2}$ is the energy of electrons. Also, $g_e = 4$ is the statistical degree of freedom of electrons and $g_\nu = 2$ is that of neutrinos of each flavor. The first- and second terms in the bracket originate from a charged-current and neutral-current interactions of ν_e with electrons, respectively. The quantum kinetic equation expressed in terms of the polarization vectors, Eq. (6.11), has an analogous form to the spin precession formula and thus useful to understand neutrino oscillation phenomena.

Since the active-spectator neutrinos $\nu_{\rm sp}$ are irrelevant to the neutrino oscillation, its time evolution can be described by the momentum-dependent classical Boltzmann equation:

$$\frac{df_{\nu_{\rm sp}}(t)}{dt} = \left(\frac{\partial}{\partial t} - H\,p\frac{\partial}{\partial p}\right) f_{\nu_{\rm sp}}(t) = C[f_{\nu_{\rm sp}}(t), t]\,, \tag{6.21}$$

where $f_{\nu_{\rm sp}}$ is the distribution function for active-spectator neutrinos, and $C[f_{\nu_{\rm sp}}(t),t]$ is the collision term for them, whose expression is given by Eq. (5.4) with a replacement $\nu_{\rm a} \to \nu_{\rm sp}$.

In order to calculate the thermalization of active- and sterile neutrinos in the expanding Universe, we must solve the Friedman equation, which gives the evolution of the scale factor $a(t)$ of the Universe:

$$H \equiv \frac{\dot{a}}{a} = \sqrt{\frac{8\pi G\rho}{3}}\,, \tag{6.22}$$

where ρ is the total energy density:

$$\begin{aligned}\rho &= \rho_\gamma + \rho_e + \rho_\nu + \rho_X \\ &= \frac{\pi^2}{15}T_\gamma^4 + \frac{g_e}{2\pi^2}\int_0^\infty dp\, p^2 \frac{E_e}{\exp(E_e/T_\gamma)+1} \\ &\qquad + \frac{g_\nu}{2\pi^2}\int_0^\infty dp\, p^3 (f_{\nu_{\rm a}} + 2f_{\nu_{\rm sp}} + f_{\nu_{\rm s}}) + \rho_X\,,\end{aligned} \tag{6.23}$$

where, in the above expression, ρ_γ, ρ_e, ρ_ν and ρ_X are the energy densities of background photons, electrons, neutrinos and the scalar particles, respectively. The total energy density of neutrinos is given by $\rho_\nu = \rho_{\nu_a} + \rho_{\nu_{\rm sp}} + \rho_{\nu_{\rm s}}$.

The evolution of ρ_X can be given by solving the integrated Boltzmann equation for X:

$$\frac{d\rho_X}{dt} = -\Gamma_X \rho_X - 3H\rho_X\,, \tag{6.24}$$

where Γ_X is the decay rate of X. This equation can be integrated analytically for non-relativistic particles X, and we find

$$\frac{\rho_X}{s} = \frac{\rho_{X,0}}{s_0}\, e^{-\Gamma_X t}\,, \tag{6.25}$$

where $\rho_{X,0}$ and s_0 are the energy- and entropy densities of X at the initial time t_0, respectively. Here, we assume that $\rho_{X,0}$ dominate the energy densities of other particles, *i.e.* $\rho_{X,0} >> (\rho_\gamma + \rho_e + \rho_\nu)_{t=t_0}$.

The standard-model particles and the sterile neutrinos obtain energy and entropy from the scalar particles X in the reheating. It is therefore required to simultaneously solve the equation of energy conservation:

$$\frac{d\rho}{dt} = -3H(\rho + P_{\rm tot})\,, \tag{6.26}$$

where $P_{\rm tot}$ is the total pressure, which can be expressed as

$$\begin{aligned}P_{\rm tot} &= P_\gamma + P_e + P_\nu \\ &= \frac{\pi^2}{45}T_\gamma^4 + \frac{g_e}{6\pi^2}\int_0^\infty dp\, \frac{p^4}{E_e}\frac{1}{\exp(E_e/T_\gamma)+1} \\ &\qquad + \frac{g_\nu}{6\pi^2}\int_0^\infty dp\, p^3 (f_{\nu_{\rm a}} + 2f_{\nu_{\rm sp}} + f_{\nu_{\rm s}})\,.\end{aligned} \tag{6.27}$$

Since all electromagnetically-charged particles are instantaneously thermalized in the reheating, they have a common temperature T_γ. Hence, we can rewrite Eq. (6.26) into the time evolution of T_γ:

$$\frac{dT_\gamma}{dt} = -\frac{-\Gamma_X \rho_X + 4H(\rho_\gamma + \rho_\nu) + 3H(\rho_e + P_e) + \frac{d\rho_\nu}{dt}}{\frac{\partial \rho_\gamma}{\partial T_\gamma}|_{a(t)} + \frac{\partial \rho_e}{\partial T_\gamma}|_{a(t)}}\,, \tag{6.28}$$

where Γ_X and $T_{\rm RH}$ are uniquely related to each other via

$$\Gamma_X = 3\,H(T_{\rm RH}). \tag{6.29}$$

Since the energy density is dominated by radiations after the reheating, we can write the Hubble expansion rate $H = H(T_{\rm RH})$ as

$$H(T_{\rm RH}) = \sqrt{\frac{g^*\pi^2}{90}}\frac{T_{\rm RH}^2}{m_{\rm pl}}\,, \tag{6.30}$$

where $m_{\rm pl} \sim 2.4 \times 10^{18}$ GeV is the reduced Planck mass, and $g^* = 10.75$ is the canonical value of the relativistic degrees of freedom for the cosmic temperature of $\mathcal{O}(1)$ MeV. By substituting Eq. (6.30) into Eq. (6.29), we find

$$T_{\rm RH} \sim 0.7\ {\rm MeV}\left(\frac{\Gamma_X}{\sec^{-1}}\right)^{1/2}\,. \tag{6.31}$$

This equation tells us that the decay rate of X is uniquely related to the reheating temperature, and the smaller decay rate of X leads to the lower reheating temperature. [5]

In order to obtain the thermalization of active- and sterile neutrinos, we numerically calculate Eqs. (6.13)–(6.16), (6.21), (6.22), (6.25), and (6.28). For this purpose, we use a modified version of the LASAGNA code [73,74], which is an efficient ODE solver optimized for calculating the sterile neutrino production in the early Universe.

6.3 Numerical result: sterile neutrino thermalization

In this section, we show the numerical results of active- and sterile neutrino thermalization in the reheating, obtained by assuming $T_{\rm RH} \sim \mathcal{O}(1)$ MeV. First, we discuss the case of ν_e–$\nu_{\rm s}$ mixing, followed by the cases of ν_μ–$\nu_{\rm s}$ and ν_τ–$\nu_{\rm s}$ mixing.

[5] Since the actual value of g^* attained after the reheating depends on the thermalization degree of active- and sterile neutrinos, Eq. (6.31) just gives a rough estimate of when the Universe comes into the radiation-dominated epoch.

6.3.1 ν_e–$\nu_{\rm s}$ mixing

The production abundance of neutrinos is often described in terms of the effective number of neutrino species $N_{\rm eff}$. In the case of ν_e–$\nu_{\rm s}$ mixing, it is defined as

$$N_{\rm eff} = N_{{\rm eff},\nu_{\rm a}} + N_{{\rm eff},\nu_{\rm s}} + 2\,N_{{\rm eff},\nu_{\rm sp}} = \rho_{\nu_{\rm a}}/\rho_{\nu_{\rm std}} + \rho_{\nu_{\rm s}}/\rho_{\nu_{\rm std}} + 2\,\rho_{\nu_{\rm sp}}/\rho_{\nu_{\rm std}}\,, \tag{6.32}$$

where $N_{{\rm eff},\nu_\alpha}$ ($\alpha = e$, s, sp) is the contribution of each neutrino species, and $\rho_{\nu_{\rm std}}$ is the energy density of neutrinos in the standard big-bang cosmology. [6] The factor of two in front of $N_{{\rm eff},\nu_{\rm sp}}$ is for summing up contributions of ν_μ and ν_τ. As can be seen from the definition, $N_{{\rm eff},\nu_\alpha} = 1$ corresponds to the full thermalization of ν_α, and then the energy spectrum of ν_α can be expressed as the thermal Fermi-Dirac distribution.

We plot in Figure 6.1 the relation between the reheating temperature $T_{\rm RH}$ and the effective number of neutrino species $N_{\rm eff}$. In the figure, we use the best fit values of mixing parameters of light sterile neutrinos reported in Ref. [127]:

$$\delta m^2 = 1.29\ {\rm eV}^2\,,\ \sin^2 2\theta = 0.035\,, \tag{6.33}$$

which was obtained from data analysis of reactor neutrino experiments. Figure 6.1 shows that both $N_{\rm eff}$ and $N_{{\rm eff},\nu_\alpha}$ increase with respect to $T_{\rm RH}$. This is because the neutrino production via $e^- + e^+ \to \nu_\alpha + \bar{\nu}_\alpha$ is more efficient at a higher temperature, and neutrinos have more time to be produced in the process. Also, an inequality $N_{{\rm eff},\nu_{\rm a}} > N_{{\rm eff},\nu_{\rm sp}}$ always holds because ν_e interact with electrons stronger than ν_μ and ν_τ as explained before. Moreover, Figure 6.1 reveals that neutrino self-interaction enhances the sterile neutrino production. The reason is that neutrino self-interaction increases the collisional-damping rate D (see Eq. (5.5)) and increase the effective production rate of sterile neutrinos, which can be approximately written as $D\,\sin^2 2\theta_{\rm M}$, where $\theta_{\rm M}$ is the in-medium mixing angle between active- and sterile neutrinos [128]. This important effect of neutrino self-interaction was not considered in Ref. [121].

Figure 6.2 shows the time evolution of $N_{{\rm eff},\nu_\alpha}$ for typical values of $T_{\rm RH}$. The behavior of $N_{{\rm eff},\nu_\alpha}$ is determined by two competing effects: dilution of neutrinos due to the entropy production induced by the decay of X and the production of neutrinos. Since neutrinos are only weakly produced in the thermal bath of photons and electrons, the former contribution is dominant for $T_\gamma > T_{\rm RH}$ and its effect becomes maximum at around $T_\gamma \sim T_{\rm RH}$, which corresponds to the cosmic time almost equal to the lifetime of X (*i.e.* $\tau_X = \Gamma_X^{-1}$). That is the reason that there is a local minimum of $N_{{\rm eff},\nu_\alpha}$ at around $T_\gamma \sim T_{\rm RH}$. On the other hand, for $T_\gamma < T_{\rm RH}$ the latter contribution, neutrino production in the thermal bath, becomes

[6] We normalize the contribution of ν_α ($\alpha = e, \mu, \tau$) to the effective number of neutrino species $N_{{\rm eff},\nu_\alpha}$ in units of the energy density of ν_e in the standard big-bang cosmology, $\rho_{\nu_{e,\,\rm std}}$. We can instead normalize ρ_{ν_α} in units of the standard energy density of ν_μ or ν_τ, but the difference between $\rho_{\nu_\alpha}/\rho_{\nu_{e,\,\rm std}}$ and $\rho_{\nu_\alpha}/\rho_{\nu_{\mu,\,\rm std}}$ (or $\rho_{\nu_\alpha}/\rho_{\nu_{\tau,\,\rm std}}$) should be quite small ($< 1\%$) and hence negligible. We note here that the value of $N_{\rm eff}$ is just a quantity which gives information on to what extent neutrinos are thermalized, and it is not an observable used for a comparison between theories and observations. Hence, an error of $N_{\rm eff}$ is irrelevant to our final results, and we do not stick to a precise value of $N_{\rm eff}$.

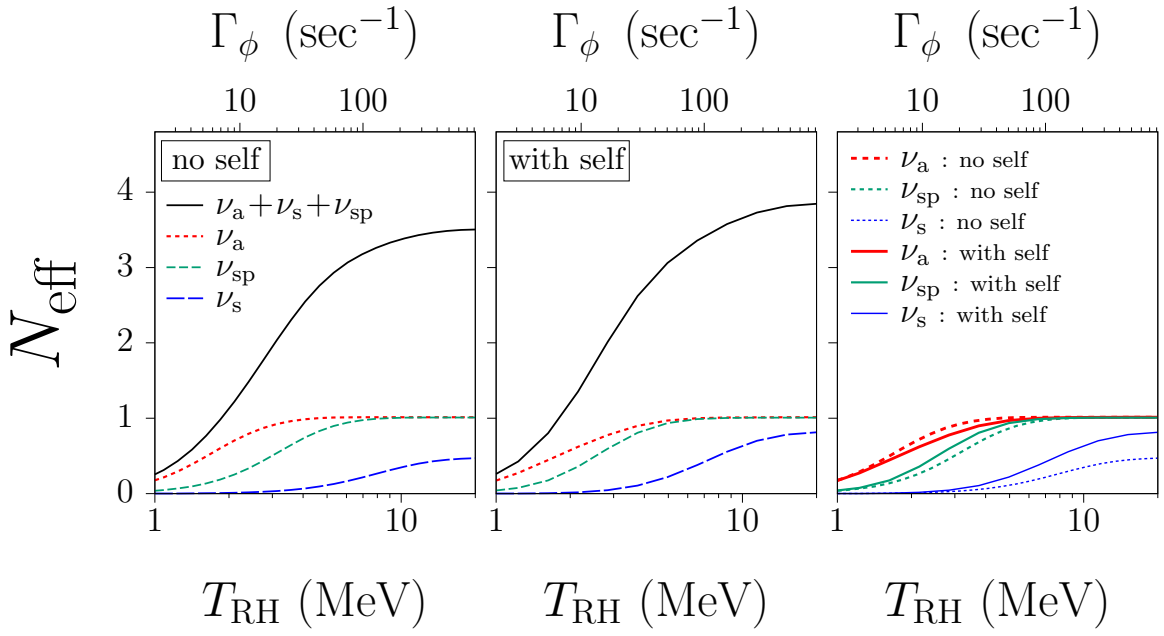

Figure 6.1: Effective number of neutrino species $N_{\rm eff} = N_{{\rm eff},\,a} + N_{{\rm eff},\,s} + 2\ N_{{\rm eff},\,sp}$ as a function of the reheating temperature $T_{\rm RH}$, where $N_{{\rm eff},\,a}$, $N_{{\rm eff},\,s}$ and $N_{{\rm eff},\,sp}$ are contributions of active mixed-, sterile- and active-spectator neutrinos, respectively. The left- and the middle panels correspond to the cases without and with neutrino self-interaction, respectively. The right figure shows the effect of neutrino self-interaction. In the left- and middle panels, the black solid line is for $N_{\rm eff}$, whereas the red short-dashed, the green middle-dashed and the blue long-dashed lines are for $N_{{\rm eff},\,a}$, $N_{{\rm eff},\,sp}$ and $N_{{\rm eff},\,s}$, respectively. In the right panel, neutrino self-interaction is taken into account in the solid lines, and the red thick-, the green medium- and the blue thin solid lines are for $N_{{\rm eff},\,a}$, $N_{{\rm eff},\,sp}$ and $N_{{\rm eff},\,s}$, respectively. In contrast, neutrino self-interaction is not considered in the dashed lines, and the red thick dashed-, the green medium dashed- and the blue thin dashed lines are for $N_{{\rm eff},\,a}$, $N_{{\rm eff},\,sp}$ and $N_{{\rm eff},\,s}$, respectively.

dominant as the former contribution becomes negligible after the decay of X. Therefore, the value of $N_{{\rm eff},\,\nu_\alpha}$ increases for $T_\gamma < T_{\rm RH}$ until neutrinos decouple from other particles at around $T_\gamma \sim 3$ MeV for ν_e and $T_\gamma \sim 5$ MeV for ν_μ and ν_τ. Also, Figure 6.2 indicates that light sterile neutrinos with masses of eV-scale start to be created via neutrino oscillation at around a temperature of 13 MeV, as discussed in the previous section (see Eq. (6.1)).

In Figure 6.3, we plot the final energy spectrum of each flavor of neutrinos for the typical values of $T_{\rm RH}$. We can see that the spectrum of sterile neutrinos is similar to those of active neutrinos, which is a characteristic feature of the non-resonant production. Also, it can be seen from Figure 6.3 that a peak position of the neutrino energy spectrum is smaller than $p/T_\gamma \sim 3.15$, which corresponds to thermally-averaged energy of fermions.

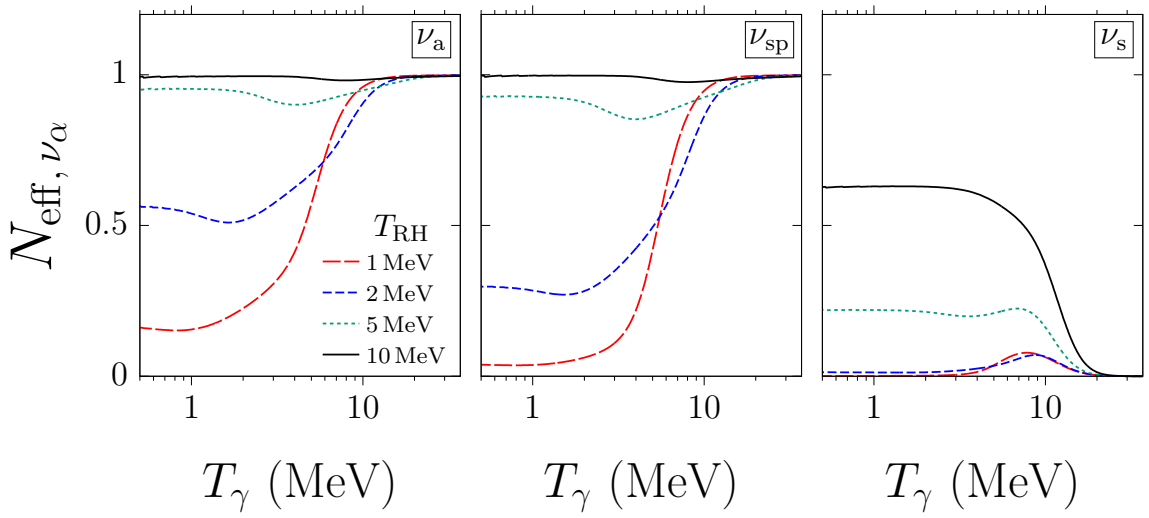

Figure 6.2: Temperature evolution of the effective number of neutrino species $N_{\rm eff}$ and a contribution of each neutrino species $N_{{\rm eff},\nu_\alpha}$ where $\alpha = {\rm a, s, sp}$. The left panel is for $N_{{\rm eff},\nu_{\rm a}}$, the middle panel is for $N_{{\rm eff},\nu_{\rm sp}}$, and the right panel is for $N_{{\rm eff},\nu_{\rm s}}$. In the figure, the red long-dashed line is for $T_{\rm RH} = 1$ MeV, the blue middle-dashed line is for $T_{\rm RH} = 2$ MeV, the green short-dashed line is for $T_{\rm RH} = 5$ MeV, and the black solid line is for $T_{\rm RH} = 10$ MeV.

This is because photon temperature T_γ increases by a factor of $(11/4)^{1/3} \sim 1.4$ compared to those of neutrinos after the annihilation of electrons, and the peak position shift to $p/T_\gamma \sim 3.15/1.4 \sim 2.25$.

Figure 6.4 shows an averaged energy of neutrinos as a function of the reheating temperature. The averaged energy of neutrinos can be expressed as a distortion parameter $R_{{\rm dist},\nu_\alpha}$ defined by

$$R_{{\rm dist},\nu_\alpha} = \frac{1}{3.15\, T_{\nu_\alpha,{\rm eff}}} \frac{\rho_{\nu_\alpha}}{n_{\nu_\alpha}}\,, \tag{6.34}$$

where $T_{\nu_\alpha,{\rm eff}}$ $(= [4\pi^2 n_{\nu_\alpha}/3\zeta(3)]^{1/3})$ is the effective temperature for each flavor of neutrinos. As can be seen from this definition, $R_{{\rm dist},\nu_\alpha} = 1$ corresponds to the thermal spectrum. Figure 6.4 reveals that the value of $R_{{\rm dist},\nu_{\rm a}}$ and $R_{{\rm dist},\nu_{\rm sp}}$ decrease as $T_{\rm RH}$ increases, and it is almost equal to unity for $T_{\rm RH} > 10$ MeV. This is because active neutrinos are only produced from the annihilation of electrons $e^- + e^+ \to \nu_\alpha + \bar{\nu}_\alpha$, and each neutrino in the final state has energy larger than the electron mass $m_e \sim 0.5$ MeV. Therefore, if neutrinos are mainly produced when the electron mass is not negligible, the value of the $R_{{\rm dist},\nu_\alpha}$ becomes larger than unity. Actually, the scattering process of neutrinos with electrons, $e^\pm + \nu_\alpha \to e^\pm + \nu_\alpha$, equilibrates neutrino spectra, but the scattering rates have almost the same value $\mathcal{O}(G_F^2)$ as that of $e^- + e^+ \to \nu_\alpha + \bar{\nu}_\alpha$, and therefore neutrinos are not completely equilibrated. Furthermore, Figure 6.4 shows the relation $R_{{\rm dist},\nu_{\rm a}} < R_{{\rm dist},\nu_{\rm sp}}$ (*i.e.* $R_{{\rm dist},\nu_e} < R_{{\rm dist},\nu_\mu}$ or $R_{{\rm dist},\nu_\tau}$) holds for any given value $T_{\rm RH}$. The reason is that

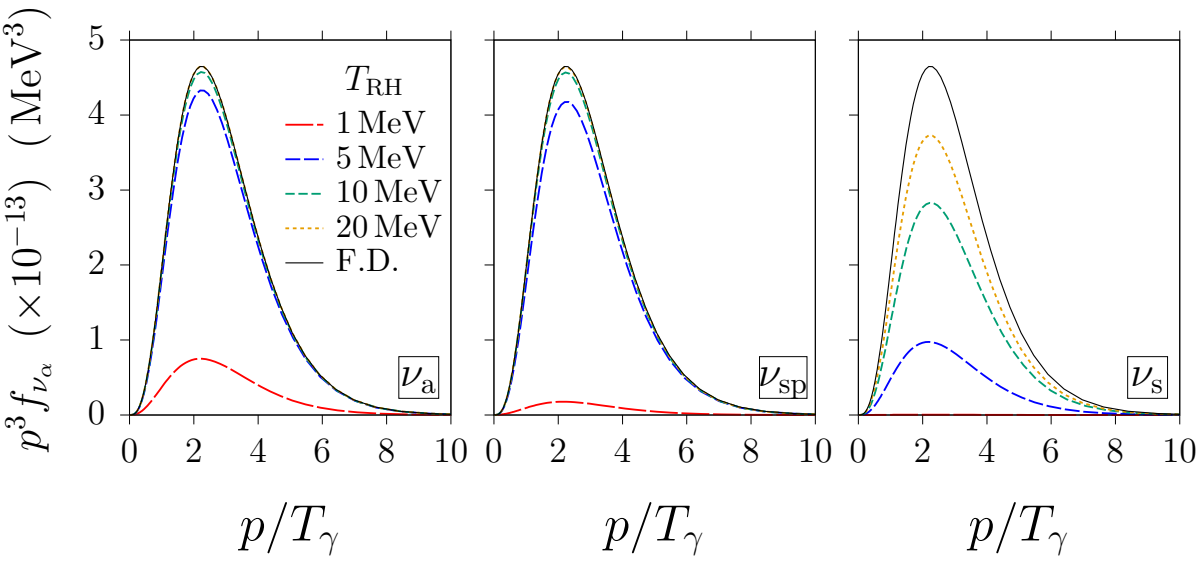

Figure 6.3: Dependence of the final energy spectra of neutrinos on the reheating temperature in the case with neutrino self-interaction. The x-axis is the neutrino energy p divided by the photon temperature T_γ. The y-axis is the differential energy spectrum of neutrinos. The spectra are evaluated at $T_\gamma = 10^{-2}$ MeV, much later than the electron annihilation and the neutrino decoupling. The left panel is for $\nu_{\rm a}$, the middle panel is for $\nu_{\rm sp}$, and the right panel is for $\nu_{\rm s}$. In the figure, the red long-dashed line is for $T_{\rm RH} = 1$ MeV, the blue middle-dashed line is for $T_{\rm RH} = 5$ MeV, the green short-dashed line is for $T_{\rm RH} = 10$ MeV, and the black solid line is for $T_{\rm RH} = 20$ MeV. In the left- and the middle panels, the lines of $T_{\rm RH} = 20$ MeV and the Fermi-Dirac spectrum are almost overlapping.

scattering rates of ν_e with electrons/positrons, $\nu_e + e^\pm \to \nu_e + e^\pm$, are larger than those for ν_μ and ν_τ. Furthermore, we can see that the value of $R_{{\rm dist},\,\nu_{\rm s}}$ has the same dependence on $T_{\rm RH}$ as those of active neutrinos, but it is larger than $R_{{\rm dist},\,\nu_{\rm a}}$ and $R_{{\rm dist},\,\nu_{\rm sp}}$. This is because sterile neutrinos do not scatter with electrons and they cannot equilibrate their energy spectrum. We note that the value of $R_{{\rm dist},\,\nu_{\rm s}}$ at $T_{\rm RH} = 5$ MeV is smaller than that obtained in Ref. [105], $R_{{\rm dist},\,\nu_{\rm s}} = 4.11$. This is possibly due to the approximations that they adopted to simplify the calculation.

Figure 6.5 shows the dependence of the dark matter fraction of sterile neutrinos $\Omega_{\rm s}/\Omega_{\rm DM}$ on the reheating temperature $T_{\rm RH}$ for each value of the active-sterile mixing angle $\sin^2\theta$ and on the active-sterile mixing angle $\sin^2\theta$ for each value of $T_{\rm RH}$. The mass of the sterile neutrino is fixed to be $m_{\rm s} = 1$ keV. The left- and right panels of Figure 6.5 are reproductions of Figure 9 and Figure 10 in Ref. [121], respectively.

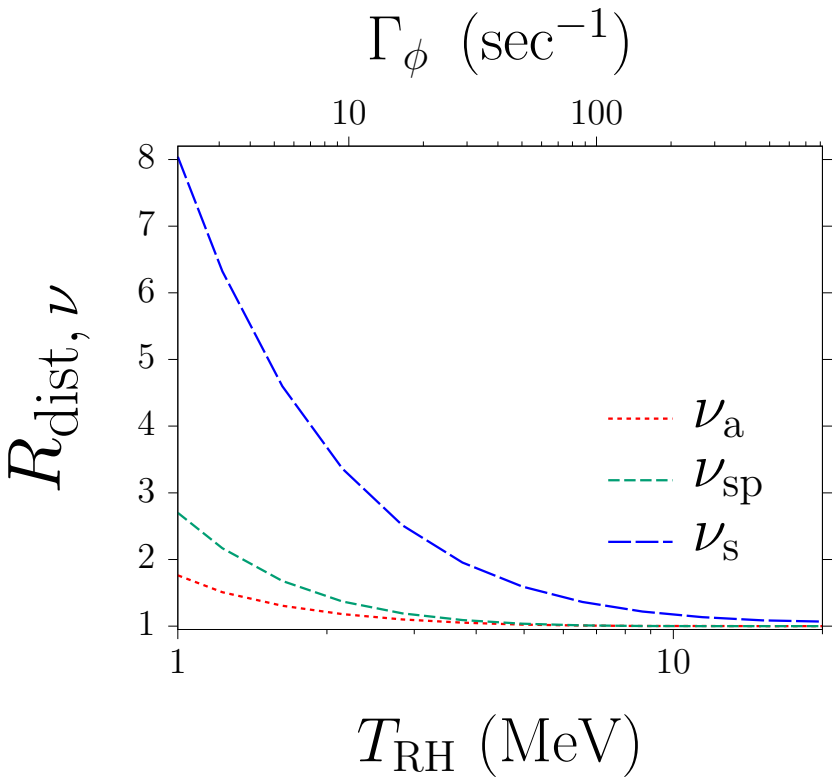

Figure 6.4: Dependence of the distortion parameter for each flavor of neutrinos $R_{\mathrm{dist},\,\nu_\alpha}$ ($\alpha = \mathrm{a}, \mathrm{s}, \mathrm{sp}$) on the reheating temperature T_{RH}. The red short-dashed line is for ν_{a}, the greed middle-dashed line is for ν_{sp}, and the blue long-dashed line is for ν_{sp}. $R_{\mathrm{dist}} = 1$ corresponds to the thermal Fermi-Dirac spectrum.

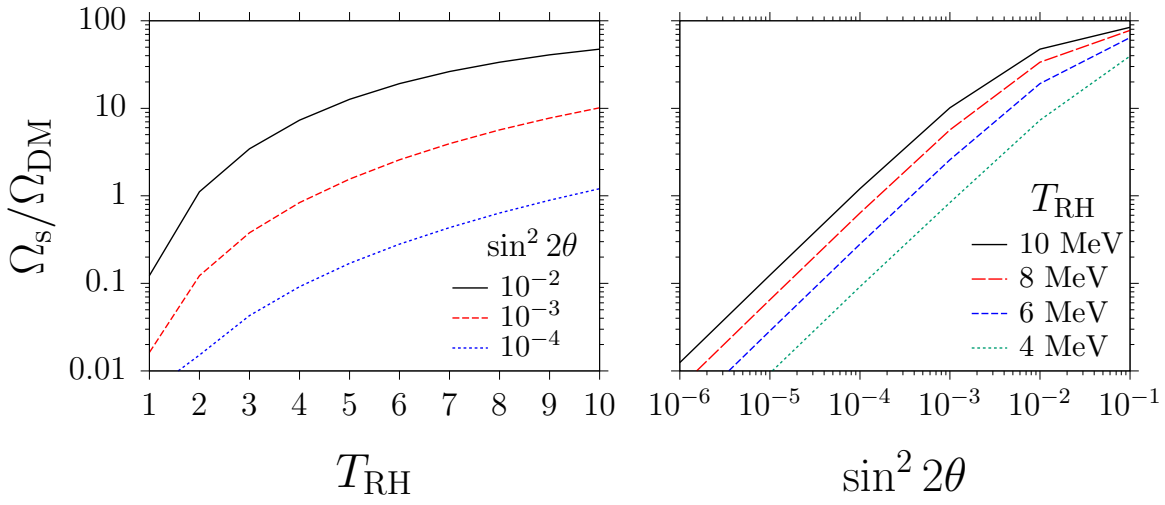

Figure 6.5: Dependence of the dark matter fraction of sterile neutrinos Ω_s/Ω_{DM} on the reheating temperature T_{RH} for each value of the active-sterile mixing angle $\sin^2\theta$ (left panel) and on the active-sterile mixing angle $\sin^2\theta$ for each value of T_{RH} (right panel). In the left panel, the black solid-, the red long dashed-, and the blue short-dashed lines are for the cases of $\sin^2 2\theta = 10^{-2}$, 10^{-3}, and 10^{-4}, respectively. In the right panel, the black solid-, the red long dashed-, the blue middle dashed-, and the green short-dashed lines are for the cases of $T_{RH} = 4, 6, 8$, and 10 MeV, respectively.

6.4 Big Bang Nucleosynthesis

In this section, we focus on BBN. First, we briefly explain the role of neutrinos in BBN, and then we introduce the formalism of the calculation of BBN. Lastly, we present numerical results, obtained by assuming $T_{\rm RH} \sim \mathcal{O}(1)$ MeV.

6.4.1 Neutrino thermalization and neutron to proton ratio

Neutrinos affect light element abundances in two ways: First, they are involved in the exchange reactions between protons and neutrons in the following:

$$n \leftrightarrow p + e^- + \bar{\nu}_e \,, \tag{6.35a}$$

$$e^+ + n \leftrightarrow p + \bar{\nu}_e \,, \tag{6.35b}$$

$$\nu_e + n \leftrightarrow p + e^- \,, \tag{6.35c}$$

which set the neutron-to-proton ratio (n/p) before the nucleosynthesis. As is well known, the neutron-to-proton ratio is one of the most important parameters of BBN, which determine the final abundances of light elements. Especially, the mass abundance of ^{4}He, Y_p, can be estimated by a simple analytical formula $Y_p \sim 1/\{1+(n/p)^{-1}_{\rm bbn}\}$ where $(n/p)_{\rm bbn}$ is the neutron-to-proton ratio just before the deuterium bottleneck opens and the synthesis of light elements begins (at the cosmic time $t_{\rm bbn} \sim 200$ sec and the temperature $T_{\rm bbn} \sim 80$ keV [28]). With the neutron lifetime τ_n and the freeze-out value of the neutron-to-proton ratio $(n/p)_f$, we can write $(n/p)_{\rm bbn} = (n/p)_f \, e^{-t_{\rm bbn}/\tau_n}$. In this study, we adopt the free neutron lifetime τ_n reported in Ref. [29]:

$$\tau_n = 880.2 \pm 1.0 \ \ {\rm sec} \ \ \ (68\%\,{\rm C.L.}). \tag{6.36}$$

In the standard big-bang cosmology, where all the active neutrinos are assumed to be fully thermalized well before an onset of BBN, the freeze-out value is known to be $(n/p)_f \sim 1/6$, which leads to $(n/p)_{\rm bbn} \sim 1/7$ and therefore $Y_p \sim 0.25$ [29]. In contrast, if neutrinos are not fully thermalized, the value of $(n/p)_f$ would be affected because both of the reaction rates of the processes (6.35a)–(6.35c), Γ_{np}, and the Hubble expansion rate $H \sim \sqrt{\rho}/m_{\rm pl}$ decrease due to the effect, and the freeze-out temperature of the processes (6.35a)–(6.35c) should be modified (see *e.g.* Refs. [26,27] for detailed discussions). Since ^{4}He is the second most abundant element in the Universe, final abundances of other light elements such as D, ^{3}He, ^{6}Li, and ^{7}Li are very sensitive to the ^{4}He abundance, and that is the main reason that light element abundances are modified if $T_{\rm RH} \sim \mathcal{O}(1)$ MeV. The important point is that since only ν_e is relevant to the processes (6.35a)–(6.35c), BBN is highly sensitive to the ν_e abundance and its energy spectrum. Hence, light element abundances are excellent probes of any physics in the early Universe, which exchange flavors of neutrinos such as neutrino self-interaction, $\nu_\alpha + \bar{\nu}_\alpha \to \nu_\beta + \bar{\nu}_\beta$ $(\alpha \neq \beta)$, or neutrino oscillation, $\nu_\alpha \to \nu_\beta$.

6.4.2 Observational abundances

An observational accuracy of light element abundances has been greatly improved over the last few decades. Especially, a precision of deuterium and helium abundances are already down to a few-percent level, and their observational data provide a precise determination of the baryon-to-photon ratio in the standard big-bang nucleosynthesis (SBBN) [29].

In our study, we adopt an observational value of the primordial mass abundance of ^{4}He, Y_p, reported in Ref. [42]:

$$Y_p = 0.2449 \pm 0.0040 \quad (68\%\,\mathrm{C.L.})\,, \tag{6.37}$$

which has been obtained by observing a recombination line of metal-poor stars in the extra-galactic HII regions or blue compact galaxies.

On the other side, we adopt the primordial value of the deuterium abundance D/H, *i.e.* the number density ratio of deuterium to hydrogen, reported in Ref. [40]:

$$\mathrm{D/H} = (2.545 \pm 0.025) \times 10^{-5} \quad (68\%\,\mathrm{C.L.})\,, \tag{6.38}$$

which has been determined by observing absorption spectra in high-redshift metal-poor quasar absorption systems.

6.4.3 Numerical calculation

We calculate the Boltzmann equations of light elements using a modified version of Kawano BBN code [23] with updated nuclear reaction rates (see Ref. [85] for more details). A contribution of X is taken into account into the Friedman equation and the energy conservation equation. Additionally, we pre-evaluate energy densities of active- and sterile neutrinos along with weak reaction rates of the processes (6.35a)–(6.35c) with the LASAGNA code and interpolate the data in the BBN code. In our study, we assume that the mass of the scalar particle m_X is smaller than the pion mass $m_\pi \sim 130$ MeV. In this case, a direct decay into hadrons is kinematically prohibited, and the scalar particles X fully decay into radiations such as photons and charged leptons. [7]

Further, in order to estimate theoretical uncertainties of light element abundances, we propagate experimental errors in the nuclear reaction rates and the free neutron lifetime by performing a Monte-Carlo calculation at each point in the 3D space of m_s, $\sin^2 2\theta$, and T_RH. Then, we can obtain observational constraints on mixing parameters of sterile

[7] If m_X is larger than m_π, hadrons should be created as a secondary particle even when the scalar particle X fully decay into radiations, and the effect induced by injected hadrons is important as shown in Ref. [1, 27, 85]. Also, it could be possible that the scalar particle directly decays into neutrinos, *e.g.* $X \to \nu_\alpha + \bar{\nu}_\alpha$ where $\alpha = e, \mu, \tau$. In such cases, a relic thermal bath of photons and electrons are mainly produced from neutrinos via weak interaction. Hence, the thermalization of active- and sterile neutrinos should be totally different from both cases of radiative and hadronic decays of X [69]. We will consider this possibility in future work.

neutrinos by performing χ^2 analysis using both theoretical and observational abundances of light elements. We define a χ^2 function as follows:

$$\chi^2 \equiv \chi^2_{\rm D/H} + \chi^2_{Y_p} = \frac{\{({\rm D/H})_{\rm th} - ({\rm D/H})_{\rm obs}\}^2}{\sigma^2_{\rm D,\,th} + \sigma^2_{\rm D,\,obs}} + \frac{\{Y_{p,\,\rm th} - Y_{p,\,\rm obs}\}^2}{\sigma^2_{Y_p,\,\rm th} + \sigma^2_{Y_p,\,\rm obs}}\,, \tag{6.39}$$

where $\chi^2_{\rm D/H}$ and $\chi^2_{Y_p}$ are χ^2 functions in terms of D/H and Y_p, respectively. Also, $i_{\rm\,th}$ ($\sigma_{i,\,\rm th}$) and $i_{\rm\,obs}$ ($\sigma_{i,\,\rm obs}$), where $i = {\rm D/H}$ and Y_p, are respectively the theoretical- and observational values (uncertainties) of light elements. The theoretical predictions and uncertainties are defined at each point in the 3D space written above, *i.e.* $i_{\rm\,th} = i_{\rm\,th}(m_{\rm s}, \sin^2 2\theta, T_{\rm RH})$ and $\sigma_{i,\,\rm th} = \sigma_{i,\,\rm th}(m_{\rm s}, \sin^2 2\theta, T_{\rm RH})$. In the computation of BBN, the baryon-to-photon ratio is the free parameter of the theory. On the other hand, a precise value of the baryon-to-photon ratio has been obtained by the Planck collaboration, and therefore we use the value as a prior of BBN in this study:

$$\eta_B = (6.14 \pm 0.04) \times 10^{-10}. \tag{6.40}$$

The region of 95% confidence level is defined as a parameter space which satisfies

$$\chi^2(m_{\rm s}, \sin^2 2\theta, \eta_B, T_{\rm RH}) < 5.991. \tag{6.41}$$

Then, we can obtain the BBN bound on sterile neutrinos by mapping it to the 2D space of the mixing parameters, *i.e.* $m_{\rm s}$ and $\sin^2 2\theta$.

6.4.4 Numerical result: ν_e–$\nu_{\rm s}$ mixing

First, we show the result of BBN in the case of ν_e–$\nu_{\rm s}$ mixing. Figure 6.6 shows the dependence of the ^{4}He and D abundances on the reheating temperature $T_{\rm RH}$ for the mixing parameters of sterile neutrinos Eq. (6.33). Light element abundances produced in BBN strongly depend on the value of the baryon-to-photon ratio $\eta_B = (n_B - \bar{n}_B)/n_\gamma$ where n_B ($\bar{n}_B$) is the number density of baryons (anti-baryons), and n_γ is the number density of photons. Since η_B is a free parameter of BBN, in Figure 6.6 we use the median value of η_B reported by Planck collaboration [3]:

$$\eta_B = 6.14 \times 10^{-10} \quad (68\%\,{\rm C.L.})\,. \tag{6.42}$$

As can be seen from Figure 6.6, light element abundances increase with the reheating temperature. This is because sterile neutrinos are more abundantly produced for large $T_{\rm RH}$ (see Figure 6.1), and therefore the total energy density of the Universe is larger than the case without the contribution of sterile neutrinos. This induces the early decoupling of the weak processes (6.35a)–(6.35c), and the neutron-to-photon ratio is increased due to the effect, which leads to large values of Y_p and D/H (see Chapter 5 or Ref. [1] for more detailed explanations). In this way, overproduction of the light sterile neutrinos is relieved in the low-reheating-temperature scenario.

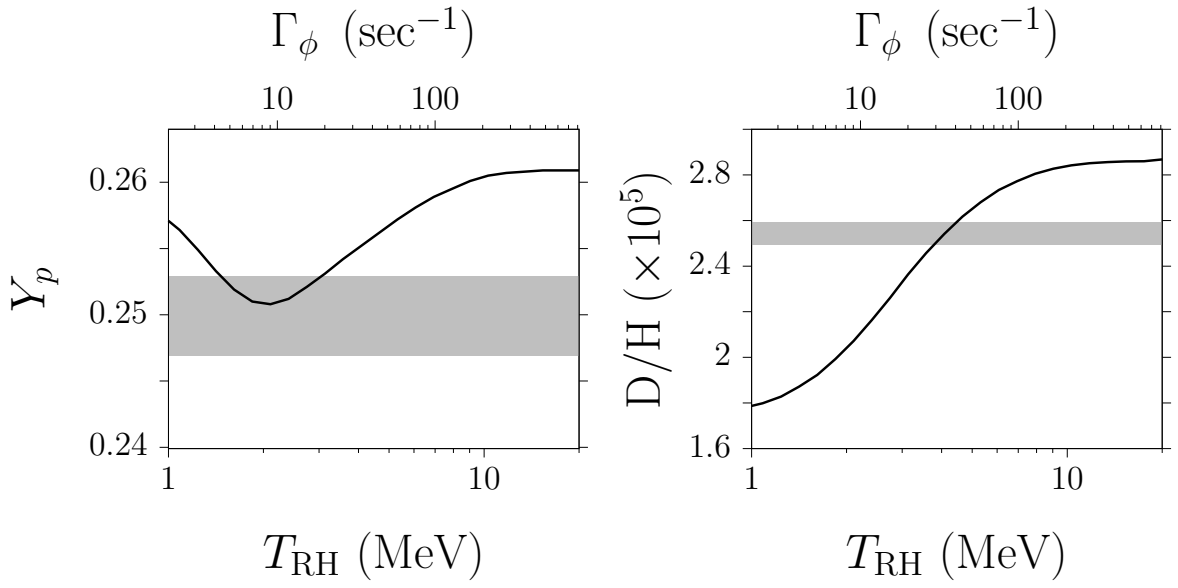

Figure 6.6: The mass abundance of ^{4}He, Y_p, and the deuterium abundance, D/H, as functions of the reheating temperature $T_{\rm RH}$. The value of the baryon-to-photon ratio is fixed at $\eta_B = 6.13 \times 10^{-10}$ in the figure. The 2-σ observational bounds on Y_p (Ref. [42]) and D/H (Ref. [40]) are also shown as the gray-shaded region.

6.5 Cosmological constraint on sterile neutrinos

In this section, we discuss cosmological constraints on sterile neutrinos, obtained from the computation of the sterile neutrino production and the synthesis of light elements.

Figure 6.7 shows the constraint on sterile neutrinos imposed by BBN. In the figure, the 2-σ allowed region of the light sterile neutrinos, obtained in Ref. [127], is also shown. Besides, we plot the dark-matter constraint on sterile neutrinos, obtained by comparing between the density parameter of sterile neutrino $\Omega_{\rm s}$ and the relic abundance of dark matter $\Omega_{\rm DM}$, *i.e.* $\Omega_{\rm s} < \Omega_{\rm DM} = 0.263$ (best fit value from Planck + BAO) [3]. To obtain the dark matter bound, the reheating temperature is fixed to 5 MeV as the density parameter of sterile neutrinos depends on the value of this parameter. [8]

It can be seen from Figure 6.7 that the existence of the light sterile neutrinos is actually in agreement with the observation of light elements synthesized in BBN for the reheating temperature of $\mathcal{O}(1)$ MeV. This result is in contrast to the previous results obtained in the framework of the standard big-bang cosmology, where neutrinos are implicitly assumed to be thermalized well before the nucleosynthesis [73, 129, 130].

As active- and sterile neutrinos obtain unique energy spectra depending on the reheat-

[8] As we have seen in Chapter 5, the reheating temperature of 5 MeV almost corresponds to the lower bound imposed by BBN for the cases without sterile neutrinos. Therefore, it can be seen as a typical value of the reheating temperature that we are interested in.

ing temperature, we would be able to verify or exclude the scenario by observing energy distributions of active neutrinos in the future neutrino experiment such as the PTOLEMY project, which is aiming at directly detecting cosmic neutrino background (CνB) with detectors on the earth.

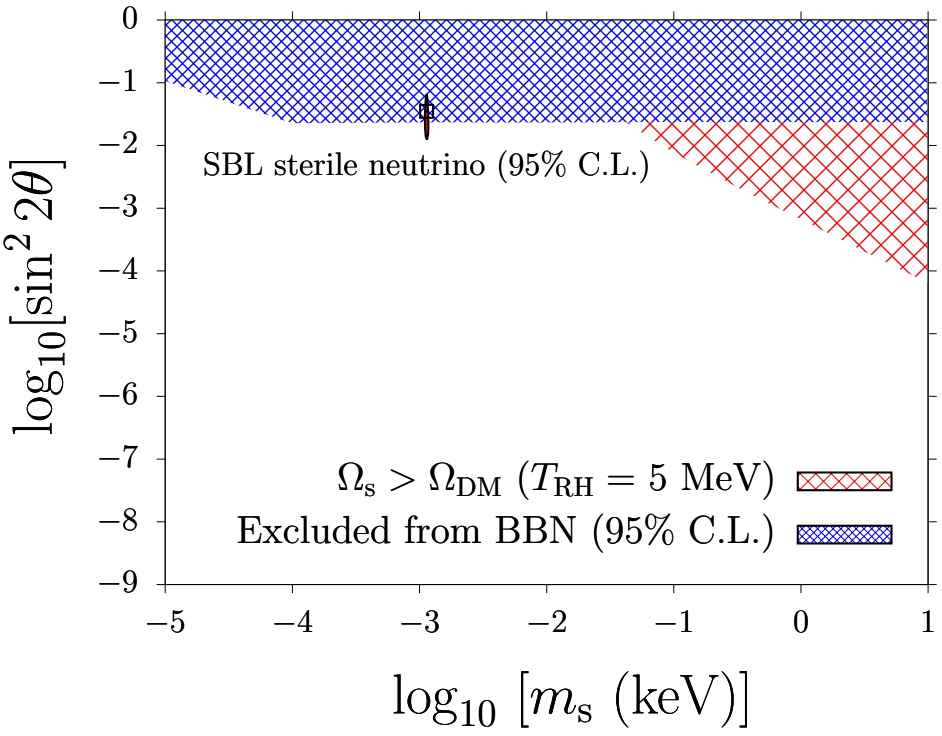

Figure 6.7: Observational constraint on the mixing parameter of sterile neutrinos. The blue fine-meshed and the red coarse-meshed regions are excluded by BBN and the overproduction of dark matter, respectively. The dark matter bound is obtained by fixing the reheating temperature to 5 MeV. Also, the 2-σ inferred region and the best-fit value of the mixing parameter for the light sterile neutrinos obtained in Ref. [127] are also shown by the red vertical region and the black box, respectively.

6.6 Conclusion of Chapter 6

In this chapter, we have investigated the possible existence of sterile neutrinos with a various range of masses in terms of cosmology assuming an MeV-scale reheating temperature.

The eV-scale sterile neutrinos, inferred from short-baseline neutrino oscillation experiments, are currently strongly and partially disfavored by several results of long-baseline neutrino oscillation experiments (MINOS/MINOS+, NOνA, and IceCube) and reactor neutrino experiments (Daya Bay, Bugey-3, and PROSPECT), respectively. However, the origin of the anomaly existing in the short-baseline neutrino experiments is still under debate, and it is therefore still interesting to examine the possibility of the light sterile neutrinos from cosmological point of view.

In our study we have performed numerical computation of the sterile neutrino production through neutrino oscillation and shown that the existence of light sterile neutrinos inferred from short-baseline neutrino oscillation experiments becomes consistent with ob-

servational results of big-bang nucleosynthesis (BBN) for the reheating temperature of $\mathcal{O}(1)$ MeV. This is in contrast to the result obtained in the standard big-bang cosmology, where neutrinos are assumed to be thermalized well before the nucleosynthesis.

As neutrinos obtain unique energy spectra depending on the reheating temperature in this scenario, we would be able to verify or exclude the scenario by observing energy spectra of active neutrinos in the future neutrino experiment such as the PTOLEMY project, which is aiming at directly detecting cosmic neutrino background with detectors on the earth.

Chapter 7

Summary and future prospects

In this chapter, we summarize the conclusions drawn in the previous chapters and provide a comment on the future prospects of our studies.

7.1 Summary of this thesis

In our studies, we have investigated the possibility of an MeV-scale reheating temperature of the Universe and discussed the active- and sterile neutrino thermalization in the scenario. Such a low reheating temperature is motivated by theories beyond the standard model of particle physics which include long-lived massive particles with masses around the weak scale $\sim \mathcal{O}(100)$ GeV, decaying only through gravitational interaction. By focusing on the roles of active- and sterile neutrinos in the production of light elements synthesized in the big-bang nucleosynthesis (BBN) and discussing their thermalization in the reheating, we have obtained observational constraints on i) lower bounds on the reheating temperature, and ii) possibilities of sterile neutrinos with a various range of its mass, which are summarized in Refs. [1] and [2], respectively.

In chapter 5, we focused on our study [1], which investigated a lower bound on the reheating temperature imposed by BBN. Since the reheating temperature is still unknown, and its value is closely related to *e.g.* a possible thermal history of the Universe, a property of exotic particles responsible for the reheating, dark matter production, and a mechanism of baryogenesis, it is of great importance to provide robust and accurate constraints on it in terms of observations. In contrast to the standard big-bang cosmology, where neutrinos are *implicitly assumed* to be completely thermalized before the onset of BBN, the MeV-scale reheating temperature leads to the flavor-dependent imperfect thermalization of neutrinos as shown in Figures 5.2–5.5. Consequently, the initial condition of BBN (*i.e.* the freeze-out value of the neutron-to-proton ratio n/p) is affected by the reduced abundances of neutrinos (especially of ν_e), and theoretical predictions of nuclear abundances are modified compared to those predicted in the standard big-bang nucleosynthesis. To consider more specifically, we have examined two possibilities for the decay mode of the long-lived massive particles X:

(a) Radiative decays:

X decays into photons (γ) or charged leptons (l), *i.e.* $X \to \gamma + \ldots$ or $X \to l + \ldots$,

(b) Hadronic decays:

X decays into quarks (q) or gluons (g), *i.e.* $X \to q + \ldots$ or $X \to g + \ldots$.

By numerically calculating the thermalization of neutrinos and the nucleosynthesis, we have obtained theoretical abundances of light elements both for the case of the radiative decay (Figures 5.7–5.8) and for the case of the hadronic decay (Figure 5.11). The notable point of our study is that we have performed detailed calculations of the neutrino thermalization, taking into account neutrino oscillation and neutrino self-interaction, in both cases of the radiative- and hadronic decays.

As a result, a comparison of the theoretical prediction with observed abundances (Eq. (3.61) for ^{4}He and Eq. (3.58) for D) leads to the 95% C.L. lower bound on the reheating temperature:

$$T_{\rm RH} \gtrsim 1.8 \text{ MeV}\,, \tag{7.1}$$

for the massive particle X which fully decays into radiation, and

$$T_{\rm RH} \gtrsim 4.1 - 4.9 \text{ MeV}\,, \tag{7.2}$$

for the massive particle X which fully decays into hadrons for the mass range of the massive particle $m_X = 10$ GeV–100 TeV (Figure 5.14). As expected, the lower bound is more stringent if the massive particle has a hadronic branching ratio. This is because injected hadrons such as pions $\pi^\pm$ additionally inter-convert neutrons and protons as *e.g.* $\pi^- + p \to \pi^0 + n$ and $n + \pi^+ \to p + \pi^0$, and thereby significantly increasing the n/p ratio compared to the 100% radiative decay cases. Furthermore, we revealed that neutrino oscillation and neutrino self-interaction enhance the thermalization of neutrinos (Figures 5.2, 5.4, and 5.5) and reduce the inter-conversion rates of neutrons with protons, thereby increasing the lower bound on the reheating temperature at the level of $\mathcal{O}(10)$% in the case of the 100% radiative decays (Figure 5.10) and $\mathcal{O}(1)$% in most cases of hadronic decays (Figure 5.12). Also, the reheating temperature $T_{\rm RH}$ and the effective number of neutrino species $N_{\rm eff}$ have a one-to-one correspondence in the scenario that we are considering, and therefore we also obtained a 95% C.L. lower bound on $N_{\rm eff}$:

$$N_{\rm eff} \gtrsim 1.0, \tag{7.3}$$

for the massive particle X which fully decays into radiation. In the same way, for the massive particle X which fully decays into hadrons, we found:

$$N_{\rm eff} \gtrsim 2.7 - 2.9 \quad \text{for} \quad m_X = 10 \text{ GeV} - 100 \text{ TeV}\,, \tag{7.4}$$

when the hadronic branching ratio Br $= 1.0$, whereas

$$N_{\rm eff} \gtrsim 1.3 - 2.5 \quad \text{for} \quad m_X = 10 \text{ GeV} - 100 \text{ TeV}\,, \tag{7.5}$$

when the hadronic branching ratio Br = 0.001. It can be seen that the possible minimum value of $N_{\rm eff}$ is not always smaller than the 95% lower bound in the standard big-bang nucleosynthesis, $N_{\rm eff} > 2.26$. However, possible detection of the effective number of neutrino species smaller than three in future observations should be clear evidence of the low reheating temperature. Additionally, it should also be useful to detect the cosmic neutrino background (CνB) and reveal the energy distribution of neutrinos for verifying the MeV-scale reheating scenario as neutrinos obtain unique non-thermal spectra depending on the value of $T_{\rm RH}$. In this way the future direct detection program of CνB such as the PTOLEMY experiment will be able to examine this scenario [87].

In chapter 6, we concentrated on our study (Ref. [2]), which investigated the possible existence of sterile neutrinos with a various range of masses in terms of cosmology assuming an MeV-scale reheating temperature. The motivation of this study is the light sterile neutrinos with eV-scale masses, inferred from results obtained in short-baseline (SBL) neutrino oscillation experiments. Such eV-scale sterile neutrinos, which have appreciable mixings with active neutrinos, are known to be copiously produced in the early Universe through neutrino oscillation, and hence its existence is inconsistent with observations of BBN and CMB. This is however only true in the standard big-bang cosmology, and some non-standard physics could save the existence of the light sterile neutrinos. The MeV-scale reheating temperature is one of the plausible possibilities because maximum production of sterile neutrinos occurs at

$$T_{\rm max} \sim 13\,{\rm MeV}\left(\frac{m_{\rm s}}{1\,{\rm eV}}\right)^{1/3}, \tag{7.6}$$

with $m_{\rm s}$ the sterile neutrino mass. Thus, for the reheating temperature of $\mathcal{O}(1)$ MeV, sterile neutrino production is always ineffective, and its final abundance is expected to be significantly suppressed, improving the agreement between light sterile neutrinos and cosmology. In our study, we have calculated the sterile neutrino abundance produced through neutrino oscillation (Figure 6.6) and then found that the parameter space for the light sterile neutrinos inferred from the SBL experiments become consistent with observational results of BBN if the reheating temperature is at the same order or below $\mathcal{O}(1)$ MeV (Figure 6.7).

7.2 Future prospects

Finally, let us comment on the future prospects of our studies. There are mainly two things worth referring to.

First, in our studies we only discussed BBN to constrain the reheating temperature (Chapter 5) and the property of sterile neutrinos (Chapter 6). On the other hand, dynamics of the cosmic microwave background (CMB) and the large-scale structure (LSS) of the Universe also depend on the expansion history of the Universe, and their results should therefore be sensitive to the thermalization of active- and sterile neutrinos. For this reason, it would be interesting to discuss observational constraints imposed by CMB and

LSS along with BBN. This requires us to perform a tough numerical computation, but it will not be a far-reaching project because there are several sophisticated- and numerically efficient codes for the computation of CMB and LSS which are publicly available.

The second future issue which deserves to be improved is the treatment of the neutrino oscillation. In Chapter 5 we approximated the full three-flavor neutrino mixings to the effective two-flavor mixing between ν_e and ν_x by neglecting the reactor neutrino mixing $(\delta m^2_{13}, \theta_{13})$. This treatment is indeed accurate enough to obtain the constraint on the reheating temperature as we revealed in the study, but it is inevitable to consider full three-flavor mixing if one hopes to discuss the effects of the CP-violating phase or the lepton chemical potentials on the neutrino thermalization because the effective two-flavor approximation is incompatible with these effects. Therefore, it is desirable to take full three-flavor mixings into account by improving the numerical efficiency of our code for a computation of the reheating and the neutrino thermalization. Similarly, in Chapter 6 we simplified the neutrino oscillation between three active- and one sterile neutrinos (3+1 mixing) to the two-flavor mixing between one active- and one sterile neutrinos (1+1 mixing). This treatment is just an approximation without any justification, and it is therefore more severe than the previous one. The numerical computation based on the 3+1 mixing is challenging, but that based on the 2+1 mixing is somewhat realistic. One would be able to attain it by performing MPI calculations with a supercomputer.

Acknowledgement

The author would like to appreciate his supervisor K. Kohri for the thorough encouragement over four-years during the Ph.D. study and valuable discussions. The author would also very much like to thank N. Hiroshima, S. Wang, R. S. L. Hansen, T. Tram, and S. Hannestad, who are collaborators of the studies in this thesis. This thesis would not be completed without their continued supports. The author is also grateful to T. Matsubara and K. Kyutoku for looking after him and giving him supportive comments. Finally, the author wishes to express his gratitude to all the members of Cosmophysics Group, KEK Theory Center, and the colleagues of SOKENDAI for sparing their time to discuss physics or other things. The author owes what he is today to these considerable persons.

Bibliography

[1] T. Hasegawa, N. Hiroshima, K. Kohri, R. Hansen, T. Tram and S. Hannestad, *MeV-scale reheating temperature and thermalization of oscillating neutrinos by radiative and hadronic decays of massive particles*, *JCAP* **12** (2019) 012 [1908.10189].

[2] T. Hasegawa, K. Kohri, S. Wang, R. Hansen, T. Tram and S. Hannestad, *MeV-scale reheating temperature and cosmological constraints on sterile neutrinos*, *In preparation, 2019* .

[3] Planck collaboration, *Planck 2018 results. VI. Cosmological parameters*, 1807.06209.

[4] S. Weinberg, *Gravitation and Cosmology*. John Wiley and Sons, New York, 1972.

[5] S. Weinberg, *Cosmology*. 2008.

[6] E. Kolb and M. Turner, *The Early Universe*, *Front. Phys.* **69** (1990) 1.

[7] S. Dodelson, *Modern Cosmology*. Academic Press, Amsterdam, 2003.

[8] A. Walker, *On Milne's Theory of World-Structure*, *Proceedings of the London Mathematical Society* **s2-42** (1937) 90.

[9] H. Robertson, *Kinematics and World-Structure*, *The Astrophysical Journal* **82** (1935) 284.

[10] H. Robertson, *Kinematics and World-Structure II.*, *The Astrophysical Journal* **83** (1936) 187.

[11] H. Robertson, *Kinematics and World-Structure III.*, *The Astrophysical Journal* **83** (1936) 257.

[12] DES collaboration, *Dark Energy Survey Year 1 results: Cosmological constraints from cosmic shear*, *Phys. Rev.* **D98** (2018) 043528 [1708.01538].

[13] D. Baumann, *Primordial Cosmology*, *PoS* **TASI2017** (2018) 009 [1807.03098].

[14] G. Gamow, *Expanding universe and the origin of elements*, *Phys. Rev.* **70** (1946) 572.

[15] R. Alpher, H. Bethe and G. Gamow, *The origin of chemical elements*, *Phys. Rev.* **73** (1948) 803.

[16] F. Hoyle and R. Tayler, *The Mystery of the Cosmic Helium Abundance*, *Nature* **203** (1964) 1108.

[17] P. Peebles, *Primeval Helium Abundance and the Primeval Fireball*, *Phys. Rev. Lett.* **16** (1966) 410.

[18] R. Wagoner, W. Fowler and F. Hoyle, *On the Synthesis of elements at very high temperatures*, *Astrophys. J.* **148** (1967) 3.

[19] A. Yahil and G. Beaudet, *Big-Bang Nucleosynthesis with Nonzero Lepton Numbers*, *Astrophys. J.* **206** (1976) 26.

[20] N. Terasawa and K. Sato, *Nucleosynthesis in the low-entropy and lepton-degenerate universe*, *The Astrophysical Journal* **294** (1985) 9.

[21] R. Wagoner, *Big bang nucleosynthesis revisited*, *Astrophys. J.* **179** (1973) 343.

[22] D. Dicus, E. Kolb, A. Gleeson, E. Sudarshan, V. Teplitz and M. Turner, *Primordial Nucleosynthesis Including Radiative, Coulomb, and Finite Temperature Corrections to Weak Rates*, *Phys. Rev.* **D26** (1982) 2694.

[23] L. Kawano, *Let's go: Early universe. 2. Primordial nucleosynthesis: The Computer way*, .

[24] O. Pisanti, A. Cirillo, S. Esposito, F. Iocco, G. Mangano, G. Miele et al., *PArthENoPE: Public Algorithm Evaluating the Nucleosynthesis of Primordial Elements*, *Comput. Phys. Commun.* **178** (2008) 956 [0705.0290].

[25] A. Arbey, *AlterBBN: A program for calculating the BBN abundances of the elements in alternative cosmologies*, *Comput. Phys. Commun.* **183** (2012) 1822 [1106.1363].

[26] M. Kawasaki, K. Kohri and N. Sugiyama, *Cosmological constraints on late time entropy production*, *Phys. Rev. Lett.* **82** (1999) 4168 [astro-ph/9811437].

[27] M. Kawasaki, K. Kohri and N. Sugiyama, *MeV scale reheating temperature and thermalization of neutrino background*, *Phys. Rev.* **D62** (2000) 023506 [astro-ph/0002127].

[28] G. Steigman, *Primordial Nucleosynthesis in the Precision Cosmology Era*, *Ann. Rev. Nucl. Part. Sci.* **57** (2007) 463 [0712.1100].

[29] Particle Data Group collaboration, *Review of Particle Physics*, *Phys. Rev.* **D98** (2018) 030001.

[30] M. Smith, L. Kawano and R. Malaney, *Experimental, computational, and observational analysis of primordial nucleosynthesis*, *Astrophys. J. Suppl.* **85** (1993) 219.

[31] R. Esmailzadeh, G. Starkman and S. Dimopoulos, *Primordial nucleosynthesis without a computer*, *Astrophys. J.* **378** (1991) 504.

[32] R. H. Cyburt, B. D. Fields, K. A. Olive and T. Yeh, *Big Bang Nucleosynthesis: 2015*, *Rev. Mod. Phys.* **88** (2016) 015004 [1505.01076].

[33] M. Asplund, D. Lambert, P. Nissen, F. Primas and V. Smith, *Lithium isotopic abundances in metal-poor halo stars*, *Astrophys. J.* **644** (2006) 229 [astro-ph/0510636].

[34] R. Cayrel, M. Steffen, H. Chand, P. Bonifacio, M. Spite, F. Spite et al., *Line shift, line asymmetry, and the 6Li/7Li isotopic ratio determination*, *Astron. Astrophys.* **473** (2007) L37 [0708.3819].

[35] M. Steffen, R. Cayrel, P. Bonifacio, H. Ludwig and E. Caffau, *6Li in metal-poor halo stars: real or spurious?*, *IAU Symp.* **265** (2010) 23 [0910.5917].

[36] A. Perez, W. Aoki, S. Inoue, S. Ryan, T. Suzuki and M. Chiba, *6Li/7Li estimates for metal-poor stars*, *Astron. Astrophys.* **504** (2009) 213 [0909.5163].

[37] K. Lind, J. Melendez, M. Asplund, R. Collet and Z. Magic, *The lithium isotopic ratio in very metal-poor stars*, *Astron. Astrophys.* **554** (2013) A96 [1305.6564].

[38] B. Fields, *The primordial lithium problem*, *Ann. Rev. Nucl. Part. Sci.* **61** (2011) 47 [1203.3551].

[39] M. Pettini and R. Cooke, *A new, precise measurement of the primordial abundance of Deuterium*, *Mon. Not. Roy. Astron. Soc.* **425** (2012) 2477 [1205.3785].

[40] E. Zavarygin, J. Webb, S. Riemer-Sørensen and V. Dumont, *Primordial deuterium abundance at z_{abs} = 2:504 towards Q1009+2956*, *J. Phys. Conf. Ser.* **1038** (2018) 012012 [1801.04704].

[41] Y. I. Izotov, T. X. Thuan and N. G. Guseva, *A new determination of the primordial He abundance using the He i λ10830 Å emission line: cosmological implications*, *Mon. Not. Roy. Astron. Soc.* **445** (2014) 778 [1408.6953].

[42] E. Aver, K. Olive and E. Skillman, *The effects of He I λ10830 on helium abundance determinations*, *JCAP* **1507** (2015) 011 [1503.08146].

[43] Planck collaboration, *Planck 2015 results. XIII. Cosmological parameters*, *Astron. Astrophys.* **594** (2016) A13 [1502.01589].

[44] B. Pontecorvo, *Mesonium and antimesonium*, *Zhur. Eksptl'. i Teoret. Fiz.* **33** (1957) .

[45] Z. Maki, M. Nakagawa and S. Sakata, *Remarks on the unified model of elementary particles*, *Progress of Theoretical Physics* **28** (1962) 870.

[46] R. Davis Jr, D. Harmer and K. Hoffman, *Search for neutrinos from the sun*, *Physical Review Letters* **20** (1968) 1205.

[47] T. Kitamura and T. Nakatsuka, *Comments on the super kamiokande project (next-generation underground facility at kamioka)*, *Il Nuovo Cimento A (1965-1970)* **103** (1990) 1443.

[48] G. Aardsma, R. Allen, J. Anglin, M. Bercovitch, A. Carter, H. Chen et al., *A heavy water detector to resolve the solar neutrino problem*, *Physics Letters B* **194** (1987) 321.

[49] Y. Fukuda, T. Hayakawa, E. Ichihara, K. Inoue, K. Ishihara, H. Ishino et al., *Study of the atmospheric neutrino flux in the multi-gev energy range*, *Physics Letters B* **436** (1998) 33.

[50] Super-Kamiokande collaboration, *Measurement of a small atmospheric muon-neutrino / electron-neutrino ratio*, *Phys. Lett.* **B433** (1998) 9 [hep-ex/9803006].

[51] P. de Salas, D. Forero, C. Ternes, M. Tortola and J. Valle, *Status of neutrino oscillations 2018: 3σ hint for normal mass ordering and improved CP sensitivity*, *Phys. Lett.* **B782** (2018) 633 [1708.01186].

[52] L. Wolfenstein, *Effects of Matter on Neutrino Oscillations*, *AIP Conf. Proc.* **52** (1979) 108.

[53] S. Mikheyev and A. Smirnov, *Resonant neutrino oscillations in matter*, *Prog. Part. Nucl. Phys.* **23** (1989) 41.

[54] L. Johns, M. Mina, V. Cirigliano, M. Paris and G. Fuller, *Neutrino flavor transformation in the lepton-asymmetric universe*, *Phys. Rev.* **D94** (2016) 083505 [1608.01336].

[55] G. Raffelt, G. Sigl and L. Stodolsky, *NonAbelian Boltzmann equation for mixing and decoherence*, *Phys. Rev. Lett.* **70** (1993) 2363 [hep-ph/9209276].

[56] G. Sigl and G. Raffelt, *General kinetic description of relativistic mixed neutrinos*, *Nucl. Phys.* **B406** (1993) 423.

[57] B. McKellar and M. Thomson, *Oscillating doublet neutrinos in the early universe*, *Phys. Rev.* **D49** (1994) 2710.

[58] A. Vlasenko, G. M. Fuller and V. Cirigliano, *Neutrino Quantum Kinetics*, *Phys. Rev.* **D89** (2014) 105004 [1309.2628].

[59] A. Vlasenko, G. M. Fuller and V. Cirigliano, *Prospects for Neutrino-Antineutrino Transformation in Astrophysical Environments*, 1406.6724.

[60] C. Volpe, D. Väänänen and C. Espinoza, *Extended evolution equations for neutrino propagation in astrophysical and cosmological environments*, *Phys. Rev.* **D87** (2013) 113010 [1302.2374].

[61] J. Serreau and C. Volpe, *Neutrino-antineutrino correlations in dense anisotropic media*, *Phys. Rev.* **D90** (2014) 125040 [1409.3591].

[62] A. Kartavtsev, G. Raffelt and H. Vogel, *Neutrino propagation in media: Flavor-, helicity-, and pair correlations*, *Phys. Rev.* **D91** (2015) 125020 [1504.03230].

[63] C. Volpe, *Neutrino Quantum Kinetic Equations*, *Int. J. Mod. Phys.* **E24** (2015) 1541009 [1506.06222].

[64] D. Notzold and G. Raffelt, *Neutrino Dispersion at Finite Temperature and Density*, *Nucl. Phys.* **B307** (1988) 924.

[65] F. Iocco, G. Mangano, G. Miele, O. Pisanti and P. D. Serpico, *Primordial Nucleosynthesis: from precision cosmology to fundamental physics*, *Phys. Rept.* **472** (2009) 1 [0809.0631].

[66] N. F. Bell, R. R. Volkas and Y. Y. Y. Wong, *Relic neutrino asymmetry evolution from first principles*, *Phys. Rev.* **D59** (1999) 113001 [hep-ph/9809363].

[67] K. Ichikawa, M. Kawasaki and F. Takahashi, *The Oscillation effects on thermalization of the neutrinos in the Universe with low reheating temperature*, *Phys. Rev.* **D72** (2005) 043522 [astro-ph/0505395].

[68] P. de Salas, M. Lattanzi, G. Mangano, G. Miele, S. Pastor and O. Pisanti, *Bounds on very low reheating scenarios after Planck*, *Phys. Rev.* **D92** (2015) 123534 [1511.00672].

[69] S. Hannestad, *What is the lowest possible reheating temperature?*, *Phys. Rev.* **D70** (2004) 043506 [astro-ph/0403291].

[70] K. Ichikawa, M. Kawasaki and F. Takahashi, *Constraint on the Effective Number of Neutrino Species from the WMAP and SDSS LRG Power Spectra*, *JCAP* **0705** (2007) 007 [astro-ph/0611784].

[71] F. De Bernardis, L. Pagano and A. Melchiorri, *New constraints on the reheating temperature of the universe after WMAP-5*, *Astropart. Phys.* **30** (2008) 192.

[72] S. Hannestad, R. Hansen, T. Tram and Y. Wong, *Active-sterile neutrino oscillations in the early Universe with full collision terms*, *JCAP* **1508** (2015) 019 [1506.05266].

[73] S. Hannestad, I. Tamborra and T. Tram, *Thermalisation of light sterile neutrinos in the early universe*, *JCAP* **1207** (2012) 025 [1204.5861].

[74] S. Hannestad, R. Hansen and T. Tram, *Can active-sterile neutrino oscillations lead to chaotic behavior of the cosmological lepton asymmetry?*, *JCAP* **1304** (2013) 032 [1302.7279].

[75] L. F. Shampine and M. W. Reichelt, *The matlab ode suite*, *SIAM journal on scientific computing* **18** (1997) 1.

[76] G. Mangano, G. Miele, S. Pastor, T. Pinto, O. Pisanti and P. D. Serpico, *Relic neutrino decoupling including flavor oscillations*, *Nucl. Phys.* **B729** (2005) 221 [hep-ph/0506164].

[77] P. Salas and S. Pastor, *Relic neutrino decoupling with flavour oscillations revisited*, *JCAP* **1607** (2016) 051 [1606.06986].

[78] N. Bell, R. Volkas and Y. Wong, *Relic neutrino asymmetry evolution from first principles*, *Phys. Rev.* **D59** (1999) 113001 [hep-ph/9809363].

[79] K. Enqvist, K. Kainulainen and M. Thomson, *Stringent cosmological bounds on inert neutrino mixing*, *Nucl. Phys.* **B373** (1992) 498.

[80] R. Foot and R. Volkas, *The Exact parity symmetric model and big bang nucleosynthesis*, *Astropart. Phys.* **7** (1997) 283 [hep-ph/9612245].

[81] M. Reno and D. Seckel, *Primordial Nucleosynthesis: The Effects of Injecting Hadrons*, *Phys. Rev.* **D37** (1988) 3441.

[82] K. Kohri, *Primordial nucleosynthesis and hadronic decay of a massive particle with a relatively short lifetime*, *Phys. Rev.* **D64** (2001) 043515 [astro-ph/0103411].

[83] M. Kawasaki, K. Kohri and T. Moroi, *Big-Bang nucleosynthesis and hadronic decay of long-lived massive particles*, *Phys. Rev.* **D71** (2005) 083502 [astro-ph/0408426].

[84] M. Pospelov and J. Pradler, *Metastable GeV-scale particles as a solution to the cosmological lithium problem*, *Phys. Rev.* **D82** (2010) 103514 [1006.4172].

[85] M. Kawasaki, K. Kohri, T. Moroi and Y. Takaesu, *Revisiting Big-Bang Nucleosynthesis Constraints on Long-Lived Decaying Particles*, *Phys. Rev.* **D97** (2018) 023502 [1709.01211].

[86] J. Hamann, S. Hannestad, G. Raffelt and Y. Wong, *Sterile neutrinos with eV masses in cosmology: How disfavoured exactly?*, *JCAP* **1109** (2011) 034 [1108.4136].

[87] PTOLEMY collaboration, *Neutrino physics with the PTOLEMY project: active neutrino properties and the light sterile case*, *JCAP* **1907** (2019) 047 [1902.05508].

[88] R. H. Cyburt, B. D. Fields, K. A. Olive and T. Yeh, *Big bang nucleosynthesis: Present status*, *Reviews of Modern Physics* **88** (2016) 015004.

[89] LSND collaboration, *Evidence for nu(mu) → nu(e) neutrino oscillations from LSND*, *Phys. Rev. Lett.* **81** (1998) 1774 [nucl-ex/9709006].

[90] MiniBooNE collaboration, *Event Excess in the MiniBooNE Search for $\bar{\nu}_\mu \to \bar{\nu}_e$ Oscillations*, *Phys. Rev. Lett.* **105** (2010) 181801 [1007.1150].

[91] MiniBooNE collaboration, *Observation of a Significant Excess of Electron-Like Events in the MiniBooNE Short-Baseline Neutrino Experiment*, 1805.12028.

[92] Daya Bay collaboration, *Measurement of the Reactor Antineutrino Flux and Spectrum at Daya Bay*, *Phys. Rev. Lett.* **116** (2016) 061801 [1508.04233].

[93] Double Chooz collaboration, *Indication of Reactor $\bar{\nu}_e$ Disappearance in the Double Chooz Experiment*, *Phys. Rev. Lett.* **108** (2012) 131801 [1112.6353].

[94] D. Abdurashitov et al., *The Russian-American gallium experiment (SAGE) Cr neutrino source measurement*, *Phys. Rev. Lett.* **77** (1996) 4708.

[95] SAGE collaboration, *Measurement of the response of the Russian-American gallium experiment to neutrinos from a Cr-51 source*, *Phys. Rev.* **C59** (1999) 2246 [hep-ph/9803418].

[96] J. Abdurashitov et al., *Measurement of the response of a Ga solar neutrino experiment to neutrinos from an Ar-37 source*, *Phys. Rev.* **C73** (2006) 045805 [nucl-ex/0512041].

[97] GALLEX collaboration, *First results from the Cr-51 neutrino source experiment with the GALLEX detector*, *Phys. Lett.* **B342** (1995) 440.

[98] GALLEX collaboration, *Final results of the Cr-51 neutrino source experiments in GALLEX*, *Phys. Lett.* **B420** (1998) 114.

[99] F. Kaether, W. Hampel, G. Heusser, J. Kiko and T. Kirsten, *Reanalysis of the GALLEX solar neutrino flux and source experiments*, *Phys. Lett.* **B685** (2010) 47 [1001.2731].

[100] P. Machado, O. Palamara and D. Schmitz, *The Short-Baseline Neutrino Program at Fermilab*, *Ann. Rev. Nucl. Part. Sci.* **69** (2019) [1903.04608].

[101] J. Park, *Searching for a Sterile Neutrino at J-PARC MLF: $JSNS^2$ experiment*, *PoS* **EPS-HEP2017** (2017) 128.

[102] IceCube collaboration, *Searches for Sterile Neutrinos with the IceCube Detector*, *Phys. Rev. Lett.* **117** (2016) 071801 [1605.01990].

[103] MINOS+ collaboration, *Search for sterile neutrinos in MINOS and MINOS+ using a two-detector fit*, *Phys. Rev. Lett.* **122** (2019) 091803 [1710.06488].

[104] NOvA collaboration, *Search for active-sterile neutrino mixing using neutral-current interactions in NOvA*, *Phys. Rev.* **D96** (2017) 072006 [1706.04592].

[105] G. Gelmini, P. Lu and V. Takhistov, *Visible Sterile Neutrinos as the Earliest Relic Probes of Cosmology*, 1909.04168.

[106] Daya Bay collaboration, *Improved Search for a Light Sterile Neutrino with the Full Configuration of the Daya Bay Experiment*, *Phys. Rev. Lett.* **117** (2016) 151802 [1607.01174].

[107] Y. Declais et al., *Search for neutrino oscillations at 15-meters, 40-meters, and 95-meters from a nuclear power reactor at Bugey*, *Nucl. Phys.* **B434** (1995) 503.

[108] PROSPECT collaboration, *First search for short-baseline neutrino oscillations at HFIR with PROSPECT*, *Phys. Rev. Lett.* **121** (2018) 251802 [1806.02784].

[109] K. Abazajian, N. Bell, G. Fuller and Y. Wong, *Cosmological lepton asymmetry, primordial nucleosynthesis, and sterile neutrinos*, *Phys. Rev.* **D72** (2005) 063004 [astro-ph/0410175].

[110] A. Mirizzi, N. Saviano, G. Miele and P. Serpico, *Light sterile neutrino production in the early universe with dynamical neutrino asymmetries*, *Phys. Rev.* **D86** (2012) 053009 [1206.1046].

[111] N. Saviano, A. Mirizzi, O. Pisanti, P. Serpico, G. Mangano and G. Miele, *Multi-momentum and multi-flavour active-sterile neutrino oscillations in the early universe: role of neutrino asymmetries and effects on nucleosynthesis*, *Phys. Rev.* **D87** (2013) 073006 [1302.1200].

[112] S. Hannestad, R. Hansen and T. Tram, *How Self-Interactions can Reconcile Sterile Neutrinos with Cosmology*, *Phys. Rev. Lett.* **112** (2014) 031802 [1310.5926].

[113] N. Saviano, O. Pisanti, G. Mangano and A. Mirizzi, *Unveiling secret interactions among sterile neutrinos with big-bang nucleosynthesis*, *Phys. Rev.* **D90** (2014) 113009 [1409.1680].

[114] M. Archidiacono, S. Hannestad, R. Hansen and T. Tram, *Cosmology with self-interacting sterile neutrinos and dark matter - A pseudoscalar model*, *Phys. Rev.* **D91** (2015) 065021 [1404.5915].

[115] M. Archidiacono, S. Gariazzo, C. Giunti, S. Hannestad, R. Hansen, M. Laveder et al., *Pseudoscalar—sterile neutrino interactions: reconciling the cosmos with neutrino oscillations*, *JCAP* **1608** (2016) 067 [1606.07673].

[116] X. Chu, B. Dasgupta and J. Kopp, *Sterile neutrinos with secret interactions—lasting friendship with cosmology*, *JCAP* **1510** (2015) 011 [1505.02795].

[117] X. Chu, B. Dasgupta, M. Dentler, J. Kopp and N. Saviano, *Sterile neutrinos with secret interactions—cosmological discord?*, *JCAP* **1811** (2018) 049 [1806.10629].

[118] G. Gelmini, S. Palomares-Ruiz and S. Pascoli, *Low reheating temperature and the visible sterile neutrino*, *Phys. Rev. Lett.* **93** (2004) 081302 [astro-ph/0403323].

[119] G. Gelmini, E. Osoba, S. Palomares-Ruiz and S. Pascoli, *MeV sterile neutrinos in low reheating temperature cosmological scenarios*, *JCAP* **0810** (2008) 029 [0803.2735].

[120] G. B. Gelmini, P. Lu and V. Takhistov, *Cosmological Dependence of Non-resonantly Produced Sterile Neutrinos*, 1909.13328.

[121] C. Yaguna, *Sterile neutrino production in models with low reheating temperatures*, *JHEP* **06** (2007) 002 [0706.0178].

[122] K. Abazajian, *Sterile neutrinos in cosmology*, *Phys. Rept.* **711-712** (2017) 1 [1705.01837].

[123] T. Venumadhav, F. Cyr-Racine, K. Abazajian and C. Hirata, *Sterile neutrino dark matter: Weak interactions in the strong coupling epoch*, *Phys. Rev.* **D94** (2016) 043515 [1507.06655].

[124] S. Dodelson and L. Widrow, *Sterile-neutrinos as dark matter*, *Phys. Rev. Lett.* **72** (1994) 17 [hep-ph/9303287].

[125] E. Akhmedov, *Do non-relativistic neutrinos oscillate?*, *JHEP* **07** (2017) 070 [1703.08169].

[126] X. Shi and G. Fuller, *A New dark matter candidate: Nonthermal sterile neutrinos*, *Phys. Rev. Lett.* **82** (1999) 2832 [astro-ph/9810076].

[127] M. Dentler, c. Hernández-Cabezudo, J. Kopp, P. Machado, M. Maltoni, I. Martinez-Soler et al., *Updated Global Analysis of Neutrino Oscillations in the Presence of eV-Scale Sterile Neutrinos*, *JHEP* **08** (2018) 010 [1803.10661].

[128] K. Kainulainen, *Light Singlet Neutrinos and the Primordial Nucleosynthesis*, *Phys. Lett.* **B244** (1990) 191.

[129] M. Cirelli, G. Marandella, A. Strumia and F. Vissani, *Probing oscillations into sterile neutrinos with cosmology, astrophysics and experiments*, *Nucl. Phys.* **B708** (2005) 215 [hep-ph/0403158].

[130] A. Melchiorri, O. Mena, S. Palomares-Ruiz, S. Pascoli, A. Slosar and M. Sorel, *Sterile Neutrinos in Light of Recent Cosmological and Oscillation Data: A Multi-Flavor Scheme Approach*, *JCAP* **0901** (2009) 036 [0810.5133].